Sustainable Energy & Fuels
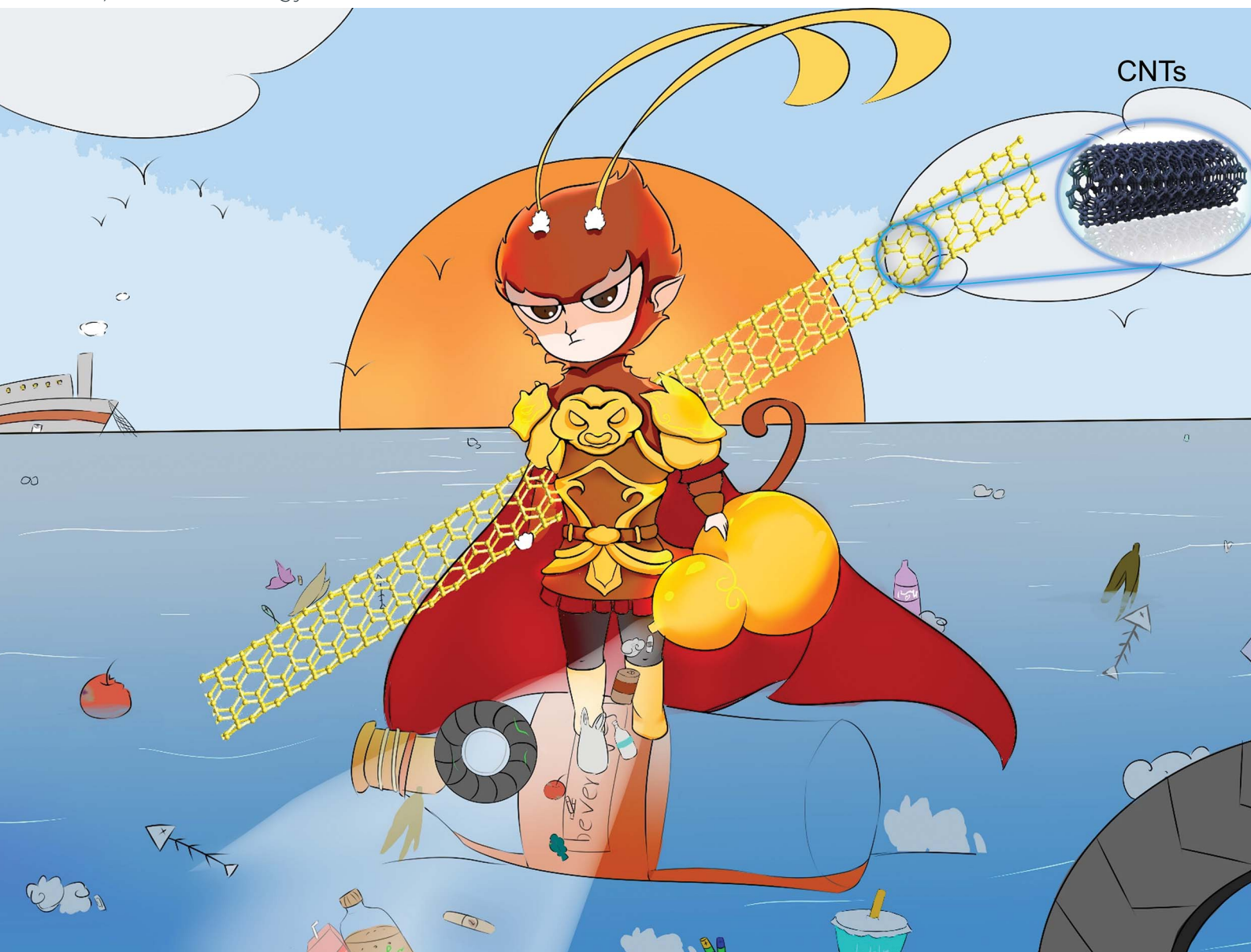
Interdisciplinary research for the development of sustainable energy technologies

CNTs

REVIEW ARTICLE
Paul T. Williams, Dan J. L. Brett *et al.*
Thermo-chemical conversion of carbonaceous wastes
for CNT and hydrogen production: a review

REVIEW

Check for updates

Thermo-chemical conversion of carbonaceous wastes for CNT and hydrogen production: a review

Ye Shui Zhang, [ID] [ab] Hua Lun Zhu,[c] Dingding Yao,[d] Paul T. Williams,*[e] Chunfei Wu, [ID] [f] Dan Xu,[ag] Qiang Hu,[d] George Manos, [ID] [a] Lu Yu,[h] Ming Zhao,[i] Paul R. Shearing [ID] [ab] and Dan J. L. Brett [ID] *[ab]

Thermo-chemical conversion of carbonaceous wastes such as tyres, plastics, biomass and crude glycerol is a promising technology compared to traditional waste treatment options (*e.g.* incineration and landfill). The process promotes the sustainable management of carbonaceous wastes and realizes the potential value of these wastes. Carbon nanotubes (CNTs) are one of the most extensively investigated and high-value materials due to their featured electrical, mechanical and physical properties. Producing CNTs from waste materials could solve the issues of waste management and simultaneously bring down the cost of CNT production. This review focuses on the four most abundant waste carbonaceous materials (waste tyres, plastics, biomass and crude glycerol) which have great potential to be alternative feedstocks for CNT production. The review considers the background of these four major types of waste to highlight the incentives in using thermo-chemical conversion to deal with these waste materials. Catalyst development for thermo-chemical conversion is discussed to summarize the most common catalysts and provide guidance for future novel catalyst improvement. Current research studies regarding CNT and hydrogen production from waste materials have been reviewed which show that the topic is highly attractive for researchers. The applications of CNTs have also been grouped based on different properties, aiming to guide the future research to explore the potential applications of CNTs synthesized from wastes. This review provides an overview of the recent developments in this research area and stimulates research to promote the deployment of the technology.

1 Introduction

An enormous amount of waste is produced globally every year which attracts people's concern in terms of waste management, cost and pollution. There are four abundant carbonaceous wastes (waste tyres, plastics, biomass and crude glycerol) from different sectors which will be introduced in this section regarding waste generation and management.

1.1 Waste tyre production and management

A large number of used tyres are generated around the world each year. It has been reported that the annual global waste tyre production is approximately 17 million tonnes.[1] The automotive retail economy is still in high demand throughout Europe accompanied by the growth of the transport sector; therefore, the increasing trend of end-of-life tyre waste generated in the EU is still expected to show an upward trend.[2]

Waste tyres are a mixture of elastomers (*e.g.* natural rubber, butadiene and styrene–butadiene rubbers), carbon black filler/strengthener, metal reinforcements, zinc, sulphur and other additives.[3] They are considered as one of the most

[a]*Electrochemical Innovation Lab (EIL), Department of Chemical Engineering, University College London, London, WC1E 7JE, UK. E-mail: d.brett@ucl.ac.uk*

[b]*The Faraday Institution, Quad One, Harwell Science and Innovation Campus, Didcot, OX11 0RA, UK*

[c]*Department of Chemical Engineering, Imperial College London, London, SW7 2AZ, UK*

[d]*Environmental Research Institute, National University of Singapore, Singapore*

[e]*Energy Research Institute, School of Chemical and Process Engineering, University of Leeds, Leeds, LS2 9JT, UK. E-mail: p.t.williams@leeds.ac.uk*

[f]*School of Chemistry and Chemical Engineering, Queen's University of Belfast, Belfast, BT9 5AG, UK*

[g]*School of Energy and Environment, Southeast University, Nanjing, P. R. China*

[h]*Bureau of Ecology and Environment in Shashi District, Jingzhou, P. R. China*

[i]*School of Environment, Tsinghua University, Beijing 100084, China*

Dr Zhang is a research fellow based at University College London UK. She has 20 publications since 2015 and her research covers a broad range of catalysis and pyrolysis, especially pyrolysis-catalysis of waste for obtaining CNTs.

Dr Yao is a research fellow at National University of Singapore, Singapore, who has expertise in converting plastic wastes into CNTs. She has four related research articles published in Appl. Catal., B in the last 4 years.

difficult waste materials to degrade due to chemical and biological resistance to degradation, which results in extremely long periods in waste landfill sites. Moreover, the waste tyre dumps could be the habitats for mosquitos and rodents that induce many diseases.[1] Therefore, most developed countries have banned the landfilling of waste tyres. In the EU, the Waste Landfill Directive has banned whole used tyres going to landfill since 2003 and shredded used tyres going to landfill since 2006.[3] The uncontrolled combustion of waste tyres produces smoke, oil and other toxic substances that pollute the atmosphere, soil, surface water and groundwater. With the demand for tyres growing globally each year, in 2020, ETRMA reported that 324 million tonnes of tyres were sold, representing 20% of the world tyre market,[4] and the environmental issues caused by waste tyre disposal is becoming more serious.[3] There is a need to find alternative methods to retreat the waste tyres. The approaches to manage the waste tyre issue include energy recovery, recycling and reuse.[1]

1.2 Waste plastic production and management

The large quantity of plastic consumption around the world results in the production of enormous amounts of waste plastics. Global annual commercial plastic production reached 359 million tonnes (Mt) in 2018 (ref. 5) and is estimated to double within the next 20 years.[6] It was reported that plastic converter demand in European countries was 51.2 million tonnes, and 29.1 million tonnes of waste plastics were generated in 2018.[5] The amount of plastic waste will inevitably

Prof. Williams is a Professor of Environmental Engineering at the University of Leeds, UK, and has a research background in both applied chemistry and process engineering. He is a Chartered Engineer and Fellow of the Institute of Energy. He has published more than 400 academic papers in the area of environmental engineering, including waste and biomass pyrolysis, waste incineration and the development of analytical methodologies for the detailed analysis of complex organic liquids, characterisation of the organic fraction of particulate emissions and the speciation of heavy metals in flue gases. He has also authored a second edition of a text book entitled 'Waste Treatment and Disposal' (John Wiley & Sons, 2005). He has an 'h' index of 50 and more than 10 000 citations to his work (Google Scholar).

increase further in 2020 because of the outbreak of COVID-19, as more plastic materials are needed whether in medical areas (especially for personal protective equipment like masks) or in daily packing areas (for food hygiene and increasing online purchases).[7] There are growing concerns that the current consumption and disposal of plastics bring substantial problems. A vast unmanaged plastic waste stream which leaks into the environment can be transformed into micro-/nano-plastics, posing a threat to the terrestrial and oceanic ecosystems.[8,9] For those collected plastic post-consumer waste, there are three options that are commonly used for disposal, including landfill, energy recovery and recycling. In Europe, though the recycling rate has doubled since 2006, the amount of plastic waste sent to landfill still accounts for 25%.[10] The landfill represents the cheapest and the least environmentally harmful waste tyre management method, while it requires hundreds of years for degradation and calls for much land area which is unrealistic in land-scarce areas such as Singapore. Energy recovery (also known as incineration) would significantly reduce the volume of plastic waste with simultaneous generation of heat, but hazardous substances may be released during incineration. Mechanical recycling provides a solution to recover some industrial plastic waste (especially PET and HDPE) into new low-grade plastic materials; however, the feasibility of such technology highly depends on the purity of waste and the availability of cost-efficient sorting equipment.[10] Chemical recycling, especially pyrolysis is another option for plastic waste management, which would be discussed in detail in a later section. It should be noted that most currently available recycling options are not cost competitive, hampering the commercialization of plastic recycling. More efficient and sustainable recycling options, which ideally not only solve the environmental issues caused by plastic but also generate value-added materials or fuels are needed to ensure the circular economy economy of plastics.[11]

1.3 Biomass waste production and management

Biomass is one of the most abundant and renewable carbon sources around the world that originates from the photosynthesis process taking place in plants utilizing carbon dioxide, water and solar light.[12] In 2017, electricity generated from biomass-based sources was the third largest renewable electricity source after hydropower and wind (596 TW h). In 2018,

Dr Wu is a Reader at Queen's University of Belfast, UK. His research interests include energy/chemical production from the catalytic thermo-chemical conversion of biomass and municipal solid wastes, and multifunctional catalytic sorbent development for carbon capture and utilisation. He has published >150 peer-reviewed journal papers (with an h-index of 45 in Google Scholar).

Prof. Brett specialises in electrochemical materials science and technology development. He is the co-founder of the UCL Electrochemical Innovation Lab (www.ucl.ac.uk/eil) that provides a sandpit environment where basic science meets industrial development leading to exploitation of new technologies. He has published >600 peer-reviewed journal papers (with an h-index of 56 in Google Scholar) and was awarded the 2009 De Nora Prize in recognition of his 'outstanding contribution to fuel cell and battery research', along with the 2011 Baker Medal from the Institute of Civil Engineers for his published work on fuel cells.

35.4 million tonnes of wood pellets were produced, of which 55% of the production was from Europe and 31% from the Americas (mainly USA).[13] Biomass waste as a low-value material has raised urgent environmental concern. The devastating environmental and health issues are caused by the disposal of very large quantities of biomass;[14,15] it is estimated to be 100 billion metric tonnes every year, including forestry residues, agricultural wastes and waste generated from food processing.[16,17] The food and green waste make up 44% of global waste.[18] Nearly 36% of waste generated globally has been landfilled and 33% of waste is disposed in open dumpsites. A limited amount of waste (~19%) can be recovered through recycling and composting, and ~11% of global waste is sent to incinerators.[19] In most developed countries, the recycling rate of the waste is higher than the global rate. In 2016, 47.4% of waste generated from 28 EU member countries has been sent to landfill or incinerators without energy recovery, and 52.6% of the waste was treated by recycling (36.7%), backfilling (10.1%) or energy recovery (5.8%).[20] However, waste management in most developing countries such as South Asia is still facing serious disposal issues as the most widespread disposal method is to dump in open sites.[21,22]

1.4 Crude glycerol production and management

Recently, biodiesel is increasingly used as a transport fuel since the derived engine emissions are much lower than the use of fossil fuels; in particular, biodiesel utilisation has a low overall carbon dioxide (CO_2) emission.[23,24] Also, biodiesel is biodegradable and nontoxic. It can be made from domestic or renewable resources, such as plain oil, animal fat, used cooking oil and algae. Biodiesel can be blended with regular diesel and used in diesel engines.[24] It can be produced by micro-emulsions, thermal cracking (pyrolysis) and trans-esterification, which is the most common method to produce biodiesel, yielding 10 wt% of glycerol as a by-product.[25,26] Considering all the benefits from biodiesel, the large scale production of biodiesel dominates the renewable energy industry in the EU. The EU expects 8.6% of its overall transport consumption in 2020 to be from biodiesel and its capacity of biodiesel production needs to reach around 23 million tonnes.[27,28] However, there is the expectation that a large amount of glycerol produced from the biodiesel production process will be usefully employed, making biodiesel more cost-competitive with the conventional diesel fuel.[29]

As a by-product of biodiesel manufacturing, the large amount of glycerol can influence the development of the biodiesel industry.[28] Volatility in the glycerol market can lead to a decrease in price, thereby bringing a series of problems including waste storage and treatment. The disposal or use of glycerol has become a challenge to make it a competitive commodity in the market. One issue is the presence of impurities in crude glycerol.[29] The impurities include water, ash, methanol and certain fatty materials. The impurities could cause catalyst deactivation and impede the performance of catalysts used in the glycerol steam reforming process.[30] There

is a need to unlock the potential value of the crude glycerol as a by-product of the biodiesel industry.[31]

An enormous amount of waste is produced globally every year and is attracting people's concern in terms of waste management, cost and pollution. Four abundant carbonaceous wastes (waste tyres, plastics, biomass and crude glycerol) from different sectors are introduced in the review. Thermo-chemical conversion of waste is more desirable compared with traditional recycling methods, as it could ease the environmental issues caused by landfilling or incineration. Also, the waste hydrocarbons can be present as an alternative feedstock for CNT and hydrogen production due to the much lower costs of feedstock.

The review summarizes the research works published in the last 20 years on the use of thermo-chemical conversion to produce high value products from waste materials, especially for obtaining CNTs. The development of this research field is discussed critically. There is a lack of research covering the applications of the CNTs produced from waste materials due to the impurities and un-controllable quality of the CNT production. So, a broad range of applications of CNTs have been covered in this review that would guide the researchers for extending the investigation to further imply the CNT products. There is potential to achieve commercialization of this technique for converting waste to high-value products.

This review would guide the researchers for further developing the technique for scaling-up. A larger scale of research would further boost the commercialization of this technique to extract values from waste materials. Also, the technique could guide the government sector to promote sustainable techniques for waste management.

The products from thermo-chemical conversion process consist of liquid, solid and gaseous products. Recently, Nanda and Berruti[32] reviewed the thermo-chemical conversion of plastic wastes to liquid fuels. Paul[33] reviewed the topic of pyrolysis-catalysis of waste plastics for hydrogen and CNT production. However, the previous reviews did not cover the applications of the CNTs which could be the future direction of this research. Solis and Silveira[34] critically reviewed different techniques based on thermo-chemical conversion and highlighted the economic feasibility of chemical recycling, which is still challenging to assess. The most important reasons are the uncontrollable quality of the products, purification methods of the products and potential applications. So, our review covers a more comprehensive summary regarding the most up-to-date research outcomes and critically discusses the research gaps to guide the researchers for next stage investigation. Although, thermo-chemical conversion of other waste materials has also been reviewed, such as biomass,[35] tyres[36] and glycerol,[37] they all focus on one single feedstock with a limited insight of the overall field. The catalyst development has been mentioned as a small proportion in the published reviews; here, we have made a more comprehensive catalyst development table to cover as much catalysts as possible. The future outlook highlights the future directions of this research, which show the potential of this technique for future development to financially and environmental benefit mankind.

2 Thermo-chemical conversion of carbonaceous wastes

Pyrolysis/gasification of waste is a thermo-chemical process which can be used for energy recovery from waste tyres, plastics, biomass and crude glycerol to prevent the waste going to landfill or incinerators.[38,39]
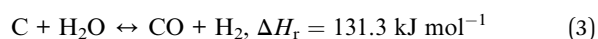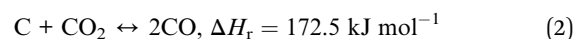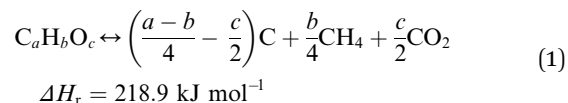
2.1 Thermo-chemical conversion of waste tyres

A typical tyre has a high carbon content of ∼81.2 wt% and a hydrogen content of ∼7.2 wt%.[40] The recovery of valuable products from tyres has been studied by many researchers, including the production of hydrogen, aromatic compounds, activated carbons, and others.[40–43] Pyrolysis as a thermal degradation process for recovering more valuable products from waste tyres has been investigated as a process option for waste tyre recycling.[41,43] The typical pyrolysis temperature for pyrolysis of tyres is around 500 °C, where the tyre is heated in an inert atmosphere for tyre degradation to produce gases, solid chars and oils. The gaseous products contain hydrogen and C_1–C_4 hydrocarbons (methane, ethene, ethane, propene, propane, butene, butane, and butadiene) and have a high calorific value of up to 65 MJ m^{-3} under atmospheric conditions, depending on the process conditions.[41] The solid char contains carbon black fillers that could be used as solid fuels or upgraded to activated carbons, which have been widely used for purification and separation.[44] Oils from pyrolysis of waste tyres are complex liquids with the texture of oil/wax, dark brown or black colours and with a sulphurous odour. The oil consists of over 100 identified compounds with chemical structures between C_5–C_{60}. The fractionation of these oils shows the presence of aliphatic hydrocarbons (including decane, undecane, dodecane, tridecane, tetradecane and others), aromatic hydrocarbons (including toluene, ethylbenzene, xylene, propylbenzene, ethylbenzene, naphthalene, phenanthrene, and pyrene), heteroatoms and polar fractions.[45]

Different compositions of tyre pyrolysis oils have been reported by different researchers. Using a circulating fluidized-bed reactor at 500 °C, Dai et al.[46] obtained a tyre pyrolysis oil which contained 26.77 wt% alkanes, 42.09 wt% aromatics, 26.64 wt% non-hydrocarbons and 4.05 wt% asphalt. Conesa et al.[47] reported that a pyrolysis oil produced with a fluidized-bed reactor at 700 °C consisted of 39.5 wt% aliphatic fraction, 19.1 wt% aromatic fraction, 21.3 wt% hetero-atom fraction and 20.1 wt% polar fraction. Aylón et al.[48] produced a tyre pyrolysis oil at 600 °C by a screw kiln reactor and contained 6.7 wt% alkane fraction, 65.5 wt% aromatic fraction and 27.8 wt% polar fraction. The difference in oil compositions is due to various tyre compositions and reaction temperatures.

Pyrolysis processes are normally carried out at relatively low temperatures (around 500 to 600 °C) with a higher yield of oils than gaseous products.[41] The typical gasification process is usually carried out at temperatures between 800 and 1200 °C, yielding more gaseous products than pyrolysis.[49] During gasification of waste tyres, hydrogen-enriched syngas is normally the target product. Syngas can be used for power generation
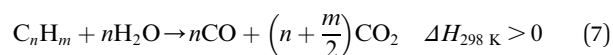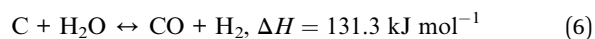
using internal combustion gas engines or for producing chemicals through the Fischer–Tropsch process.[50–53] Hydrogen is regarded as a clean energy carrier for a projected future hydrogen economy, as it can be produced from many sources, its combustion only generates water and it has broad applications e.g. fuel cells.[54]
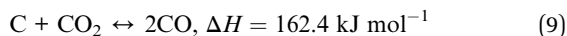
Tyres are a type of polymeric material made of single or double-bonded carbon atoms, where the rubbers are characterized by carbon–carbon double bonds.[55] The thermal decomposition of tyre rubber produces sub-units of the tyre rubber's molecular structure which are highly reactive free radicals.[56] The mechanism of tyre decomposition can be explained by reactions (1)–(5):[57]

$$C_aH_bO_c \leftrightarrow \left(\frac{a-b}{4} - \frac{c}{2}\right)C + \frac{b}{4}CH_4 + \frac{c}{2}CO_2 \tag{1}$$
$$\Delta H_r = 218.9 \text{ kJ mol}^{-1}$$

$$C + CO_2 \leftrightarrow 2CO, \Delta H_r = 172.5 \text{ kJ mol}^{-1} \tag{2}$$

$$C + H_2O \leftrightarrow CO + H_2, \Delta H_r = 131.3 \text{ kJ mol}^{-1} \tag{3}$$

$$CH_4 + H_2O \leftrightarrow CO + 3H_2, \Delta H_r = 205.8 \text{ kJ mol}^{-1} \tag{4}$$

$$CO + H_2O \leftrightarrow CO_2 + H_2, \Delta H_r = -50.8 \text{ kJ mol}^{-1} \tag{5}$$

2.2 Thermo-chemical conversion of waste plastics

Thermo-chemical recycling has been seen as a promising technology with a low carbon footprint for disposing of waste plastics. Quite a number of projects have been conducted on chemical recycling of waste plastics to produce liquid fuels. However, many challenges still exist in the product homogeneity from a mixed feedstock, optimization of liquid quality, and minimization of handling cost, before such technology is accepted and widely applied for plastic waste.[58] Many researchers also investigated the gasification of plastic waste for producing hydrogen or syngas.[59–63] It is often suggested that large quantities of waste plastics are available and can be used to produce significant amounts of hydrogen. Polyethylene, including HDPE and LDPE, is one of the main types of waste plastics.[64] Many researchers have focused on the thermal decomposition of plastics, and their results are indicative of the viability of using plastics to produce hydrogen.[59–61,65] Gasification of waste plastics to produce synthesis gases (H_2, CH_4 and CO) could effectively convert all of the carbon compounds in waste plastics to valuable products.[66] The reactions can be explained by eqn (6)–(9).[67] By using waste plastics to replace the conventional feedstock for hydrogen production, there is a promising potential to mitigate the high demand for fossil fuels.[65]

$$C + H_2O \leftrightarrow CO + H_2, \Delta H = 131.3 \text{ kJ mol}^{-1} \tag{6}$$

$$C_nH_m + nH_2O \rightarrow nCO + \left(n + \frac{m}{2}\right)CO_2 \quad \Delta H_{298 \text{ K}} > 0 \tag{7}$$

$$H_2O + CO \leftrightarrow H_2 + CO_2, \Delta H = -41.2 \text{ kJ mol}^{-1} \qquad (8)$$

$$C + CO_2 \leftrightarrow 2CO, \Delta H = 162.4 \text{ kJ mol}^{-1} \qquad (9)$$
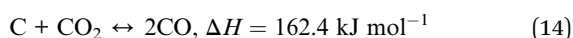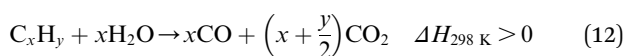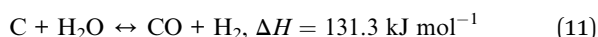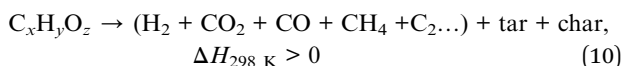
In the thermo-chemical conversion of waste plastics to produce hydrogen, catalysts play a key role in maximizing hydrogen production. Also, two-stage pyrolysis-catalysis systems are more controllable than one-stage catalysis processes because they separate the pyrolysis residues containing contaminants from catalysts.[64] From previous studies, nickel-based catalysts are the most common catalysts used for hydrogen production from plastics by thermal processing, mainly because of their high thermal stabilities and hydrogen selectivity.[59,62,64] Many types of Ni-based catalysts have been investigated such as Ni/Al_2O_3,[68] Ni–Mg–Al[64] and Ni/MgO catalysts.[69]

2.3 Thermo-chemical conversion of waste biomass

Biomass waste contains a higher fraction of oxygen and a lower percentage of hydrogen and carbon compared with petroleum resources.[70] Thermo-chemical conversion/pyrolysis-gasification/reforming of biomass has been extensively studied by researchers through supercritical water gasification,[71] microwave-assisted gasification[72] and chemical looping gasification.[71] Pagliaro[23] summarized the chemistry of energy from biomass and highlighted that it will play a crucial role in future biorefineries. The energy from biomass includes biomass for glycerol and biodiesel production; the biodiesel can be used to produce energy, or the CO_2 and H_2O could be the source of biomass through photosynthesis, and glycerol can be catalytically converted to chemicals, fuels and drugs. A bio-refinery can be considered as an integral unit that can accept different biological feedstocks and convert them to a range of useful products including chemicals, energy and materials.[23] The chemical reactions occurring during thermo-chemical conversion of biomass can be described through eqn (10)–(15):[73]

$$C_xH_yO_z \rightarrow (H_2 + CO_2 + CO + CH_4 + C_2...) + \text{tar} + \text{char},$$
$$\Delta H_{298 \text{ K}} > 0 \qquad (10)$$

$$C + H_2O \leftrightarrow CO + H_2, \Delta H = 131.3 \text{ kJ mol}^{-1} \qquad (11)$$

$$C_xH_y + xH_2O \rightarrow xCO + \left(x + \frac{y}{2}\right)CO_2 \quad \Delta H_{298 \text{ K}} > 0 \qquad (12)$$

$$CH_4 + H_2O \leftrightarrow 3H_2 + CO, \Delta H = 206.3 \text{ kJ mol}^{-1} \qquad (13)$$

$$C + CO_2 \leftrightarrow 2CO, \Delta H = 162.4 \text{ kJ mol}^{-1} \qquad (14)$$

$$CO + H_2O \leftrightarrow CO_2 + H_2, \Delta H = -41.2 \text{ kJ mol}^{-1} \qquad (15)$$
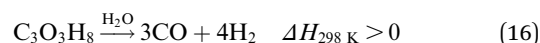
2.4 Thermo-chemical conversion of crude glycerol

Increasing the value of glycerol is an effective way to meet the challenges of the future development of biodiesel production.[15] Considering the relatively high costs of producing biodiesel and
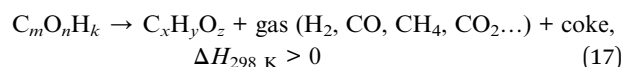
the purification of crude glycerol, the development of converting glycerol to value-added chemicals is important.[15,21,22] Many reactions occur during the pyrolysis of glycerol across the temperature range of 650 to 800 °C. Products from pyrolysis of glycerol include gases, liquids and chars. Gas components include H_2, CO, CO_2, CH_4, and C_2H_2. The liquid components include methanol, ethanol, acetone, acetaldehyde, acrolein, acetic acid and water.[74] The liquid, gas and char are produced by dehydration reactions when the temperature is relatively low. When the temperature is relatively high, H_2, CO and char are produced as the main products by consecutive thermal cracking reactions.[74] Valliyappan *et al.*[74] surmised that the total char production from pyrolysis of glycerol is below 10 wt%, which means that the process is quite feasible.

The chemical process for conversion of glycerol to CO and H_2 is shown in eqn (16). CO and H_2 are the main gaseous products from thermo-chemical conversion of glycerol. There are also small contents of other gases such as CO_2, CH_4, C_2H_4, C_2H_5 and C_3H_6. There are also simultaneous reactions happening during the decomposition of glycerol, as shown in eqn (17).[74] Subsequent reactions, such as water–gas shift and methanation reactions, are shown as eqn (18) and (19).[30,75]

Decomposition of glycerol:

$$C_3O_3H_8 \xrightarrow{H_2O} 3CO + 4H_2 \quad \Delta H_{298 \text{ K}} > 0 \qquad (16)$$

Simultaneous reactions:

$$C_mO_nH_k \rightarrow C_xH_yO_z + \text{gas} (H_2, CO, CH_4, CO_2...) + \text{coke},$$
$$\Delta H_{298 \text{ K}} > 0 \qquad (17)$$

Water–gas shift reaction:

$$CO + H_2O \Leftrightarrow CO_2 + H_2, \Delta H = -41.2 \text{ kJ mol}^{-1} \qquad (18)$$

Methanation reaction:

$$CO + 3H_2 \rightarrow CH_4 + H_2O, \Delta H = -206.1 \text{ kJ mol}^{-1} \qquad (19)$$

2.5 Discussion of thermo-chemical conversion of carbonaceous waste

The production and disadvantages of conventional waste management for the four most abundant waste carbonaceous materials (waste tyres, waste plastics, biomass and crude glycerol from the biodiesel industry) have been discussed in Sections 1.1–1.4. There is a need to develop recovery methods to further improve the energy recovery efficiency from these waste materials. Thermo-chemical conversion/pyrolysis–gasification as a relatively mature and effective route to convert these four waste materials to profitable liquid, gaseous and solid products is explained in Sections 2.1–2.4, which are summarized in Fig. 1.[76,77] Liquid products containing naphtha, tars and phenols can be applied straightaway or upgraded as fuels.[78] Gas products containing syngas (H_2 + CO), methane and other gases can also be used as fuels;[79] and solid products are mainly chars

that can be upgraded to activated carbons.[80] As gasification is different from pyrolysis, it requires gasifying agents such as water, air or CO_2 to enhance the gaseous products, and this consequently results in lower production of oils. The gaseous products are mainly H_2, CO, CO_2, CH_4 and H_2O.[76] As there are many products produced through thermo-chemical conversion of carbonaceous waste, the development of the technique should focus on the most valuable products which have great potential to reach a higher recovery rate or financial values. So, hydrogen gas and CNTs (CNTs) will be further discussed as the targeting products.

3 Hydrogen and CNT production

As discussed in Section 2.5, the products from thermo-chemical conversion of carbonaceous waste are generally grouped as gaseous, liquid and solid products, and the targeting products of hydrogen and CNTs are mainly covered in this review. Therefore, the production and background of hydrogen and CNTs are discussed in this section to explain the reasons for targeting these two products, especially CNTs from the thermo-chemical conversion of pure gas precursors and carbonaceous wastes.

3.1 Hydrogen

There is around 5×10^{11} N m^3 of hydrogen produced in the world, and around 96% of hydrogen is produced from fossil fuels. Hydrogen is mainly produced through methane reforming (48%), oil/naphtha reforming (30%), coal gasification (18%) and electrolysis (3.9%).[81] Costs and alternative material sources are key challenges for the development of a sustainable hydrogen economy. Therefore, using alternative sources to generate hydrogen is imperative.

Hydrogen is considered as a clean energy fuel which has the potential to reduce the world consumption of fossil fuels to meet sustainable development targets. Currently, the methods to produce hydrogen energy are not renewable. The costs and alternative sustainable energy sources are issues for hydrogen economy development.[82] There is increasing research interest in investigating new feedstocks to produce hydrogen. Waste hydrocarbons are a significant potential source as it can help solve waste disposal issues and maximise the value of wastes by producing hydrogen and value-added products such as CNTs.

3.2 CNTs

Since the discovery of CNTs in the early 1990s, CNTs have been popularly applied in a wide range of science and engineering fields due to their unique physical and chemical properties.[83,84] Single-walled carbon nanotubes (SWCNTs) are formed by a single graphite sheet wrapped around to form a cylinder with the diameter in the range of 0.8–1 nm. Multi-walled carbon nanotubes (MWCNTs) are formed by nested cylinders of graphene sheets in which the diameters are typically in the range of 5–20 nm but can also exceed 100 nm. The length of CNTs varies from 100 nanometers to centimeters.[85] CNTs have several featured properties including relatively high tensile strength

(around 100 GPa) which is 100 times greater than that of stainless steel, high modulus (around 1 TPa),[86] a large aspect ratio of length to diameter, a cylindrical structure, low density (around 1100–1300 kg m^{-3}) which equates to one-sixth of that of stainless steel, small size on the nano-scale, and good chemical and environmental stability. CNTs have relatively high thermal conductivities of about 3500 W m^{-1} K^{-1} at room temperature, similar to those of diamond and a relatively high electrical conductivity of 10^9 A cm^{-2} comparable to that of copper.[87,88] The applications of CNTs are widely varied, making CNTs a high-value material.

Bulk CNTs have been used for a wide range of applications including rechargeable batteries, automotive parts, sporting goods and boat hulls.[86] The initial applications of CNTs on super-capacitors, actuators and lightweight electromagnetic shields have already achieved commercial impact. CNTs can be used as multifunctional coating materials. For example, MWCNTs can be added to paint which can discourage algae and barnacles attached on boat hulls and therefore reduce biofouling.[89] MWCNTs have been widely used in lithium-ion batteries by blending MWCNTs with active materials and a polymer binder.[90,91] MWCNTs can increase the electrical connectivity and mechanical integrity; therefore, the rate capacity and life cycle of batteries can be enhanced.[92,93] Considering the low electron scattering and band gap of high quality SWCNTs, they have been used in transistors. CNTs have also been used in biosensors and medical devices because of their chemical and dimensional compatibility with biomolecules.[94]

However, the commercial applications of CNTs have still not reached their full potential, and there is still room for the development of CNT production from wastes as a complementary process for large-scale CNT production. The existing methods for CNT production are energy and resource intensive and include but are not limited to the electric arc-discharge method, laser ablation method, catalytic chemical vapour deposition (CVD), flame synthesis and a solar energy route.[95] Among these methods, CVD is currently the most promising and preferred method for large-scale production. The typical reactor used for CVD is a fluidized bed reactor which improves the gas diffusion and heat transfer to catalyst nanoparticles.[95] The low-cost feedstock, efficiency improvement, energy consumption reduction and waste reduction are the main factors that affect the scale-up of CNTs produced by CVD.[96] There is a successful example of scaled-up camphor CVD for MWCNT production that has been commercialized in Japan (Meijo Nano Carbon Co. Ltd.).[97] It has been reported that due to the relatively low price of camphor, the cost for producing CNTs has been reduced to around $100 kg^{-1}, which is the lowest commercial price reported for purified CNTs.[85]

Nevertheless, researchers are still looking for more efficient and cost-effective ways for large-scale production of CNTs which has been defined as the production of 10 000 tonnes of CNTs per year. Hence, in recent years, there have been efforts regarding possible alternative routes for producing CNTs or investigating alternative feedstocks.[85]
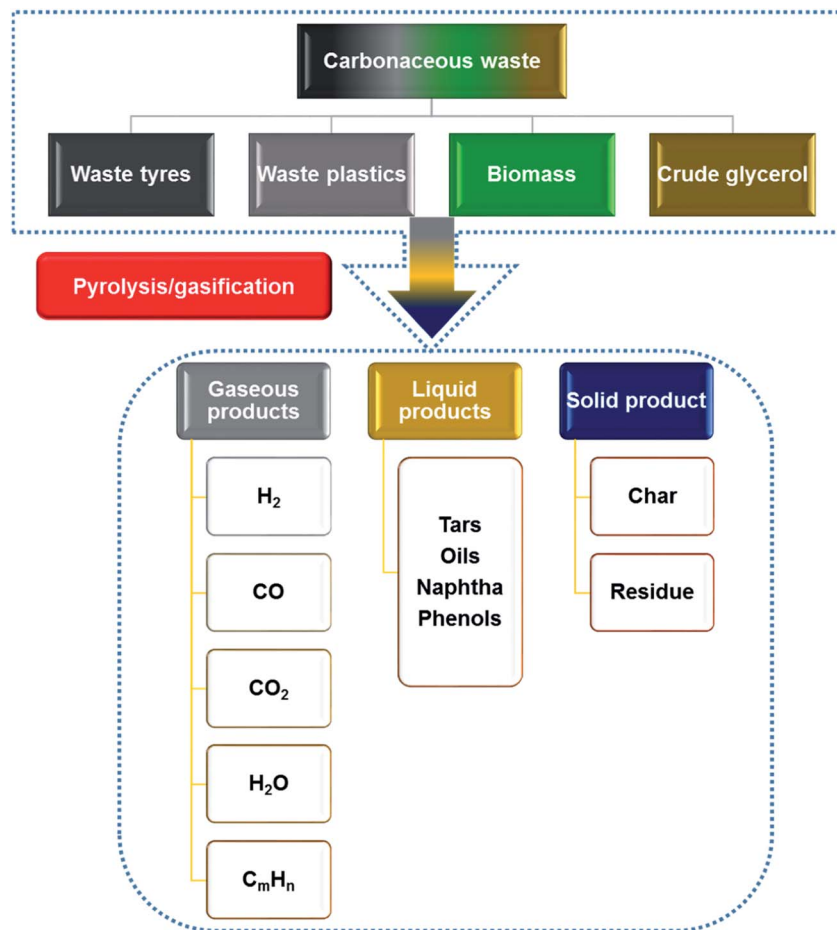
Fig. 1 Products from the pyrolysis and gasification of carbonaceous materials.

3.2.1 Conventional methods for CNT production and purification. CNTs are currently mainly produced by electric arc discharge,[83] laser ablation, catalytic CVD, flame synthesis, solar energy route and others.[98] The electric arc discharge method requires two graphite electrodes with 1 mm gap under an inert gas atmosphere at a pressure of 500 torr. A current of 50–120 A with a voltage of 20–25 V produces an arc which occurs between the two electrodes. The carbon evaporates from the electrodes which then condense on the cathodes with CNT formation. The advantage of this method is that both SWCNTs and MWCNTs can be synthesised at low cost.[99] The laser ablation method employs the same conditions as the arc-discharge method, including condensation of the graphite vapour to form CNTs. Graphite to CNT conversions of 60–90% can be achieved by using the laser ablation method.[100]

Dasgupta et al.[101] noted that both the arc discharge and laser ablation methods have the issue of requiring a large amount of energy to induce the reorganization of carbon atoms into CNTs. The temperature for the process needs to reach 3000 °C or higher for effective crystallization and good graphite alignment of CNTs. Difficulties have emerged in meeting the basic required conditions for the large-scale production of CNTs, such as a vacuum environment and continuous graphite target replacement. CNTs produced by the arc-discharge method and

laser ablation are normally in a carbonaceous soot form, which consists of amorphous carbon and metal particles from catalysts. This will significantly affect the purity and quality of the products. Transition metal carbide has been considered by many researchers to promote filamentous carbon deposition.[102–104] Aligned SWCNTs can be synthesised by an attractive coagulation-based spinning of CNT suspensions, which has the potential to enlarge the scale and be extended to the production of MWCNTs.[105]

CVD is the most common and popular method to commercially synthesise CNTs. The CVD method is based on the thermal decomposition of hydrocarbon vapour, and the process can be promoted by adding metal-based catalysts. The general process includes the passing of a hydrocarbon vapour through a tubular reactor at temperatures of 600 to 1200 °C, in the presence of a catalyst. As the hydrocarbon decomposes in the reactor, CNTs grow on the surface of the catalyst. The growth ends with the system cooling down to room temperature. Precursors for CNT synthesis by the CVD method can be of various phases, such as liquid and solid hydrocarbons.[97] The CVD method is more energy-saving compared with the arc discharge method and the laser ablation method. Also, the structure of CNTs can be properly controlled in the CVD process, such as the wall number, length, diameter and

alignment. In consideration of the advantages of CVD, such as mild operations, low cost and a well-controlled process, CVD has great promise as a feasible method for large-scale production of CNTs.[106] However, the disadvantage still exists that the CNTs produced are a mixture of MWCNTs and SWCNTs.[99]

3.2.2 Catalysts and precursors for CNT production by CVD.

Although noble metals are the most effective catalysts to promote hydrogen production,[107,108] they are not the ideal catalysts for large scale applications considering their high costs. Currently, Ni-, Fe- and Co-based catalysts have been commonly used for the gasification of hydrocarbons.[97] The most common carbon precursors used for CNT production are methane,[109,110] ethylene,[111,112] acetylene,[113] benzene,[114] xylene[115] and carbon monoxide.[116] Hernadi et al.[109] investigated Fe-based catalysts with different supports to produce CNTs via CVD using different hydrocarbons including acetylene, ethylene and propylene. They found that a Fe/silica catalyst presented the highest activity for CNT formation compared with other types of catalysts, such as graphite and ZSM-5.

Weidenkaff et al.[117] produced MWCNTs with diameters in the range of 5 to 20 nm from carbon monoxide and gaseous hydrocarbons by CVD in the presence of a Fe-based catalyst in a fluidized bed reactor. Venegoni et al.[118] produced MWCNTs from a mixture of hydrogen and ethylene in the presence of an Fe/SiO$_2$ catalyst by a CVD method in a fluidized bed reactor. Homogeneous MWCNTs were produced with diameters in the range of 10 to 20 nm. Morançais et al.[119] selectively synthesised MWCNTs from ethylene by the CVD method in a fluidized bed reactor, in the presence of a Fe/Al$_2$O$_3$ catalyst. The improved CVD process with efficient mixing of carbon precursors and catalysts resulted in a high selectivity of MWCNTs and a high purity. Philippe et al.[120] also produced MWCNTs by a CVD method with a fluidized bed reactor in the presence of a Fe/Al$_2$O$_3$ catalyst. They also proposed a two-stage MWCNT growth mechanism based on their experiments and characterizations, which started with the MWCNT nucleation and grew by reconstruction as well as simultaneous carburization of the catalytic film. When the catalytic film was consumed, the catalyst particles inside of the mesoporous support were reduced and tangled CNTs were formed. Li et al.[121] used Fe/Al$_2$O$_3$ catalysts prepared by an ion-beam assisted deposition method to produce well-aligned CNT arrays with lengths in a range of 500 μm to 1.5 mm by the CVD method. See et al.[122] used Fe/Co/Al$_2$O$_3$ catalysts in their experiments to investigate process parameters for CNT synthesis in a fluidized bed. The results showed that the synthesis temperature affected the formation of CNTs greatly while the influence on the CNT diameter, quality, and yield was not clear. With the increase of synthesis temperature in all of their experiments, the yield of carbon increased rapidly and the increment of the CNT yield is small. It was indicated that the selectivity to CNTs decreased when the catalytic temperature increased. Nevertheless, See and co-researchers[123] found that the quality of CNTs improved with the increase of reaction temperature in relation to the graphitization of CNTs. The results also showed that a higher fluidization ratio resulted in a pronounced increase of carbon yield compared with the increase of the deposition time. The type of catalyst and the

interaction between the catalyst and the temperature were proved to have significant effects on carbon yields. The selectivity to CNTs significantly depended on the type of catalyst. In addition, their experimental results showed that the Fe–Co/Al$_2$O$_3$ catalyst had a relatively higher selectivity toward CNT formation than the Fe/Al$_2$O$_3$ catalyst.

Some researchers have used Co-based catalysts to enhance the growth of CNTs obtained from hydrocarbon reforming.[124] Qian et al.[124] used Co- and Ni-based catalysts in methane decomposition to enhance CNT production in a fluidized bed reactor. They compared the decomposition of methane with and without catalyst reduction. The yield of CNTs produced by the process without catalyst reduction was 3 to 4 times less than the CNT yield from the methane decomposition process with catalyst reduction. They explained that the in situ catalyst reduction provides energy for endothermic methane decomposition. Also, the in situ catalyst reduction consumed hydrogen and carbon to form water and carbon monoxide, which promoted hydrogen and CNT formation. Kong et al.[110] synthesised CNTs by CVD from methane in the presence of different catalysts. They reported the effect of different metals (Fe-, Ni-, Co- and Fe/Co-based) and different supports (alumina and silica) on the formation of CNTs.

Wei et al.[125] investigated the thickness of Fe- and Ni-based catalyst films on CNT formation by the CVD method. They found that there was no correlation between the thickness of the catalyst film and the formation of CNTs. However, the vertically oriented CNTs formed by using plasma-enhanced CVD with the nickel catalyst showed a strong correlation between the diameter of CNTs and the thickness of the catalyst film. Fang et al.[126] reported that Ce–Ni mixed oxide can be one of the most effective and stable catalysts in steam reforming of ethanol to produce hydrogen and carbon nano-materials. The results from their research showed that the Ce–Ni catalyst is not only active for hydrogen production but also is the most effective catalyst to produce carbon nano-materials. They also found that co-precipitation is the most suitable method for catalyst preparation in terms of hydrogen and carbon nano-material production for ethanol steam reforming. The co-precipitation method can form small size NiO with a diameter of 15 nm and CeO$_2$ with a diameter of 4 nm. These led to less formation of nano-fibrous carbon materials. In addition, the size of nano-fibrous carbon materials depended on the size of Ni nanoparticles. Ce–Ni catalysts prepared by the co-precipitation method can form smaller and more homogeneous carbon filaments compared to the catalysts prepared by other methods. The graphitic filaments are CNTs and carbon nanofibres (CNFs).

Ni-based catalysts have significant catalytic activity; their catalytic activity and stability are determined by the size of NiO and CeO$_2$ and the interaction between nickel and cerium species, which are defined by the method of preparation. Considering the strong relationship between the catalytic stability and the type of carbon formation, catalytic stability can be analysed according to the size of graphitic filaments.[127]

Fe, Co and Ni are the most common metals used in CNT synthesis for two reasons: first, the carbon solubility can reach

high levels at high temperature and second, carbon diffusion can attain high rates in these metals. Apart from the common transition metals used in CNT production, Cu, Au, Ag, Pt and Pd were also found to catalyse hydrocarbon decomposition to form CNTs.[128] Kong et al.[129] synthesised single-walled CNTs (SWCNTs) of high quality by CVD of methane with Fe-based catalysts at 1000 °C. Different catalyst supports were investigated, and the authors concluded that the catalysts supported by amorphous silica particles could produce SWCNT bundles. However, the catalysts supported by crystalline alumina nanoparticles produced individual SWCNTs and small bundles. Fan et al.[111] produced self-oriented regular arrays of CNTs by CVD of ethylene with patterned porous silicon as the substrate. Satishkumar et al.[112] produced bundles of aligned CNTs by pyrolysis of ferrocene and hydrocarbon mixtures. They found that the ferrocene–acetylene mixture is ideal for producing compact aligned nanotube bundles. The bundles of CNTs were associated with nanoparticles in a size range of 2–13 nm, and the alignment of catalyst nanoparticles was dominated by the ferromagnetism of transition metal nanoparticles. Li et al.[113] enlarged the scale of aligned CNT production by CVD of xylene with iron nanoparticle embedded mesoporous silica catalyst. The growth direction of aligned CNTs was controlled by the pores of the mesoporous silica catalyst support. Sen et al.[114] investigated the effects of metallocenes such as ferrocene, cobaltocene and nickelocene on CNT synthesis by pyrolysis of benzene. The wall thickness of nanotubes was associated with the metallocene content.

Organometallocenes have also been widely used as catalysts to produce CNTs because the metal particles can be liberated in situ and effectively promote hydrocarbon decomposition to form CNTs.[97] Wei et al.[115] synthesised multi-walled CNTs using a promoted method by exposing a silica substrate to a xylene and ferrocene mixture at 800 °C. The authors reported that the mixture of xylene and ferrocene vapour enhanced the selectivity to multi-walled CNTs. Nikolaev et al.[116] synthesised SWCNTs by gas-phase catalytic reforming of carbon monoxide. The catalysts were obtained by in situ decomposition of iron pentacarbonyl in a hot carbon monoxide flow.

Cyclohexane[130,131] and fullerene[132,133] are also commonly used as carbon precursors to produce multi-walled CNTs. Liu et al.[130] prepared CNTs by catalytic decomposition of cyclohexane. Li et al.[131] synthesised three-dimensional hierarchical CNTs by electrochemical iron deposition of cyclohexane. The CNTs were shown to have high electrical conductivity. Nerushev et al.[132] used fullerene and acetylene as carbon sources to investigate the dependence of catalytic particle size in a CVD process. They found that the diameter of CNTs increased when the catalytic particle size increased. Morjan et al.[133] used fullerene as a carbon precursor to synthesize multi-walled CNT films by an iron-catalysed thermo-chemical vapour deposition process. The structural properties of CNTs produced from fullerene were different from the CNTs produced from acetylene.

Catalyst supports used in CNT production by the chemical vapour deposition process include graphite,[134] quartz,[135,136] silicon,[137,138] silicon carbide,[139,140] silica,[141,142] alumina,[143–146] alumina-silicate (zeolite),[147,148] CaCO$_3$,[149] and magnesium oxide,[150–152] among others. The interactions between catalytic particles and supports play an important role in CNT formation. The formation of chemical bonds between catalytic metal particles and supports could inhibit the catalytic ability of metal particles. Also, the morphology and textural properties of catalyst supports could affect the yield and quality of CNTs.[97] For example, zeolite with nano-scale pores can significantly enhance CNT yields with a relatively small particle size.[148]

Alumina materials have been reported to be better catalyst supports than silica due to their strong metal–support interaction which could promote metal dispersion on catalysts.[153] Stainless steel meshes have been applied by many researchers in CNT production from different sources.[154–158] For example, the use of a stainless steel mesh as a catalyst support has been introduced in CNT and hydrogen production from the reforming of toluene, which can easily separate the CNT products from the catalysts.[154] Alves et al.[155] produced CNTs using a stainless steel type 304 alloy which consisted of 67% iron, 18–20% chromium and 11% nickel. They concluded that stainless steel can promote CNT growth which has also been reported by other researchers.[156,157] Sano et al.[156] produced aligned multi-walled CNTs on the surface of stainless steel by phenol decomposition. The stainless steel mesh was activated by intensive oxidation in air and then reduced in H$_2$. Wal and Hall[158] used an activated type 304 stainless steel mesh as a catalyst to produce CNTs from a mixture of C$_2$H$_2$/benzene or CO/benzene mixture by CVD.

3.2.3 CNT purifications. To improve the purity of CNTs formed by different methods and to apply them in different industries, non-CNT impurities (metal or metal oxides from the catalysts and amorphous carbon) should be removed. The two most popular methods used to remove impurities from CNT products are the dry method which involves oxidizing in air, and the wet treatment which involves dissolving in an acid. The dry method depends on the higher thermal stability of CNTs compared with amorphous carbon and other highly reactive impurities. The wet method is normally applied after the dry treatment and dissolves the metals or metal oxides in nitric acid. Filtration and centrifugation steps are also applied to improve the quality and the yield of CNTs. Ebbesen et al.[159] used a dry method to oxidize CNTs produced by the electric arc discharge method, to remove impurities. The CNTs produced were oxidized at 750 °C and held for half an hour. However, the method was unsuccessful as most of the carbon, even CNTs, was burnt off. Xu et al.[160] purified CNTs produced by the CVD method using carbon monoxide in a combined dry and wet method. The produced CNTs were first dry-treated to remove active amorphous carbon. Then, the samples were wet-treated in HCl to remove the iron catalyst particles. When the oxidation temperature was 350 °C, 98% of CNTs were obtained with a significant reduction of iron content from 30 to 1%. The total weight loss of the CNT yield was around 30 wt%. Moon et al.[161] obtained CNTs with 96% purity, which were also treated by a combination method. The CNTs produced by the electric arc discharge method were first heated to 450 °C and held for 50 minutes to remove amorphous carbon. Then, the produced CNTs with impurities were dissolved in HCl to remove catalyst
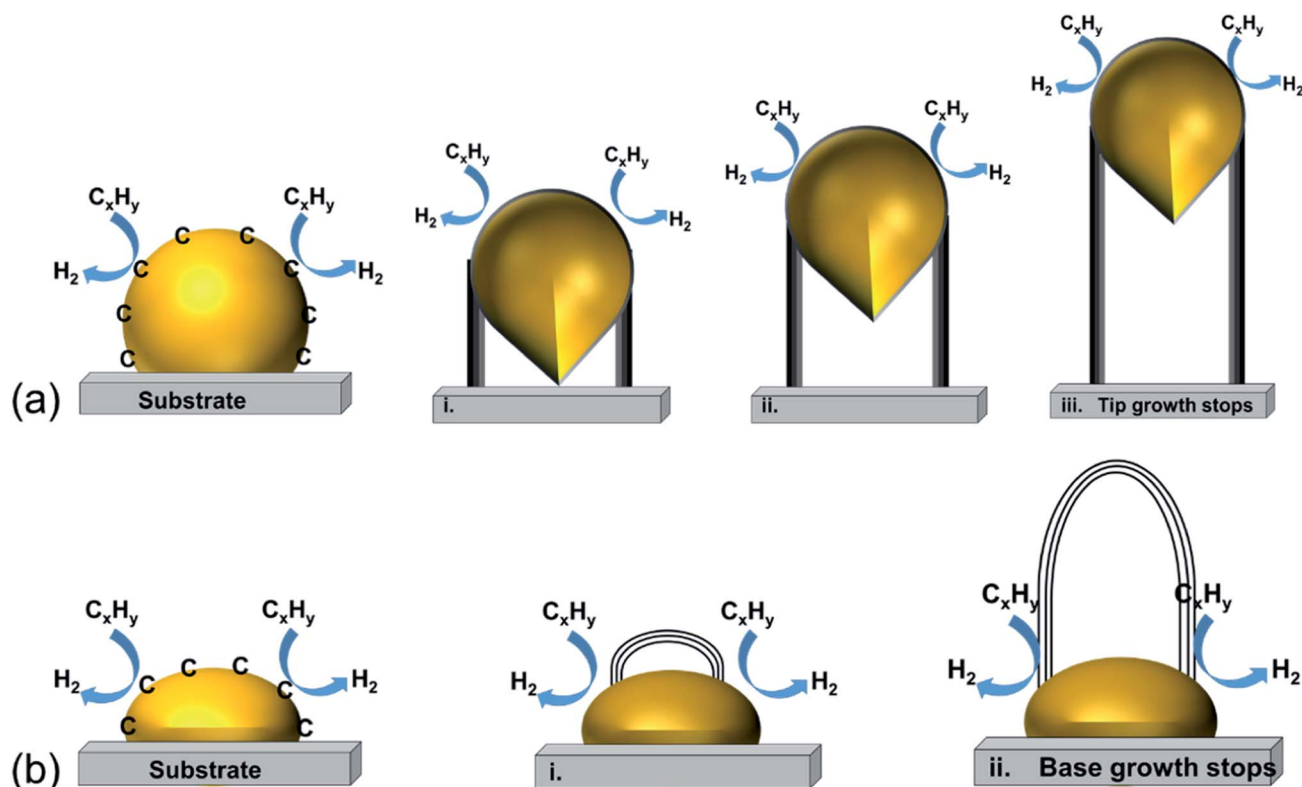
Fig. 2 The most accepted mechanism for CNT growth: (a) tip-growth model and (b) base-growth model.[162] (This publication is distributed under the terms of the Creative Commons Attribution-NonCommercial-ShareAlike-3.0 License, which permits use, distribution and reproduction for non-commercial purposes, provided the original is properly cited and derivative works building on this content are distributed under the same license.)

particles and finally the CNTs were boiled in 30% nitric acid to unbundle the CNTs.

Overall, common CNT synthesis methods like CVD always come with impurities from the production process, such as amorphous carbon and catalyst metal particles. Furthermore, the incorporation of dry and wet treatments can improve the purity of CNTs dramatically.

3.2.4 Mechanism of CNT growth. The mechanism of CNT growth has been debated since they were discovered. Mechanisms proposed by different researchers are based on different catalysts, substrates, hydrocarbons and carrier gases. However, the most acceptable mechanism for CNTs formed by the CVD method has been proposed by Kumar in 2011.[162,163] They claimed that hydrocarbon vapours start to decompose into carbon and hydrogen atoms when in contact with metal nanoparticles at higher temperatures; then the carbon atoms dissolve into the metals until the metals are saturated with carbon at a certain temperature; the carbon precipitates out and crystallizes as hollow tubes which have no dangling bonds and are thus energetically stable. There are two models to explain this growth mechanism according to the catalyst metal and support interaction as shown in Fig. 2.

Fig. 2(a) shows the tip-growth model and describes the growth of CNTs on the catalyst where there is a weak metal–support interaction when the metal particles are at an acute contact angle with the support. The hydrocarbons decompose

on the tip of the metal particle, then carbon atoms diffuse down through the metal particles and accumulate at the bottom of the metal particles. Because of the weak interaction between the metal particles and the support, the accumulated carbon on the bottom of the particle would push the metal particle away from the support. The accumulated carbon are hollow carbon CNTs which can keep growing until they reach the carbon solubility of the metal particle. Fig. 2(b) illustrates the base-growth model which describes the growth of CNTs on the catalyst where there is a strong metal–support interaction. The strong metal–support interaction indicates that the metal particle has an obtuse contact angle with the support. The beginning stage of hydrocarbon decomposition and carbon atom diffusion is similar to that of the tip-growth model. Due to the strong interaction between metal particles and support, the carbon precipitates out on top of the metal particles as a hemispherical dome. As more and more hydrocarbons decompose and diffuse to the lower peripheral surface of the metal particles, the carbon atoms accumulate as crystallized CNTs.[97,162] The authors also broadly concluded that SWCNTs are formed when the catalyst particle sizes are of a few nanometers in size and the MWCNTs are formed when the catalyst particle sizes are of a few tens of nanometers. CNT growth is affected by a number of parameters, including the hydrocarbon precursors and the type of catalyst. Other factors such as the synthesis temperature, pressure, residence time, reactor type and flow rate of reactant can also

influence the quality of CNT formation. Tessonnier and Su[164] reached a similar conclusion that the diameter of the SWCNTs increases as the size of the catalyst particles increases. However, the nature of the CNTs would change at a certain point where double walled carbon nanotubes and MWCNTs are formed. They also highlighted that large metal particles at diameters above micro-meter size could dominate graphene or graphite formation. The shapes of catalyst particles also affect the features of filamentous carbon formation; round shape catalyst particles lead to hollow CNTs, while irregular metal particles with sharp edges lead to fishbone carbon nanofibers.[165]

In 2011, Tessonnier and Su[164] proposed a vapour–solid–solid growth mechanism based on the vapour–liquid–solid mechanism proposed by Baker et al. in 1970s,[134] as shown in Fig. 3(I)–(III). The vapour–liquid–solid mechanism includes three main steps. The first step (I) is the elementary carbon atom formation by the absorption and dissociation of a gaseous carbon precursor on the surface of the catalyst particle. In the second step (II), the carbon atoms dissolve in the bulk of nanoparticles, the liquid metastable carbide forms and carbon diffusion occurs within the particles. Finally, in the third step (III), the carbon atoms precipitate out at the side of the catalyst particles to accumulate as carbon filaments. Steps (II) and (III) could be alternatively described as (IV) and (V) that carbon species diffuse only on the surface of the catalyst particle. The vapour–liquid–solid mechanism has been supported by many other researchers as the calculated activation energy for carbon nanofiber formation agrees with the calculation of carbon dissolution in metals.[134,166,167]

There are still debates on the vapour–liquid–solid mechanism because the diffusion step is not clear, especially the nature of the driving force pushing the carbon atoms to diffuse on the catalyst particle surface has not been stated clearly. The vapour–liquid–solid mechanism could explain the CNT growth mechanism when the metal particles melt. The study of the CNT growth mechanism has been modified as the carbon diffusion occurs at the surface of the catalyst particle instead of through the bulk of catalyst particles, which has been supported by many researchers. Tessonnier and Su[164] investigated the vapour–solid–solid mechanism including the carbon precursor dissociation, carbon atom diffusion on the surfaces of catalyst particles and carbon precipitation to form CNTs. They also proposed a hypothesis about the sub-diffusion of carbon atoms according to the calculation that each carbon atom could gain 0.3 eV energy by diffusing on the sub-surface.

3.2.5 Recent CNT growth mechanism development. The CNT growth mechanism is complex and may vary under different reaction regimes, catalysts and feedstocks, especially for the waste material which has a complex composition.

In 2018, Yang et al.[168] proposed a multi-route reaction in the gas-phase-assisted vertically aligned CNT growth mechanism in temperature gradient chemical vapour deposition of acetylene, whose growth kinetic characterization shifted from a single rate-limiting reaction to a multi-route reaction. C_2H_2 contributed to CNT growth through dissociation, followed by path one of bulk diffusion or path two of surface diffusion without gas-phase reactions. The secondary products (C_4 and C_6 species) were formed and approached the Fe-based catalyst substrate by the enhanced gas-phase reactions, which could be path three or others. The authors highlighted that the findings could help understand the vertically aligned CNT growth from thermally rearranged precursors, which would then guide the diameter-controlled and low-temperature growth.

In 2019, Li et al.[169] reported the vaporizing phenomenon of the Na catalyst in low-temperature ($\sim$400 °C) CNTs catalyzed by sodium-based ingredients coupled with an oxidative
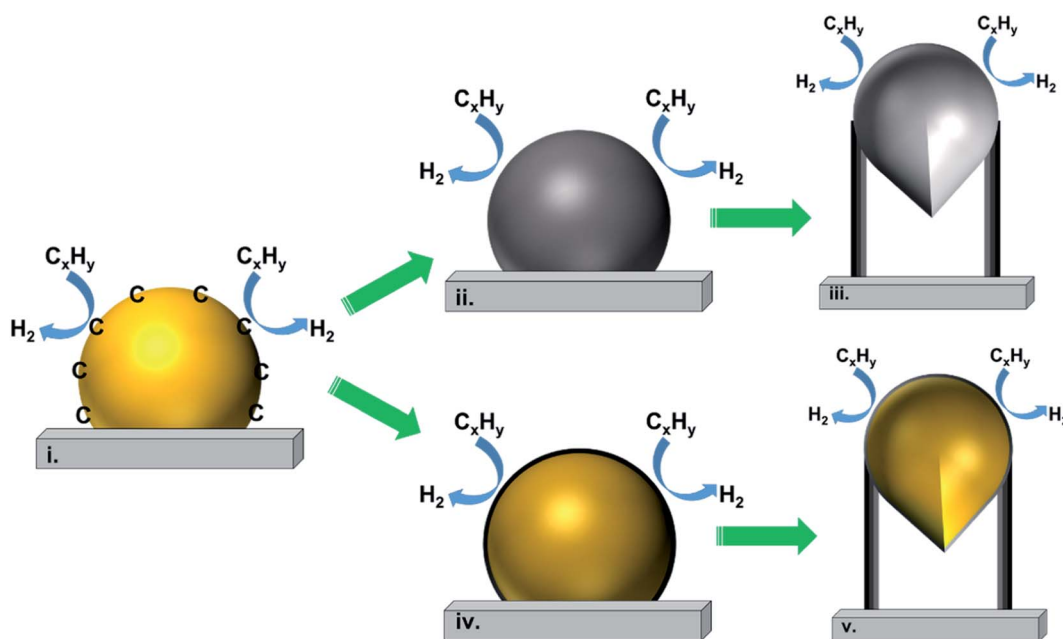

Fig. 3 The vapour–liquid–solid mechanism of carbon nanotube growth, which is reproduced from ref. 164 with permission from John Wiley and Sons.

dehydrogenation of acetylene, which is feasible for the synthesis of metal-free CNTs. The authors proposed a plausible CNT growth mechanism as C_2H_2 reacts with metallic liquid Na to produce Na_2C_2 where sodium carbide could have several stoichiometries, then Na_2C_2 decomposes in the presence of H_2 to produce metallic Na and a free C precursor. The graphitic structures of carbon will start assembling once free condensed C is present on the surface.

In 2020, Ashok et al.[170] proposed the growth mechanism of bamboo-like N-doped CNTs from the polymerization of melamine. The C atoms keep accumulating at the base of the NiCo–graphene interface, and more atoms are nucleated on the edge and bottom of the deformed particle with the formation of bamboo knots over the outer layer. A restoring cohesive force developed through an increase in the surface tension force and the compressive stress from the growth walls of the CNTs. This could provoke the catalytic particle to be released from the newly formed graphene layer, and the growth process is repeated to form a complete bamboo-like structure with multiple knots. The authors also mentioned that the growth mechanism of CNTs is specifically different from bamboo-like CNTs whose most favourable route is a chain of adsorption–decomposition–diffusion–nucleation. The nucleated carbon atoms that are excreted through the surface of the catalyst and form a multiple graphene layer that is in line with the diameter of the catalytic nanoparticle form MWCNTs.

4 Influence of waste feedstock on CNT and hydrogen production

It is known that both amorphous and filamentous carbons are formed during the catalytic conversion of carbonaceous feedstocks.[171] As the carbon deposition deactivates the catalyst and reduces the efficiency of thermo-chemical conversion of waste feedstock, enhancing the production of CNTs as well as reducing the production of amorphous carbon will add significant value to the process of hydrogen production from waste carbonaceous feedstocks.

The catalyst deactivation resulting from carbon formation on the surface of catalyst would decrease the efficiency of the catalytic process.[29,172] However, CNTs produced in the process of tyre gasification for hydrogen production can be regarded as a secondary product, instead of considering it as unwanted coke. It is therefore interesting to manipulate the gasification process e.g. using a catalyst to maximize the production of CNTs. Thus, the economic feasibility of hydrogen production would be effectively increased from waste hydrocarbons by thermo-chemical conversion.

Although the most common method to synthesise CNTs is via a CVD process from hydrocarbons like methane, benzene, xylene or other hydrocarbons,[173,174] waste hydrocarbons such as waste tyres, plastics and crude glycerol, with their high content of hydrocarbons also represent a potential feedstock for the production of CNTs. A large amount of publications have been reviewed by Bazargan[98] in relation to the synthesis of CNTs from waste plastics.

4.1 Waste tyres for CNT and hydrogen production

As tyres have high carbon and hydrogen contents,[81] the recovery of valuable products from tyres has been studied by many researchers.[6,29,31,81] Pyrolysis as a thermal degradation process to recover more valuable products from waste tyres has been investigated.[29,31] Recent works[50,175–178] have shown that under certain process conditions, carbon deposited on the surfaces of catalysts during pyrolysis catalysis of waste tyres is composed mainly of CNTs. Yang et al.[179] successfully used waste tyres as an alternative carbon source to produce CNTs by a CVD method over a cobalt-based catalyst. This indicated that there is potential for waste tyres to be used as carbon precursors to synthesise CNTs. Murr et al.[180] investigated a novel electric arc discharge method for the synthesis of MWCNTs from tyre powder. Poyraz et al.[181] produced CNTs from devulcanized ground tyre rubber particles. The short-term microwave irradiation devulcanization of ground tyre rubber was first carried out in a microwave for less than 4 min. The microwave-treated ground tyre rubber particles were coated with polypyrrole as a substrate to grow CNTs by a secondary microwave treatment. The successful growth of CNTs was confirmed by TGA, FTIR, SEM and TEM techniques.

4.2 Waste plastics for CNT and hydrogen production

Co-production of hydrogen and CNTs by pyrolysis-catalysis of plastics has become more attractive to researchers for simultaneously solving the plastic waste related issues and upcycling the waste to get value-added products.[182] Among all kinds of plastics, PE (LDPE and HDPE), PP, PS and their mixtures have displayed their superior potential to be used as feedstocks for the synthesis of carbon nanomaterials. Kukovitskii et al.[183] confirmed that crooked CNTs with 10–40 nm diameters were produced from polyethylene by pyrolysis at 420–450 °C and 4 atm in a quartz tube in the presence of a nickel plate catalyst in the early 90s. The CNT production rate could reach up to 200–300 mg h^{-1}. Recently, quite a few researchers have worked on the production of CNTs within a flexible pyrolysis-catalysis system at atmospheric pressure. Liu et al.[184] investigated the influence of temperature on MWCNTs and hydrogen-rich syngas production from polypropylene by a pyrolysis catalytic-reforming process. The two-stage reaction process involved polypropylene pyrolysis over a HZSM-5 zeolite catalyst in a crew kiln reactor and further catalysis of the pyrolysis vapour over a nickel-based catalyst in a moving-bed reactor. They found that 700 °C was the optimum temperature for MWCNT and hydrogen production. Recently, Jie et al.[185] also used waste plastics as the feedstock to produce hydrogen and MWCNTs but using a different technique of microwave-initiated catalytic deconstruction of plastic waste under 1000 W microwave irradiation.

4.3 Waste biomass (including bio-oil) for CNT and hydrogen production

Waste biomass is a biodegradable, eco-friendly resource, which is a low-cost, readily available, widely distributed, renewable carbon source with the ability to make renewable fuels and

high-value carbon materials.[12] Wang et al.[12] recently reviewed the technology of the preparation of CNTs from biomass in the last few decades and summarized the CNT production from biomass, together with the application of biomass as a catalyst and a catalyst support, which have been extensively investigated. The authors also pointed out the potential of the biomass-based carbon nano-material market.

He et al.[186] utilized the Ni/α-Al$_2$O$_3$ catalyst for catalytic reforming of biomass-derived organics (toluene, 1-methyl-naphthalene, phenol, ethanol, etc.). It was found that phenol and ethanol yielded a higher amount of hydrogen and CNTs than the other two organics, due to the enhancement of the oxygen functional group in phenol and ethanol. In addition, the lower molecular weight and the higher degree of saturation of organics stimulated CNT growth. Zhang et al.[187] prepared high-quality three-dimensional graphene foams by utilizing waste biomass pyrolysis gases. The resulting 3DGFs exhibited excellent performance in environmental and energy-storage applications. Nevertheless, considering the congenital characteristic of biomass that contains sufficient oxygen and strong chemical bonding, as well as multiple ash components, it is difficult to realize direct conversion from biomass to CNMs.

4.4 Crude glycerol for CNT and hydrogen production

Glycerol can be a potential feedstock for producing H$_2$, with a theoretical production ratio of glycerol/hydrogen of 1 : 4.[188,189] Comparing all the processes of glycerol production, the recovery of hydrogen from the glycerol reforming process is the most effective way to improve the utilization of glycerol.[190–192] Avasthi et al.[29] summarized that hydrogen production from glycerol could be a very good option because the amount of hydrogen produced from glycerol reforming processes was stoichiometrically higher than the hydrogen production from conventional methods e.g. methane reforming. At high temperatures, gasification of glycerol can produce H$_2$ and CO. The Fischer–Tropsch synthesis is a way to produce green biodiesel using syngas as the feedstock, at a H$_2$/CO ratio of around 2 : 1.[188,193] The gas produced from glycerol can be used to produce electricity because of the medium heating value.[188,194] Valliyappan et al.[195] produced syngas by pyrolysis of glycerol at atmospheric pressure and at different nitrogen flow rates and temperatures with different types or sizes of packing materials in the reactor. Simonetti et al.[196] focused on syngas production from glycerol by gas-phase reforming. They used carbon-supported platinum (Pt) and platinum–rhenium (Pt–Re) catalysts in the experiments and measured the rates of glycerol conversion and H$_2$/CO ratio by controlling the reaction conditions. The interaction of CO with the surface was decreased by the primary promotional effect of Re. Therefore, the coverage of CO decreased and the catalyst operated more effectively when the gaseous CO was presented. Peres et al.[197] found that the optimized output of converting glycerol to gas in their pyrolysis of glycerol (they used commercial glycerol with a purity of 99% in experiments) reached up to 80 wt%. The highest hydrogen concentration was up to 40%, and the highest CO concentration was up to 48%.

Similar to carbon deposition in waste tyre and plastic pyrolysis catalysis/catalytic reforming processes, coke formation on the surface of catalysts during hydrogen production from glycerol reforming processes is also a challenge which cannot be avoided. Efficiencies of the reforming process could be reduced dramatically due to catalyst deactivation. Therefore, it would reduce the heat transfer from gas to catalyst.[29,172] Ebshish et al.[172,198] reported that coke formation during their glycerol steam reforming process was due to the acidic properties of the catalyst support, which affected the glycerol conversion process including hydrogen production. Chiodo et al.[199] concluded that coke formation is mainly due to the large amounts of olefins that exist in the reaction streams. Investigations on how to convert coke to value-added products would increase the feasibility of glycerol reforming to such products.[27] Wu et al.[27] reported that 500 N m^3 hydrogen fuel produced from 1 tonne of glycerol through gas-phase catalytic reforming along with ∼2.8 kg CNT production could have a considerable impact on the economics of glycerol utilization. Charisiou et al.[200] also detected CNT formation through the glycerol steam reforming reaction. However, for future applications, this process needs further investigation because of the impurities contained in the crude glycerol which include spent and excess alkali metal catalysts, salts, excess methanol, fatty acids and esters.

5 Catalyst development for thermo-chemical conversion of carbonaceous wastes

5.1 Active metal types (monometallic type – Ni-, Fe-, and Co-based – and multi-metal based)

5.1.1 Non-noble transition metal-based catalysts. Transition metals are considered as efficient catalysts for the reforming of hydrocarbons.[201] Currently, Ni-, Fe-, Cu- and Co-based catalysts are normally used for the gasification of waste polymers.[7,116–119] Ni-based catalysts are most frequently used in the production of hydrogen by thermo-chemical processing of plastics and biomass, primarily because of their stability at high temperatures and high selectivity for hydrogen.[59,64,65,69] Acomb et al.[202] investigated different metal catalysts (Ni/Al$_2$O$_3$, Co/Al$_2$O$_3$, Cu/Al$_2$O$_3$ and Fe/Al$_2$O$_3$) for both hydrogen and CNT production from LDPE by a catalytic pyrolysis process at 800 °C. Except for the Cu-based catalyst, MWCNTs were successfully formed with the three other catalysts. Fe-based and Ni-based catalysts gave the highest amounts of CNT and hydrogen production due to the weaker metal–support interaction of Ni/Al$_2$O$_3$ and Fe/Al$_2$O$_3$ catalysts, and the interaction between the catalytic site and catalyst support was believed to be the key factor that affected CNT formation. The Fe/Al$_2$O$_3$ catalyst gave the highest CNT production due to its adequate metal–support interaction and larger carbon solubility of iron. The authors mentioned that purification processes would be necessary to separate CNTs from contaminants in future applications. Wu et al.[27] also pointed out that intensive work was required to separate CNTs from Ni–Mg–Al catalysts for end-use applications.

Ni-based catalysts are some of the most widely used catalysts in the catalytic reforming of tyres. Several Ni-based catalysts have been investigated by Elbaba et al.[50,175,177,178] to improve the production of hydrogen from waste tyres. They used a two-stage pyrolysis coupled with a catalytic steam reforming reactor in the presence of nickel catalysts to produce a syngas with a high content of hydrogen (65 vol%) from waste tyres.[178] The authors[50,178] reported that hydrogen production could be increased with a higher nickel content in catalysts. Zhang et al.[189,203–206] also used Ni-based catalysts to produce hydrogen and CNTs from waste tyres by catalytic pyrolysis/catalytic steam reforming. Ni-based catalysts are also the most common catalysts used in the glycerol reforming process.[207] Different catalyst supports have been investigated in steam reforming/catalytic-gasification processes. Adhikari et al.[208] considered that active catalysts for ethanol steam reforming could also be active in glycerol steam reforming. They used Ni-based catalysts in glycerol reforming experiments to produce hydrogen. The recent research they carried out on a crude glycerol conversion process showed that the maximum hydrogen production and purity of 68% could be achieved at 600 °C. Czernik et al.[209] investigated the glycerol steam reforming process in a fluidized-bed reactor by using a commercial Ni-based catalyst. The hydrogen production efficiency reached around 80% of the theoretical yield. Adhikari et al.[210] focused their research on the kinetics and reactor modelling of hydrogen production using Ni/MgO, Ni/TiO_2 and Ni/CeO_2 catalysts in a glycerol reforming process. They reported an activation energy of 103 kJ mol^{-1}. The surface area of the Ni/CeO_2 catalyst was the highest (67.0 m^2 g^{-1}) and therefore it gave the maximum hydrogen selectivity (74.7%) compared with the Ni/MgO and Ni/TiO_2 catalysts under same experimental conditions: 600 °C, a water to glycerol molar ratio of 12 : 1 and a feed flow rate of 0.5 ml min^{-1}.[210,211]

Alkali metals are effective for eliminating tar formation or upgrading the gaseous products formed in the thermo-chemical conversion of biomass, and the presence of alkali carbonates increased the carbon conversion to gases from biomass gasification processes.[212] Hauserman[213] investigated primary alkali catalysts for hydrogen production from wood gasification. The alkali catalyst from wood ash after gasification showed a high content of alkali metals (CaO, 44.3 wt%; MgO, 15 wt%; and K_2O, 14.5 wt%).

Although the Ni-based catalyst is effective in the catalytic conversion process, there is still room for development of the catalysts. As the current research indicates that when using Ni-based catalysts in the reforming process, efficiency mainly depends on the temperature of the reaction which needs to be at a minimum of 550 °C. An impregnation method was used by Buffoni et al.[214] to modify a catalyst by adding ZrO_2 and CeO_2 oxides onto a commercial α-Al_2O_3 support to boost the activity and stability of the Ni catalyst. The results proved that the modified Ni–Ce/α-Al_2O_3 catalyst could reduce the coke formation and was more stable in the reforming process. This is because the character of Ni/Ce restrains lateral dehydration, rearrangement and condensation reactions which result in coke formation with intermediate components.[214] A precipitation method was used by Zhang et al.[215] to prepare an M/CeO_2 (M =

2% Ir, 15% Co and 15% Ni in weight) catalyst. The conversions of glycerol to hydrogen achieved up to 85% at a temperature as low as 400 °C using the Ir/CeO_2 catalyst in the glycerol reforming process.[215] To achieve the same conversion efficiency using Co/CeO_2 and Ni/CeO_2 catalysts required temperatures of 425 and 450 °C, respectively.[172,215]

Modifications of the Ni-based catalysts by adding promoters have been investigated by researchers to improve the catalytic activity. Wu et al.[27] used Ni–Mg–Al catalysts for a glycerol pyrolysis/catalytic-gasification process. They found that the catalysts stayed effective after six hours of testing in terms of hydrogen production and the concentrations of gases. Iriondo et al.[216] investigated hydrogen production from a glycerol reforming process by using an alumina supported nickel-based catalyst modified with Mg, Zr, Ce, and La. They found that the addition of promoters to catalysts could promote hydrogen selectivity in the glycerol reforming process. The results showed that when Mg was used as a promoter in the catalyst, the improved surface area of the catalyst resulted in high hydrogen selectivity. Also, when Zr was used as a promoter in the catalyst, the capacity of activating steam increased. Higher catalyst stability was achieved when Ce and La were used as promoters. The conversion of glycerol could stay at 100% over 50 h when using a Ni/Al_2O_3–ZrO_2 catalyst.[172] Iriondo et al.[172,217] also investigated the possibility of improving the activity of an alumina supported Ni-based catalyst by adding intermediate amounts of La to the catalyst. Hao et al.[218] synthesised CNTs by using an Fe/Mo/Al_2O_3 catalyst in the catalytic pyrolysis of polypropylene in a nano-agglomerate fluidized bed reactor. The researchers[218] studied the formation of CNTs during this process including the initial fragmentation of the support of the catalyst, sub-agglomerate formation and the growth of CNTs which expanded the agglomerates. The CNT product yield was high when the agglomerates were fully developed. Ateyya A.[219] used a Fe–Mo/MgO catalyst with different Fe/Mo ratios for the catalytic pyrolysis of polyethylene waste to produce carbon nanomaterials. MWCNTs, CNFs and graphene nanosheets were detected individually, or as a binary or ternary mixture depending on the Fe/Mo ratio. Higher Fe or Mo ratios were found to be optimal for enhancing the growth of CNTs and CNFs.

Fe- and Ni-based bimetallic catalysts have also been investigated in waste plastic pyrolysis-catalysis processes.[203,220–224] He et al.[221] recently studied the effect of the addition of Fe to the Ni catalyst on CNT growth. The interaction in the Ni–Fe alloy promoted the generation of metal carbide for enhancing CNT growth and H_2 production. Yao et al.[220] investigated the effects of Ni : Fe molar ratios at 1 : 3, 1 : 2, 1 : 1, 2 : 1 and 3 : 1 on the production of hydrogen and CNTs from waste plastics in a two-stage pyrolysis-catalysis steam reforming process at 800 °C. The results showed that the ratio of Ni : Fe at 1 : 3 supported by γ-Al_2O_3 gave the highest H_2 yield of 84.72 mg g^{-1} plastic. Zhang et al.[203] also studied the effect of different Fe/Ni weight ratios (00 : 20, 05 : 15, 10 : 10, 05 : 15, and 20 : 00) on hydrogen production from waste plastics in a two-stage fixed bed reactor. The authors pointed out that the presence of Fe and Ni together on the MCM-41 supported catalysts produced a synergistic

enhancement of the total gas yield, especially for hydrogen production. The Fe : Ni weight ratio of 10 : 10 produced the highest gas yield of 95 wt% and the highest H_2 production of 46.1 mmol H_2 g^{-1} plastic. Yao et al.[224] co-produced hydrogen and CNTs from the steam gasification of real-world waste plastics (a mixture of disposable drink cups, lunch boxes and plastic wraps) over Fe/Ni supported Al_2O_3 catalysts, yielding 287 mg $g_{plastic}^{-1}$ of CNTs and 31.8 mmol $g_{plastic}^{-1}$ of H_2 for the bimetallic Ni–Fe/γ-Al_2O_3 catalyst at 800 °C in the absence of steam.

5.1.2 Noble metal-based catalysts. It has been reported that not only the transition metal-based catalysts but also noble metals such as Pt, Pd and Rh could also be used in the reforming process. However, noble metal-based catalysts will increase the cost of production from the reforming process.[172,207,215,225] Pt-based catalysts with various catalyst supports have been investigated to achieve the high catalytic activity and reduce the cost of catalysts. Soares and Simonetti et al.[192,196] found that a carbon-supported platinum (Pt/C) catalyst gave the best performance of glycerol reforming when compared to other Pt catalysts with different supports. The supported Pt catalysts consisting of Al_2O_3, ZrO_2, CeO_2/ZrO_2 and MgO/ZrO_2 were deactivated after glycerol conversion. On the other hand, the Pt/C catalyst showed much better stability and selectivity to H_2/CO at around 620 K. The Pt/Al_2O_3 catalyst was able to activate the reaction for certain periods and then was suddenly deactivated. However, the high catalytic activity of Pt/C catalysts required the temperature to be lower than 570 K. Also, considering that the Fischer–Tropsch synthesis of syngas from glycerol reforming to fuel required reaction temperatures between 470 and 550 K, Soares and Simonetti[192] found that a carbon-supported Pt–Re catalyst could be used in this temperature range. When the Pt/Re ratio was 1 : 1, it gave a better reaction stability, higher activity and selectivity of H_2/CO at the desired temperature. The authors prepared the carbon supported Pt–Re catalysts by the incipient wetness method, impregnating carbon black with aqueous solutions of $H_2PtCl_6\cdot6H_2O$ and $HReO_4$. The carbon support needed to be dried up for 12 hours at 373 K before impregnation. For every gram of support, 1.7 g of solvent was needed. After impregnation and drying at 403 K for 12 hours, catalyst preparation was done.[192,196] Slinn et al.[226] found that when using a Pt/Al_2O_3 catalyst in the glycerol reforming process, optimum hydrogen production could be achieved at 860 °C with a flow rate of 0.12 mol glycerol per min per kg catalyst and a steam to carbon (S/C) ratio of 2.5. The optimized hydrogen selectivity was 70% and the glycerol conversion to gas was 100%.

As Ni-based catalysts are some of the most widely used and effective catalysts in the catalytic conversion process, various kinds of noble metal-based catalysts have been investigated to compare the catalytic activities with the Ni/Al_2O_3 catalyst. Adhikari et al.[208] performed different experiments at 900 °C, with a water to glycerol molar ratio of 9 : 1 and a feed flow rate of 0.15 ml min^{-1} by using 14 different catalysts in a glycerol steam reforming process. These included Al_2O_3, Rh/Al_2O_3, Pt/Al_2O_3, Pd/Al_2O_3, Ir/Al_2O_3, Ru/Al_2O_3, Ni/Al_2O_3, Ce/Al_2O_3, Rh/Ce/Al_2O_3, Pt/Ce/Al_2O_3, Pd/Ce/Al_2O_3, Ir/Ce/Al_2O_3, Ru/Ce/Al_2O_3, and Ni/Ce/

Al_2O_3. The catalysts were prepared on 92% alumina ceramic foam monoliths, which contained 8% silica, by the wetness technique using nitrate and chlorate precursors. Among the 14 different catalysts, Ni/Al_2O_3 and Rh/CeO_2/Al_2O_3 resulted in the best H_2 selectivity and glycerol conversion. The results showed that the highest hydrogen selectivity of 80% was achieved by using Ni/Al_2O_3, and the H_2 selectivity realized using Rh/CeO_2/Al_2O_3 was 71%. They also found that the increase in the water/feedstock ratio led to an increase of H_2 selectivity and glycerol conversion. However, the efficiency of H_2 production from the glycerol conversion process was reduced because of the increase of energy needed for water evaporation. Sanchez et al.[225] found that the glycerol reforming efficiency could increase from 96.8% to 99.4% when the temperature was increased from 600 to 700 °C at 1 atm pressure and a 16 : 1 water/feedstock ratio using a Ni/Al_2O_3 catalyst (5.8 wt% Ni). The maximum glycerol conversion efficiency reached 99.7% at 650 °C and started to decrease at 600 °C over time. However, Chiodo et al.[199] found that a Rh/Al_2O_3 catalyst showed higher activity and better stability compared to a Ni/Al_2O_3 catalyst in hydrogen production from their glycerol steam reforming process.

Hirai et al.[227] found that H_2 selectivity could reach up to 90% in the glycerol steam reforming process with complete conversion at 600 °C by using a Ru/Y_2O_3 catalyst. Also, a Ru/Y_2O_3 catalyst with 3 wt% Ru loading was considered as a more durable catalyst for limiting deactivation of catalysts caused by carbon deposition in the glycerol steam reforming process. They reported that this catalyst demonstrated a very high activity in a prolonged experiment. In their experiments, Groups 8–10 metals were used to prepare the catalysts over Y_2O_3, ZrO_2, CeO_2, La_2O_3, SiO_2, MgO, and Al_2O_3 supports. The results showed that the order of catalyst activity was as follows: Ru ≈ Rh > Ni > Ir > Co > Pt > Pd > Fe. In addition, Kikuchi et al.[228] found the order of the activity of the catalyst on silica in steam reforming methane was as follows: Ru ≈ Rh > Ni > Ir > Pt ≈ Pd > Co ≈ Fe. Hirai et al.[227] summarized that active metals in steam reforming of methane also afforded high activity in the glycerol steam reforming process. Their results showed that Ru exhibited the highest H_2 yield at a reaction temperature of 600 °C. Although Al_2O_3 could be a favorable support for the steam reforming of hydrocarbons, Ru on an Al_2O_3 support gave the lowest conversion in the glycerol steam reforming process. The greater the CH_4 produced and the lower the CO_2 produced, the less the amount of H_2 was produced. So, the Ru/Y_2O_3 catalyst showed the best performance in the glycerol steam reforming process. The optimal Ru loading was attained at 500 °C. The results also showed that when the Ru loading increased, the H_2 yield increased until the Ru loading was up to 3 wt%. The further increase of Ru loading up to 5 wt% had no significant effect on the H_2 yield.[227]

Noble metals have also been added into the Ni-based catalysts as promoters to investigate the effects on the catalytic activity. Catalytic performances of Ni/CeO_2–Al_2O_3 catalysts were promoted by the addition of noble metals (Pt, Pd, Ru, Ir). The results showed that the modified catalyst with noble metals led to higher H_2 yields than the catalysts without noble metal promoters. The best result from their glycerol reforming

process was achieved when the Ni/Pt/CeO$_2$–Al$_2$O$_3$ catalyst was used at 700 °C.[229] Profeti et al.[229] found that a Ni/CeO$_2$–Al$_2$O$_3$ catalyst can be promoted by noble metals (Pt, Ir, Pd, and Ru) since the dispersed CeO$_2$ on alumina can prevent the formation of active nickel aluminate. The addition of noble metals could stabilize Ni sites in the reduced state in the reforming process, leading to a decrease in coke formation and an increase in glycerol conversion. In their experiments, a higher catalytic performance together with the highest H$_2$ yield and a lower CO yield was achieved by using the Ni/Pt catalyst. Ni/CeO$_2$–Al$_2$O$_3$ catalysts were prepared by a sequential impregnation method. The first step was to incorporate CeO$_2$ on γ-Al$_2$O$_3$ using the incipient wetness method. An aqueous solution of Ce(NO$_3$)$_2$ prepared in a rotary evaporator at 60 °C was also required. For the removal of adsorbed contaminants, the γ-Al$_2$O$_3$ pellets needed to be sieved to 80–100 mesh particles and treated at 550 °C for three hours under the synthetic flow. The sample was calcined at 550 °C for 3 hours under a 20 cm^3 min^{-1} airflow after drying at 80 °C for 10 hours. Then, Ni was incorporated on the CeO$_2$–Al$_2$O$_3$ support by using the incipient wetness method with an aqueous solution of Ce(NO$_3$)$_2$·6H$_2$O. Finally, the catalysts were obtained by calcination at 550 °C for three hours and drying at 80 °C for 10 hours. Cui et al.[230] investigated the performance of a La$_{1-x}$Ce$_x$NiO$_3$ catalyst in the glycerol steam reforming process by comparing its catalytic activity with that of a Pt metal catalyst. They found that Ni can be easily reduced in the La$_{0.3}$Ce$_{0.7}$NiO$_3$ structure. The results were calculated by a non-stoichiometric method and compared with the thermodynamic equilibrium. The result showed that the catalyst had the highest activity in the glycerol steam reforming process. The glycerol conversion efficiency was close to the thermodynamic equilibrium when the temperature was in the range of 500 to 700 °C. The minimum carbon formation on the surface of the catalyst was achieved by using the La$_{0.3}$Ce$_{0.7}$NiO$_3$ catalyst.[172]

5.2 Catalyst supports (artificial – Al-, Si, Si–Al, and activated carbon – and natural-based supports)

Alumina support has been applied widely in many reactions and considered to be the most effective support for catalysts. Mirodatos et al.[145] found that Ni/Al$_2$O$_3$ catalysts demonstrated the highest amount of carbon deposition in the methanation reaction compared to Ni/SiO$_2$ catalysts. Ni/Al$_2$O$_3$ catalysts presented the highest catalytic stability in reforming processes. A similar situation occurred in the reforming of methane using Ni/Al$_2$O$_3$ and Ru/Al$_2$O$_3$ catalysts carried out by Zhang et al.[146] and Slagtern et al.[231]

There are also some other common catalyst supports which have been used in hydrocarbon reforming processes to obtain hydrogen, such as γ/α-Al$_2$O$_3$, MgO, MgAl$_2$O$_4$, SiO$_2$, ZrO$_2$, CeO$_2$ and TiO$_2$.[232] Adhikari et al.[210] found that hydrogen production from glycerol reforming reached a maximum of 56.5% using a Ni/MgO catalyst and compared it with that from Ni/TiO$_2$ and Ni/CeO$_2$ catalysts at 650 °C and 1 atm.[233] The catalysts were prepared using Ni(NO$_3$)$_2$·6H$_2$O over three supports including MgO, TiO$_2$ and CeO$_2$, by the wet impregnation method. The

same content of Ni loading (15 wt%) was used in all prepared catalysts. All catalysts were dried at 110 °C for 12 hours and then calcined at 500 °C in air for 6 hours. The final step was to sieve the catalyst using sieves with 16–35 mesh sizes. Dou et al.[198] used a commercial Ni-based catalyst and dolomite sorbent in the glycerol conversion process. CO$_2$ removal progressed simultaneously with hydrogen production from the glycerol conversion process. The results showed that the optimum temperature for the reactions was around 500 °C. Rossetti et al.[234] prepared Ni-based catalysts supported on TiO$_2$, ZrO$_2$ and SiO$_2$ by synthesizing supports in a liquid phase. These were followed by impregnation with the active phase and calcination at 800 °C. The metal–support interaction and surface acidity are the most important parameters for assessing catalysts. The metal–support interaction strongly depends on the catalyst preparation procedure. If the metal–support interaction is stronger, the activity and the stability of catalysts will be relatively higher. The surface acidity of catalysts can be modified using different catalyst supports.

Different catalyst supports also have an effect on the performance of a catalyst through the interaction of the active metal with the support, surface area and porosity of the support material, among others. Miyazawa et al.[235] investigated the performance of nickel catalysts on various supports for steam reforming of tars derived from biomass pyrolysis. Ni/Al$_2$O$_3$, Ni/ZrO$_2$, Ni/TiO$_2$, Ni/CeO$_2$ and Ni/MgO catalysts were studied. The Ni–Al$_2$O$_3$ catalyst was reported as the most active one and the Ni–MgO catalyst showed the lowest activity in relation to hydrogen production. It was suggested that the type of support influenced the nickel metal particle size, which was key to the catalyst activity. Inaba et al.[236] investigated Ni/SiO$_2$, Ni–ZrO$_2$, Ni–CeO$_2$ and a series of Ni-zeolites for hydrogen production from the gasification of cellulose. The production of hydrogen followed the order Ni/SiO$_2$ > Ni/ZrO$_2$ > Ni/CeO$_2$. The production of hydrogen using the Ni-zeolites depended on the type of zeolite. Wu and Williams[59] used a two-stage pyrolysis-catalytic steam reforming process to produce hydrogen from polypropylene using various substrate supports with nickel, including Ni/Al$_2$O$_3$, Ni/MgO, Ni/CeO$_2$ and Ni/ZSM-5. The ZSM-5 zeolite performed as a relatively good support for the Ni-based catalyst with a high rate of hydrogen production; this could be due to the high surface area compared with other catalysts. He et al.[237] synthesized CNTs through toluene steam reforming with Ni/γ-Al$_2$O$_3$ and Ni/α-Al$_2$O$_3$ catalysts. They reported that the strong interaction between Ni particles and γ-Al$_2$O$_3$ led to the base-growth mechanism of CNTs that the active sites of Ni-based catalyst will be covered. In contrast, the Ni/α-Al$_2$O$_3$ catalyst with a weaker interaction would lead to the tip-growth mechanism that would increase the Ni dispersion and promote the reforming reaction. Similar results were also reported by Yao et al.[224] in the co-production of hydrogen and carbon nanotubes from real-world waste plastics in a fixed-bed reactor.

MCM-41 is a mesoporous material with a high surface area (up to 1000 m^2 g^{-1}), pore diameters of ∼2–10 nm and a flexible structure of amorphous silica walls.[238] It has been used as a catalyst for hydrogen production, Wu et al.[238] investigated Ni on a MCM-41 support for H$_2$ production from biomass and

Table 1 Summary of different catalysts used in the thermo-chemical conversion of the carbonaceous waste process

Catalysts	Active content	Precursors	Catalyst synthesis method	Feedstock	Reaction conditions	Reactor
Ni-based	—	—	C11-NK, a commercial nickel-based naphtha reforming catalyst	Pine sawdust derived bio-oil, crude glycerine, trap grease	750–850 °C	Bench-scale bubbling fluidized-bed[209]
Ni-Mg-Al	Molar ratio 1 : 1 : 1	$Ni(NO_3) \cdot 6H_2O$, $Al(NO_3)_3 \cdot 9H_2O$, $Mg(NO_3)_2 \cdot 6H_2O$	Co-precipitation	Plastics (PP, PS and HDPE); waste tyres (natural rubber styrene–butadiene rubber and polybutadiene rubber); crude glycerol	800–850 °C	Two-stage fixed-bed[38,59,64,171,178]
Ni-Al	Molar ratio 1 : 2	$Ni(NO_3)_2 \cdot 6H_2O$, $Al(NO_3)_3 \cdot 9H_2O$	Precipitation	PP	800 °C	Two-stage fixed-bed[59]
Ni/CaO	17 wt%	$Ni(NO_3)_2 \cdot 6H_2O$, CaO	Impregnation	Methane	550–750 °C	Fixed-bed[146]
Ni/CaO/C		$Ni(NO_3)_2 \cdot 6H_2O$, CaO, activated carbon	Impregnation, increasing pH and sol–gel	LDPE + pine sawdust	800 °C	Two-stage fixed-bed[63]
Ni/MgO	9.62–15 wt%	$Ni(NO_3)_2 \cdot 6H_2O$; MgO	Incipient wetness	PP, glycerol, wood-derived tar	500–800 °C	Two-stage fixed-bed;[59] tubular furnace;[211,233] laboratory-scale continuous feeding dual-bed reactor[235]
Ni/zeolites	7.5–10 wt%	$Ni(NO_3)_2 \cdot 6H_2O$; H-β (27); H-mordenite (18.3); Na-mordenite (18.3); H-ZSM-5 (29); Na-ZSM-5 (29); USY (14); Na–Y (5.7); ZY-5.2; ZY-30; ZY-80 Ni/chabazite; ZSM5-30; ZSM5-50; ZSM5-80; β-zeolite-25; Y-zeolite-30 (the numbers in parentheses denote Si/Al₂ ratios)	Impregnation	Cellulose, naphthalene, HDPE	500–800 °C	Fixed-bed;[236] two-stage fixed-bed;[240] clear fused quartz compression tube[248]
Ni/ZSM-5	10 wt%	$Ni(NO_3)_2 \cdot 6H_2O$; ZSM-5	Incipient wetness	PP	800 °C	Two-stage fixed-bed[59]
Ni/MCM-41	5–20 wt%	$Ni(NO_3)_2 \cdot 6H_2O$; MCM-41	Impregnation	Wood, cellulose	200–800 °C	Two-stage fixed-bed;[238] TGA-MS[239]
Ni/CeO₂	10–15 wt%	$Ni(NO_3)_2 \cdot 6H_2O$; CeO₂	Incipient wetness/impregnation; deposition–precipitation	PP, glycerol, ethanol	250–800 °C	Two-stage fixed-bed,[59] fixed-bed,[210,225] tubular reactor;[210,211,233] fixed-bed quartz micro-reactor;[215] laboratory-scale continuous feeding dual-bed reactor[235]
Ni/Al₂O₃	2–30 wt%; 18% NiO				200–900 °C; N₂	

Table 1 (Contd.)

Catalysts	Active content	Precursors	Catalyst synthesis method	Feedstock	Reaction conditions	Reactor
		Ni(NO$_3$)$_2$·6H$_2$O; α/γ-Al$_2$O$_3$; Al$_2$O$_3$ ceramic foam monoliths (92% Al$_2$O$_3$ and 8% SiO$_2$)	Incipient wetness/impregnation; commercial catalyst (Ni-3288 Engelhard)	PP, LDPE, toluene, cellulose, glycerol waste tyres, styrene–butadiene rubber, butadiene rubber and natural rubber, tyre oil, methane, wood derived tar		Two-stage fixed-bed;[59,175,177,202,205] fixed-bed;[68,146,198,214,225] conventional autoclave with a magnetic stirrer;[69] tubular furnace;[208,225] fixed-bed linear quartz micro-reactor;[199] laboratory-scale continuous feeding dual-bed reactor;[235] TGA-MS;[239] packed bed reactor[248]
Ni/CeO$_2$–Al$_2$O$_3$	Ni 2–20 wt%, NiO 16 wt%, CeO$_2$ 0–30 wt%	Ni(NO$_3$)$_2$·6H$_2$O, Ce(NO$_3$)$_3$·6H$_2$O, γ-Al$_2$O$_3$, Ce(NO$_3$)$_2$	Co-impregnation; incipient wetness/impregnation; sequential impregnation	PP, waste tyres, glycerol	450–900 °C	Two-stage fixed-bed;[50,59] fixed-bed;[214,216,225,229] tubular furnace[208]
Ni-Pt/CeO$_2$–Al$_2$O$_3$	Ni 5 wt%, Pt 0.3 wt%, CeO$_2$ 10 wt%	Ni(NO$_3$)$_2$·6H$_2$O, Ce(NO$_3$)$_2$; γ-Al$_2$O$_3$, H$_2$PtCl$_6$·2H$_2$O	Sequential impregnation	Glycerol	450–600 °C	Fixed-bed[229]
Ni-Ir/CeO$_2$–Al$_2$O$_3$	Ni 5 wt%, Ir 0.3 wt%, CeO$_2$ 10 wt%	Ni(NO$_3$)$_2$·6H$_2$O, Ce(NO$_3$)$_2$; γ-Al$_2$O$_3$, IrCl$_4$·xH$_2$O	Sequential impregnation	Glycerol	450–600 °C	Fixed-bed[229]
Ni-Pd/CeO$_2$–Al$_2$O$_3$	Ni 5 wt%, Pd 0.3 wt%, CeO$_2$ 10 wt%	Ni(NO$_3$)$_2$·6H$_2$O, Ce(NO$_3$)$_2$; γ-Al$_2$O$_3$, PdCl$_2$	Sequential impregnation	Glycerol	450–600 °C	Fixed-bed[229]
Ni-Ru/CeO$_2$–Al$_2$O$_3$	Ni 5 wt%, Ru 0.3 wt%, CeO$_2$ 10 wt%	Ni(NO$_3$)$_2$·6H$_2$O, Ce(NO$_3$)$_2$; γ-Al$_2$O$_3$, RuCl$_3$·H$_2$O	Sequential impregnation	Glycerol	450–600 °C	Fixed-bed[229]
Ni/natural olivine	2.8 wt%	Ni(NO$_3$)$_2$·6H$_2$O; (Mg$_{0.92}$Fe$_{0.08}$)$_2$SiO$_4$	Impregnation	Methane	600–850 °C; steam or CO$_2$	Fixed-bed[249]
Ni/dolomite	5–20 wt%	Ni(NO$_3$)$_2$·6H$_2$O; (NH$_4$)$_2$CO$_3$; dolomite	Impregnation	Toluene, waste tyres	550–800 °C	Fixed-bed;[68] two-stage fixed-bed[176,177]
Ni/SiO$_2$	8.9 wt%	Ni(NO$_3$)$_2$·6H$_2$O; H$_4$Si	Impregnation	Glycerol	650–700 °C	Fixed bed[234]
Ni/SiO$_2$–Al$_2$O$_3$	5–20 wt%, Al$_2$O$_3$ to SiO$_2$ mole ratios (3 : 5, 1 : 1, 3 : 2, 2 : 1)	Ni(NO$_3$)$_2$·6H$_2$O; SiO$_2$–Al$_2$O$_3$, C$_9$H$_{21}$O$_3$Al; SiO$_2$	Impregnation, sol–gel	Toluene, waste tyres	550–800 °C	Fix-bed;[68] two-stage fixed-bed[250]
Ni/ZrO$_2$	8.8–15 wt%	Ni(NO$_3$)$_2$·6H$_2$O; ZrOCl$_2$·8H$_2$O; ZrO$_2$	Precipitation, impregnation	Glycerol, wood-derived tar	500–700 °C	Fixed-bed;[234,251] laboratory-scale continuous feeding dual-bed reactor[235]
Ni/ZrO$_2$/Al$_2$O$_3$	Ni 2 wt%, NiO 17 wt%, ZrO$_2$ 7 wt%	Ni(NO$_3$)$_2$·6H$_2$O; Zr(NO$_3$)$_4$·5H$_2$O; γ-Al$_2$O$_3$	Impregnation	Glycerol	600–850 °C	Fixed-bed[214,216]
Ni/La$_2$O$_3$ Ni/La$_2$O$_3$/Al$_2$O$_3$	3–17 wt%	Ni(NO$_3$)$_2$·6H$_2$O; La$_2$O$_3$	Impregnation	Methane Glycerol	550–750 °C 500–600 °C	Fixed-bed[146] Fixed-bed[216,217]

Table 1 (*Contd.*)

Catalysts	Active content	Precursors	Catalyst synthesis method	Feedstock	Reaction conditions	Reactor
	Ni 16 wt%, NiO 17 wt%, La$_2$O$_3$ 3–15 wt%	Ni(NO$_3$)$_2$·6H$_2$O; La(NO$_3$)$_3$·6H$_2$O; CeO$_2$; γ-Al$_2$O$_3$	Impregnation/co-impregnation	Glycerol	600 °C	Fixed-bed[216]
Ni/MgO/Al$_2$O$_3$	NiO 16.2 wt%, MgO 2.5 wt%	Ni(NO$_3$)$_2$·6H$_2$O; Mg(NO$_3$)$_2$·6H$_2$O; γ-Al$_2$O$_3$	Impregnation	Cellulose	200–350 °C	Conventional autoclave with a magnetic stirrer[69]
Na$_2$CO$_3$	—	Sodium carbonate	Commercial catalysts			
Ir/CeO$_2$	2 wt%	H$_2$Ir$_4$Cl$_6$·6H$_2$O; CeO$_2$	Deposition–precipitation	Ethanol, glycerol	250–600 °C	Fixed-bed quartz micro-reactor[215]
Ir/Al$_2$O$_3$	2.5%	H$_2$Cl$_6$Ir; Al$_2$O$_3$	Incipient wetness	Glycerine	600–900 °C	Tubular furnace[208]
Ir/Ce/Al$_2$O$_3$	2.5%	H$_2$Cl$_6$Ir; Ce(NO$_3$)$_3$·6H$_2$O; Al$_2$O$_3$	Incipient wetness	Glycerine	600–900 °C	Tubular furnace[208]
Ce/Al$_2$O$_3$	2.5%	Ce(NO$_3$)$_3$·6H$_2$O; Al$_2$O$_3$	Incipient wetness	Glycerine	600–900 °C	Tubular furnace[208]
Ce/zeolites	5–30 wt%	Ce(NO$_3$)$_3$·6H$_2$O	Impregnation	Cellulose	500–600 °C	Fixed-bed[236]
Co/CeO$_2$	15 wt%	Co(OAc)·4H$_2$O; CeO$_2$	Deposition–precipitation	Ethanol, glycerol	250–600 °C	Fixed-bed quartz micro-reactor[215]
Rh/Al$_2$O$_3$	2.5–5%	Rh(NO$_3$)$_3$; Al$_2$O$_3$	Incipient wetness	Glycerine	600–900 °C	Tubular furnace;[208] fixed-bed linear quartz micro-reactor[199]
Rh/SiO$_2$	30 wt%	HN$_4$O$_{10}$Ru; SiO$_2$	Impregnation	Cellulose	500–600 °C	Fixed-bed[236]
Rh/Ce/Al$_2$O$_3$	2.5%	Rh(NO$_3$)$_3$; Ce(NO$_3$)$_3$·6H$_2$O; Al$_2$O$_3$	Incipient wetness	Glycerine	600–900 °C	Tubular furnace[208]
Rh/Ce/SiO$_2$	Rh 2 wt%, Ce 30 wt%	C$_{15}$H$_{21}$O$_6$Rh, SiO$_2$; Ce(NO$_3$)$_3$·6H$_2$O	Impregnation	Cellulose	500–600 °C	Fixed-bed[236]
Ru/Al$_2$O$_3$	2.5%	HN$_4$O$_{10}$Ru; Al$_2$O$_3$	Incipient wetness	Glycerine	600–900 °C	Tubular furnace[208]
Ru/Y$_2$O$_3$	3 wt%	—	Impregnation	Glycerol	600 °C	Fixed-bed flow type reactor[227]
Ru/Ce/Al$_2$O$_3$	2.5%	HN$_4$O$_{10}$Ru; Ce(NO$_3$)$_3$·6H$_2$O; Al$_2$O$_3$	Incipient wetness	Glycerine	600–900 °C	Tubular furnace[208]
Pt/Al$_2$O$_3$	2.5%	H$_2$PtCl$_6$, Al$_2$O$_3$; [Pt(NH$_3$)]$_4$(NO$_3$)	Incipient wetness	Glycerine	600–900 °C; 225–300 °C	Tubular furnace;[208] tubular stainless steel reactor[192]
Pt/Ce/Al$_2$O$_3$	2.5%	H$_2$PtCl$_6$; Ce(NO$_3$)$_3$·6H$_2$O; Al$_2$O$_3$	Incipient wetness	Glycerine	600–900 °C	Tubular furnace[208]
Pt–Ni/La$_2$O$_3$/Al$_2$O$_3$	Pt 2 wt%, NiO 2.5–12.6 wt%, 6 wt% La$_2$O$_3$	Ni(NO$_3$)$_2$·6H$_2$O; La(NO$_3$)$_3$·6H$_2$O; CeO$_2$; γ-Al$_2$O$_3$	Consecutive wet impregnation	Glycerol	500–600 °C	Fixed-bed[217]
Pd/Al$_2$O$_3$	2.5%	Pd(NO$_3$)$_2$; Al$_2$O$_3$	Incipient wetness	Glycerine	600–900 °C	Tubular furnace[208]
Pd/Ce/Al$_2$O$_3$	2.5%	Pd(NO$_3$)$_2$; Ce(NO$_3$)$_3$·6H$_2$O; Al$_2$O$_3$	Incipient wetness	Glycerine	600–900 °C	Tubular furnace[208]
Pt–Re/C	5.6 wt% (Pt : Re 1 : 1, 10 : 1 and 1 : 2)	H$_2$PtCl$_6$·6H$_2$OH; ReO$_4$; carbon black; HReO$_4$	Incipient wetness impregnation	Glycerol	700 °C	Fixed-bed[196]
Pt/C	5 wt%	—	Commercial catalysts from E-TEK	Glycerol	225–300 °C	Tubular stainless steel reactor[192]

Table 1 (Contd.)

Catalysts	Active content	Precursors	Catalyst synthesis method	Feedstock	Reaction conditions	Reactor
Pt–Ru/C	—	—	Commercial catalysts from E-TEK	Glycerol	225–300 °C	Tubular stainless steel reactor[192]
Pt/ZrO$_2$	—	H$_2$PtCl$_6$; ZrO(NO$_3$)$_2$·xH$_2$O	Incipient wetness impregnation	Glycerol	225–300 °C	Tubular stainless steel reactor[192]
Pt/CeO$_2$/ZrO$_2$	—	H$_2$PtCl$_6$; (NH$_4$)$_2$Ce(NO$_3$)$_6$; ZrO(NO$_3$)$_2$·xH$_2$O	Incipient wetness impregnation; co-precipitation	Glycerol	225–300 °C	Tubular stainless steel reactor[192]
Pt/MgO/ZrO$_2$	—	[Pt(NH$_3$)$_4$](NO$_3$)$_2$; Mg(NO$_3$)$_2$·6H$_2$O; ZrO(NO$_3$)$_2$·xH$_2$O	Incipient wetness impregnation; co-precipitation	Glycerol	225–300 °C	Tubular stainless steel reactor[192]
Fe-based	99.99 wt%	—	Commercial iron powder from Johnson Matthey	Ethylene	600 °C	Tube reactor[103]
Fe/Al$_2$O$_3$	10 wt%	Fe(NO$_3$)$_3$·9H$_2$O; γ-Al$_2$O$_3$	Impregnation	Tyre, LDPE	800 °C	Two-stage fixed-bed reactor[189,202]
Fe/Ni/MCM-41	Total 20 wt%, Fe/Ni ratios (00 : 20, 05 : 15, 10 : 10, 15 : 05, 20 : 00)	Fe(NO$_3$)$_3$·9H$_2$O; Ni(NO$_3$)$_2$·6H$_2$O; MCM-41	Impregnation	Simulated waste plastics	800 °C	Two-stage fixed-bed reactor[252]
Fe/Ni/Al$_2$O$_3$	10 wt%, molar ratio of Ni : Fe at (1 : 3, 1 : 2, 1 : 1, 2 : 1 and 3 : 1)	Ni(NO$_3$)$_3$·6H$_2$O; Fe(NO$_3$)$_3$·9H$_2$O; α/γ-Al$_2$O$_3$	Impregnation	Simulated waste plastics, real-world waste plastics	800 °C	Two-stage fixed-bed reactor[203,220–224]
Co/Al$_2$O$_3$	10 wt%	Co(NO$_3$)$_2$·6H$_2$O; γ-Al$_2$O$_3$	Impregnation	Tyre, LDPE	800 °C	Two-stage fixed-bed reactor[189,202]
Cu/Al$_2$O$_3$	10 wt%	Cu(NO$_3$)$_2$·3H$_2$O; γ-Al$_2$O$_3$	Impregnation	Tyre, LDPE	800 °C	Two-stage fixed-bed reactor[189,202]

Zhao et al.[239] compared Ni–Al$_2$O$_3$ and Ni/MCM-41 for hydrogen production from cellulose. Zhao et al.[239] reported that the highly ordered mesoporous structure of an MCM-41 support improved the dispersion of active nickel particles and subsequently increased the interaction between the nickel sites and gaseous products. However, few studies have investigated the production of H$_2$ from waste plastics using Ni/MCM-41 or the role of the addition of metal promoters such as Fe- to Ni-catalysts. Yao et al.[240] investigated a series of zeolite supported Ni-based catalysts (Ni/ZSM5-30, Ni/β-zeolite-25 and Ni/Y-zeolite-30) for the catalytic steam reforming of polyethylene process with a two-stage pyrolysis-catalytic steam reforming reactor. The authors found the ranking of syngas selectivity of each catalyst as Ni/ZSM5-30 > Ni/β-zeolite-25 > Ni/Y-zeolite-30 catalyst. In addition, the Ni/ZSM-5 catalyst showed excellent coke resistance and thermal stability.

5.3 Discussion of catalyst development for thermo-chemical conversion of carbonaceous waste

Catalysts play an important role in the waste hydrocarbon pyrolysis-catalysis/catalytic gasification process/thermo-chemical conversion processes. A comprehensive table and a summarized figure about different catalysts have been reviewed in the thermo-chemical conversion process and are shown in Table 1 and Fig. 4, respectively. The most common catalysts used in this process are transition metals-based catalysts like Ni-, Co-, Cu- and Fe-based catalysts. Noble metal-based catalysts, such as Rh, Pt, Pd, Ir, Ru and Ce also promote the catalysis or reforming process. However, the cost of noble metals is considerable, and as such, noble metal-based catalysts could not be commercialized for the large-scale production, for thermo-chemical conversion of waste feedstock.

Catalyst supports also affect the process and play an important role in terms of hydrogen selectivity and catalyst stability because of their basic characteristics and redox properties.[241] The most commonly used catalyst supports are alumina, zeolite and silica. Catalyst synthesis methods are also very important which mainly include incipient wetness impregnation, precipitation and sol–gel. Although the impregnation is the most used method, the reported sol–gel method could significantly improve the catalyst porosity and nickel dispersion, which leads to the highest activity among the catalysts prepared by impregnation and co-precipitation.[242]

In addition, a fixed-bed reactor is the most typical reactor used in thermo-chemical conversion, which also has been modified and renamed as two-stage fixed-bed, tubular reactor, clear fused quartz compression tube, fixed-bed quartz micro-reactor, fixed-bed linear quartz micro-reactor, packed-bed reactor, fixed-bed quartz micro-reactor and tubular stainless steel reactor. There are also other types of reactors, such as bench-scale bubbling fluidized-bed, laboratory-scale continuous feeding dual-bed reactor, conventional autoclave with a magnetic stirrer and TGA-MS. Kikuchi et al.[228] summarized a table about the types and methods of gasification and smelting processes for a semi-pilot scale test for hydrogen-rich fuel gas produced from different wastes. Muhammad et al.[243] reviewed different pyrolysis techniques for synthesizing carbon nanomaterials.[228] Williams[33] recently reviewed the specific reactor designs for hydrogen production from waste plastics.
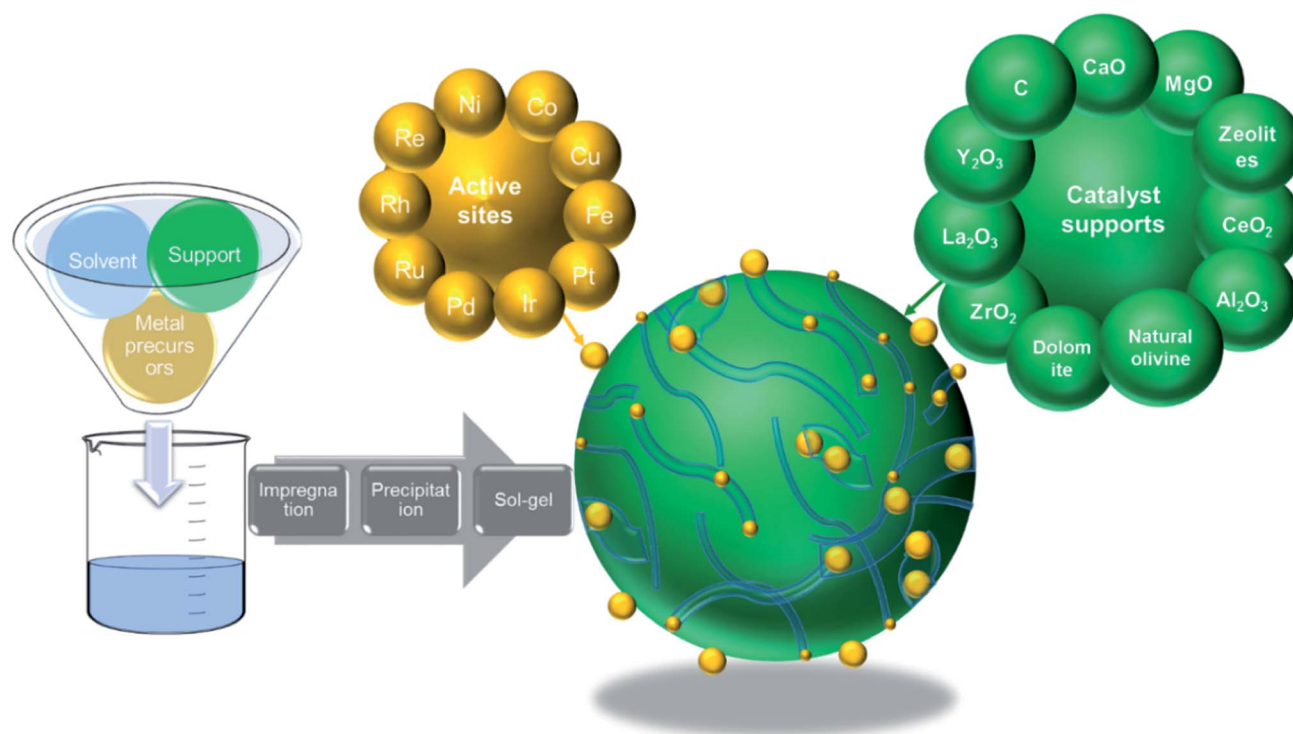

Fig. 4 A summary of how reviewed catalyst materials have been applied in catalytic conversion processes.

So, the types of reactors of pyrolysis techniques are not included in this review.

Catalyst deactivation resulting from coke formation on the surface of the catalyst is one of the challenges in hydrogen production from tyre gasification.[235,244–247] Catalyst deactivation is also affected by sulphur poisoning. Elbaba et al.[50] found that the deactivation of a Ni/Al$_2$O$_3$ catalyst in gasification of a waste tyre for hydrogen production was due to sulphur poisoning and carbon deposition. It was noted that there were different forms of carbons generated in the process, including amorphous carbon and graphite carbons, for instance, CNTs. Giannakeas et al.[248] found the evidence from X-ray diffraction results regarding the deposition of carbons on the surfaces of reacted catalysts, which caused catalyst deactivation in waste tyre reforming.

6 Evaluation of process parameters on CNT and hydrogen production from thermo-chemical conversion of carbonaceous waste

6.1 Process conditions for thermo-chemical conversion of carbonaceous wastes

Pyrolysis of waste tyres can be influenced by process conditions including the type of raw material, sample size, residence time, temperature and feeding rate that have been studied by many researchers.[47,51,190,253–255] Dai et al.[46] investigated the pyrolysis temperatures, residence times and particle sizes of samples by using a circulating fluidized-bed reactor in which pyrolysis and secondary reactions occurred. They reported that secondary reactions were favored by a longer residence time, and carbonization is favored at lower temperature and heating rates. Gas product yields increased with the increment of temperature from 400 to 800 °C. The yields of CH$_4$, H$_2$ and CO were also increased with the increment of temperature. However, the yields of CO$_2$ and heavier hydrocarbon gases decreased. As the residence time increased, the production of syngas and light hydrocarbon increased, while CO$_2$ production decreased. This is because the enhanced secondary reactions, such as further cracking of heavy pyrolysis oils, char reduction and shift reactions. The temperature and residence time played predominant roles in the production of gas and tar/oil. Furthermore, the particle size of feedstock showed only a slight influence on gaseous production.

Aylón et al.[48] carried out tyre pyrolysis using a moving-bed reactor at different temperatures (600, 700 and 800 °C). The yield of pyrolysis oil decreased dramatically from 41.5 to 27.5 wt% as the temperature increased from 600 to 800 °C. However, gaseous production significantly increased from 17.9 to 31.5 wt%. The reason for the promoted tar cracking reactions at higher temperatures was due to the enhanced primary cracking of heavy hydrocarbons. Cunliffe and Williams[255] investigated the temperature and chemical class fractions of tyre pyrolysis oil using a fixed-bed reactor. They found a clear increase of the aromatic fraction from 36.7 to 45.6 wt% and a decrease of the aliphatic fraction from 51.3 to 36.1 wt% as the temperature

increased from 450 to 600 °C. They also pointed out that the extended residence time of pyrolysis gases in the reactor could increase the fraction of aromatic compounds. Kyari et al.[253] compared pyrolysis products from seven different types of tyres (countries of origin: Poland, Korea, Japan, South Africa, Italy and Great Britain) also with a fixed-bed reactor to investigate the influence of tyre origin on the yields of pyrolysis products. They found that the yields of gases, chars and oil products were not significantly affected by the type of tyres. However, the composition of the pyrolysis gas and pyrolysis oil varied between different tyres. Leung et al.[51] studied the influence of operational parameters (equivalence ratio, tyre feed rate, temperatures and particle sizes) on hydrogen production from waste tyre gasification using a tubular reactor. They concluded that the yield of gaseous product was proportional to the equivalence ratio, tyre feed rate and tyre particle size. The yield of char decreased slightly when the equivalence ratio, feed rate or particle size increased. The yield of oil reduced considerably with the increase of the equivalence ratio and tyre feeding rate. The gaseous products were mainly H$_2$, CO, CO$_2$, H$_2$S and other light hydrocarbons (C$_2$–C$_4$), with relatively high heating values ranging between 20 and 37 MJ m^{-3}. Rodriguez et al.[254] used an unstirred stainless steel 0.0035 m^3 autoclave to run tyre pyrolysis experiments at temperatures in the range of 300 to 700 °C with 100 °C intervals. They found that the pyrolysis temperature significantly affected the gas production in the waste tyre pyrolysis process, and the highest temperature of 700 °C resulted in the highest gas yield. The calorific value of the pyrolysis gases was in the range of 68 to 84 MJ m^{-3}, which is much higher than the values found in the literature (20–37 MJ m^{-3}).[256–258] Ucar et al.[190] also investigated the pyrolysis of two types of tyres (passenger car tyre and truck tyre) using a fixed-bed reactor. They reported that there was no significant difference in the composition of gases. Hydrogen production from the waste car tyre was higher than that from the waste truck tyre. The composition of pyrolysis oil obtained from the two types of tyres was different. For example, the oil produced from the passenger car tyre contained more sulphur and aromatic compounds compared to the oil produced from the truck tyre. Solid char obtained from the truck tyre contained less ash, which is more suitable for upgrading to activated carbon.[190]

6.2 Effects of reaction conditions on CNT production

In addition to the effect of catalysts and precursors on CNT production, process conditions such as temperature and addition of oxidants also play dominant roles. Zhou et al.[259] and Zhao et al.[260] concluded that the orientation of graphene sheets of CNTs can be turned to 0–90° relative to the filament axis. The nature of the carbon precursor and synthesis temperature could lead to the re-construction of carbon particles.

Hata et al.[137] investigated water addition in SWCNT formation by a CVD method. The results showed that water could stimulate the catalyst activity and increase the catalysis lifetime by an etching effect, which oxidized the carbon encapsulated on the catalyst particles. The enhanced aligned SWCNTs with 2.5 mm height were formed within 10 minutes with 99.98% carbon
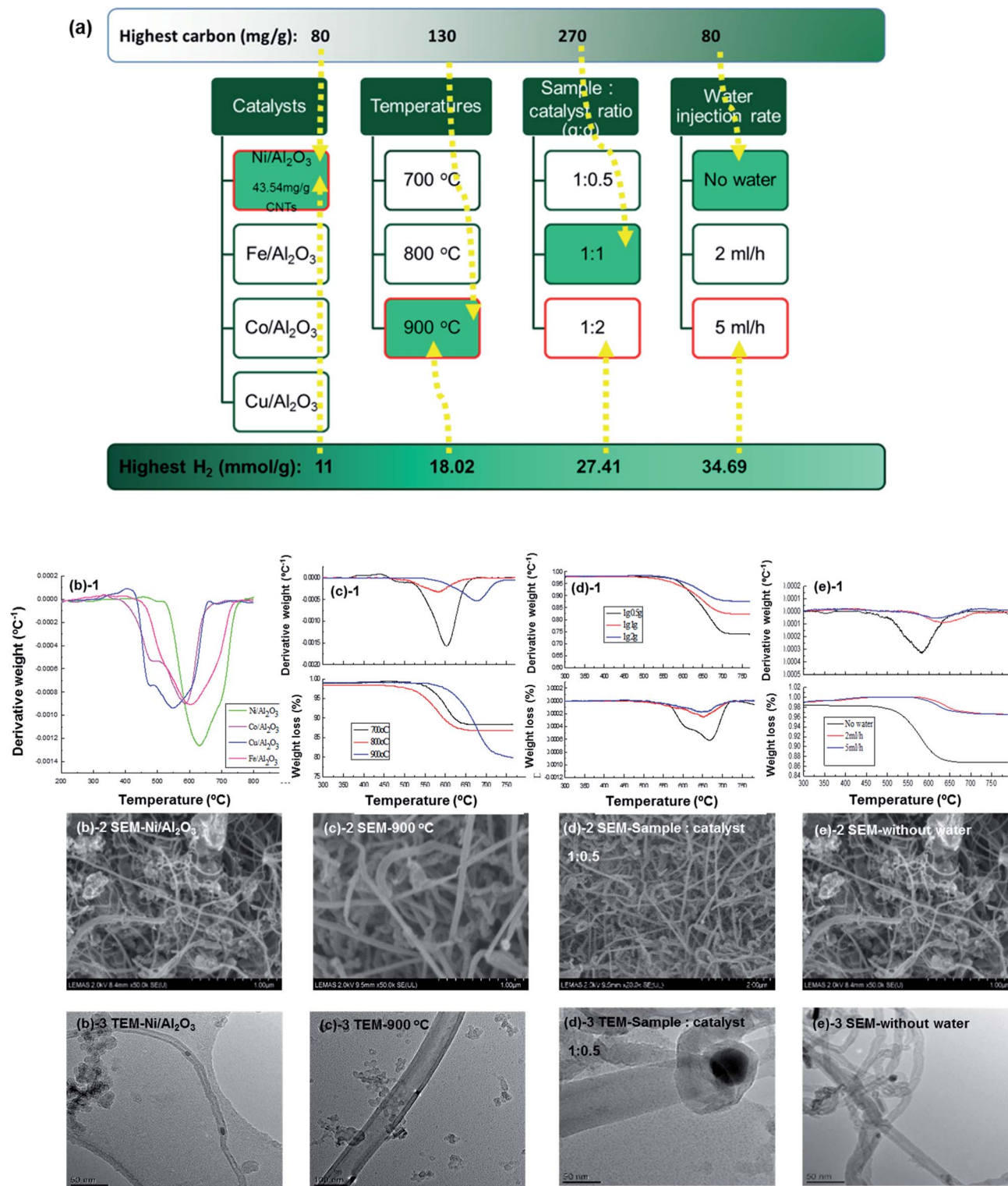
Fig. 5 A summary of the findings obtained by Zhang et al.[189,204,264] about CNT and hydrogen production from pyrolysis-catalysis of waste tyres. (a) Optimum conditions for CNT and hydrogen production under different process conditions (catalysts, temperatures, sample-to-catalyst ratios and water injection rates); (b)-1 DTG of carbon produced with different catalysts (Ni/Al_2O_3, $Co/Al_2O_3/Fe/Al_2O_3$ and Cu/Al_2O_3); (b)-2 and (b)-3 SEM and TEM micrographs of CNTs produced with Ni/Al_2O_3; (c)-2 and (c)-3 SEM and TEM micrographs of CNTs produced at 900 °C; (d)-2 and (d)-3 SEM and TEM micrographs of CNTs produced with the sample-to-catalyst ratio of 1 : 0.5; (e)-2 and (e)-3 SEM and TEM micrographs of CNTs without water.

purity by this water-assisted CVD of ethylene, also called "super growth". However, the oxidant (normally less than 1000 ppm) could also etch CNTs. Magrez *et al.*[261] mixed CO_2 with ethylene to grow CNTs at a ratio of 1 : 1. Zhang *et al.*[262] added ethanol (C_2H_5OH) to the CNT formation process to grow vertically aligned CNT forests. The modified process had insufficient H_2O or CO for the etching effect in this process with ethanol addition. However, there was still a small amount of water formed by the ethanol decomposition. The results showed that the walls of the CNTs could be reduced by ethanol addition and the catalyst lifetime also increased by more than three times. They used online dewpoint and mass spectrometry measurements and found that the decomposition of ethanol forming active carbons could enhance the growth of CNTs, and the water was used to etch the amorphous carbons accumulated on the surface of catalysts, whereas the catalyst activity was subsequently improved and the lifetime was prolonged. Motta *et al.*[263] investigated the effects of sulphur on SWCNT and MWCNT production at high temperatures between 1200 and 1300 °C in the presence of Fe-based catalysts. The results showed that sulphur could enhance the growth of CNTs by the diffusion of sulphur atoms into the first layers of iron atoms to form Fe–S. The surface energy could potentially be modified by the liquid Fe–S layer due to the lower melting point compared to iron. Also, the presence of sulphur prevented the diffusion of carbon inside bulk catalyst particles, promoting the production of SWCNTs instead of MWCNTs which need sub-surface diffusion of carbon atoms.

In 2017, Zhang *et al.*[189,204,264,265] completed a more comprehensive study on MWCNTs produced from waste tyres, and a summary of the results obtained under different process conditions is presented in Fig. 5. The preliminary investigations concerned different metal catalysts (Ni/Al_2O_3, Co/Al_2O_3/Fe/ Al_2O_3 and Cu/Al_2O_3), which were investigated to determine the effect on the production of CNTs and hydrogen by pyrolysis-catalysis of waste truck tyres. The results showed that the addition of catalysts in the pyrolysis-catalysis of waste tyre process can increase hydrogen production. The Ni/Al_2O_3 catalyst gave the highest hydrogen production at 18.14 mmol g_{tyre}^{-1} along with the production of relatively high-quality CNTs which were homogeneous.[189]

The influence of catalyst support was investigated with different $SiO_2 : Al_2O_3$ ratios (3 : 5, 1 : 1, 3 : 2, 2 : 1) with nickel. The results showed that the Ni-based $SiO_2 : Al_2O_3$ supported catalyst at a 1 : 1 ratio at 900 °C with the tyre sample to catalyst ratios at 1 : 2 gave the highest hydrogen production at 27.41 mmol g^{-1}, and the 1 : 1 ratio gave the highest filamentous carbon production at 201.5 mg g^{-1}.[250] The influence of process parameters on hydrogen and CNT production was investigated with the Ni/Al_2O_3 catalyst. Hydrogen production reached the highest level of 27.41 mmol g^{-1} at 900 °C with a sample-to-catalyst ratio of 1 : 2. The highest filamentous carbon production was obtained with the sample to catalyst ratio of 1 : 1 at 900 °C. The influence of water injection rate was also investigated that water introduction inhibited filamentous carbon production but increased hydrogen production.[204]

Three different tyre rubbers were investigated to understand the mechanism of CNT formation from the pyrolysis-catalysis of waste tyres.[205,264] The results showed that natural rubber, which is the main component of most tyres, dominated hydrogen production at 25 mmol g^{-1} and styrene–butadiene rubber gave the highest carbon formation at 40 wt%. The study was further extended to investigate waste plastics and different types of waste plastic feedstocks used in the pyrolysis catalysis/catalytic reforming process to produce hydrogen and CNTs.[265] As the separation of CNTs from catalysts is a challenge, a nickel metal catalyst was loaded on a stainless steel mesh and applied in the high-density polyethylene pyrolysis-catalysis process. The benefit of this catalyst has shown that the formation of carbon could be easily separated by physical shaking from the stainless steel–nickel mesh catalyst.[265] However, further investigation on waste plastics was concentrated on hydrogen production and where CNTs were the by-products of the process. Fe–Ni bimetallic catalysts supported by MCM-41 with different Fe : Ni ratios were investigated using simulated mixed waste plastics. A synergistic effect of iron and nickel was observed, particularly for the (10 : 10) Fe/Ni/MCM-41 catalyst, where the highest gas yield (95 wt%) and the highest H_2 production (46.1 mmol $g_{plastic}^{-1}$) have been achieved, along with the lowest carbon deposition, which was 6 wt% with the formation of CNTs.[252]

6.3 Discussion of process parameters on CNT and hydrogen production from thermo-chemical conversion of carbonaceous waste

A summary of the influence of process parameters on the production of CNT and hydrogen is shown in Fig. 6. Relevant
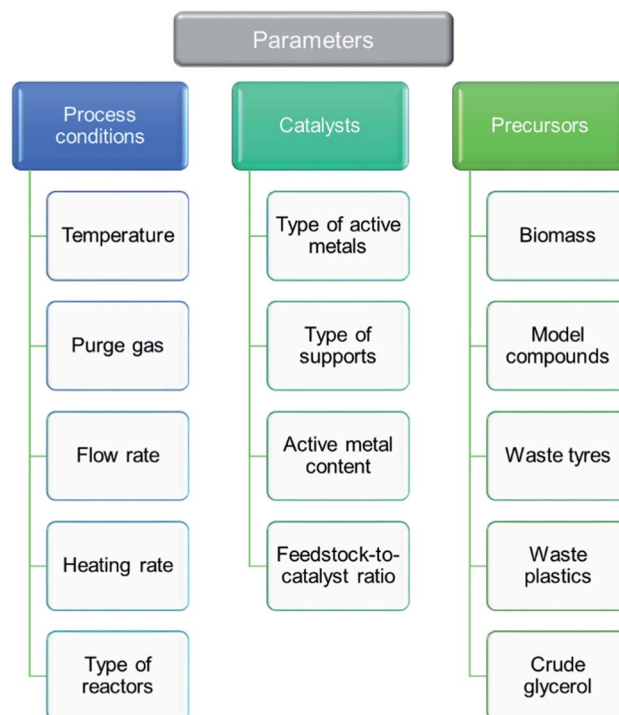
Fig. 6 Summary of the relevant process parameters that can affect CNT and hydrogen production.

process conditions include the temperature, purging gas, flow rate, heating rate and type of reactors. There are various parameters involved in the catalysis process, such as the type of active metals and supports, active metal contents, and feedstock-to-catalyst ratios. The precursor also plays a dominant role in the formation of CNTs, and the production of hydrogen including four most abundant waste carbonaceous materials (biomass, tyres, plastics and crude glycerol) has been reviewed.

From the literature, reaction parameters such as the temperature and the addition of oxidants such as water and CO_2 could improve the yield of CNTs by improving the catalyst activity and prolonging the catalyst life. The most common precursors for CNT synthesis are ethanol, methane, ethylene, acetylene, benzene, xylene and carbon monoxide, while ethanol has become the most popular precursor for SWCNTs synthesised at low temperatures.[85,140] The molecular structure of the precursors affects the morphology of CNTs directly. Hydrocarbons with linear structures such as methane, ethylene, acetylene result in a dominance of linear structured CNTs, since the hydrocarbon could decompose into atomic carbons, linear dimers or trimers of carbon and form the straight hollow filamentous carbons. Likewise, cyclic hydrocarbons such as benzene, xylene and cyclohexane would lead to a dominance of curved CNT formation, with bridges inside of the tubes.[132] SWCNT formation generally requires a higher temperature than for MWCNTs, which is 600–900 °C and 900–1200 °C, respectively.[97]

The most popular transition metals used for the production of CNTs and hydrogen from waste polymers are Fe, Ni, and Co due to their high solubility of carbon at high temperatures, high diffusion rates, relatively high melting points and low equilibrium-vapour pressures. It is also known that Fe, Ni and Co have stronger adhesion to CNTs. These transition metal-based catalysts are also suitable for CNTs formulated by arc-discharge and laser-vaporization methods in addition to the CVD method. Solid organometallocenes like ferrocene, cobaltocene and nickelocene are used as catalysts for CNT formation because they could liberate metal particles *in situ* and effectively improve the catalytic activity.[97] It has been reported that the same metal-based catalyst supported on different supports could have different catalytic activities. The common catalyst supports are graphite, quartz, silicon, silicon carbide, silica, alumina, zeolite, calcium oxide, and magnesium oxide, among others. The quality and yield of CNTs are affected by the morphology and textures of supports. Aluminium supports are more suitable for CNT formation compared to silica supports, because a stronger metal interaction would promote a higher metal dispersion.[153]

7 Applications of CNTs

In recent years, CNTs have been one of the most frequently investigated materials due to their physical, chemical, mechanical and thermal properties, and their potential applications in different industries which have grown rapidly since they were first discovered by Iijima.[83] The commercial interest

in CNTs is reflected in their production of thousands of tonnes every year. The wide range of applications will be reviewed in this section and summarized into different groups based on their different properties.

7.1 Applications based on electrical properties

To date, lithium-ion batteries (LIBs) have dominated the global battery market. They have a higher energy density and a longer lifespan compared to lead-acid, nickel–cadmium, or nickel–metal hydride batteries.[266,267] However, some issues such as resource availability, limited energy density, *etc.* are being exposed. Lithium–sulfur batteries (LSBs) possess a much higher theoretical energy density of 2600 W h kg^{-1} than that of LIBs.[268] However, the high solubility of polysulfide intermediates and the consumption of metallic lithium anode restrain the large-scale production.

MWCNTs can be blended with active materials and polymer binders in LIBs for laptops and mobile phones, since they can substantially enhance electrical connectivity and mechanical integrity, consequently increasing the electrochemical performance of the cells due to three reasons.[269,270] First, CNTs can act as electron- and ion-transport facilitators to construct a robust and interpenetrating conductive network when integrated with electroactive phases. Therefore, the diffusion of Li$^+$ can be improved to increase the energy density and the specific capacity of LIBs.[271] Cao *et al.*[272] synthesized Fe_2O_3 hollow spheres anchored on CNT composites for the application in LIBs. The Fe_2O_3/CNT hybrid delivered a reversible specific capacity of 1176 mA h g^{-1}, which is approximately a 40-fold enhancement compared to bare Fe_2O_3 (31.2 mA h g^{-1}). Second, the structure characteristics of MWCNT also play an important role in electrochemical performance. Li *et al.*[273] found that highly fluorinated MWCNTs with larger diameters of around 50 nm displayed better electrochemical performance in lithium/solid cathode systems because the larger diameter of MWCNTs could effectively avoid the diffusion path of lithium ions from being plugged by the swelled LiF crystals. The high strength and one-dimensional structure of CNTs can buffer the volume change of materials like sulphur, silicon, metal oxides, *etc.* in the process of battery cycling. The addition of CNTs can also maintain a complete conductive network and improve the cycling performance of these materials.[274–278] Zhang *et al.*[276] prepared nickel sulfide anchor on CNT nanocomposites for all-solid-state LIBs. The NiS-CNT nanocomposites exhibited a much higher reversible capacity of 259.6 mA h g^{-1} at 1 A g^{-1} than that of bulk-NiS owing to the presence of MWCNTs that increased the specific area of NiS-CNT composites, accommodated the volume changes and prevented the structural distortion. Third, when metallic lithium is used as the negative electrode, the formation of lithium dendrites results in durability limitations and safety issues. The introduction of CNTs with a high specific surface area and a superior electrical conductivity to those of lithium metal anodes can suppress the dendrite growth by means of changing the local current density, controlling the lithium nucleation and accommodating lithium deposition.[279] In addition, due to its fascinating features,

Table 2 A summary of CNT applications

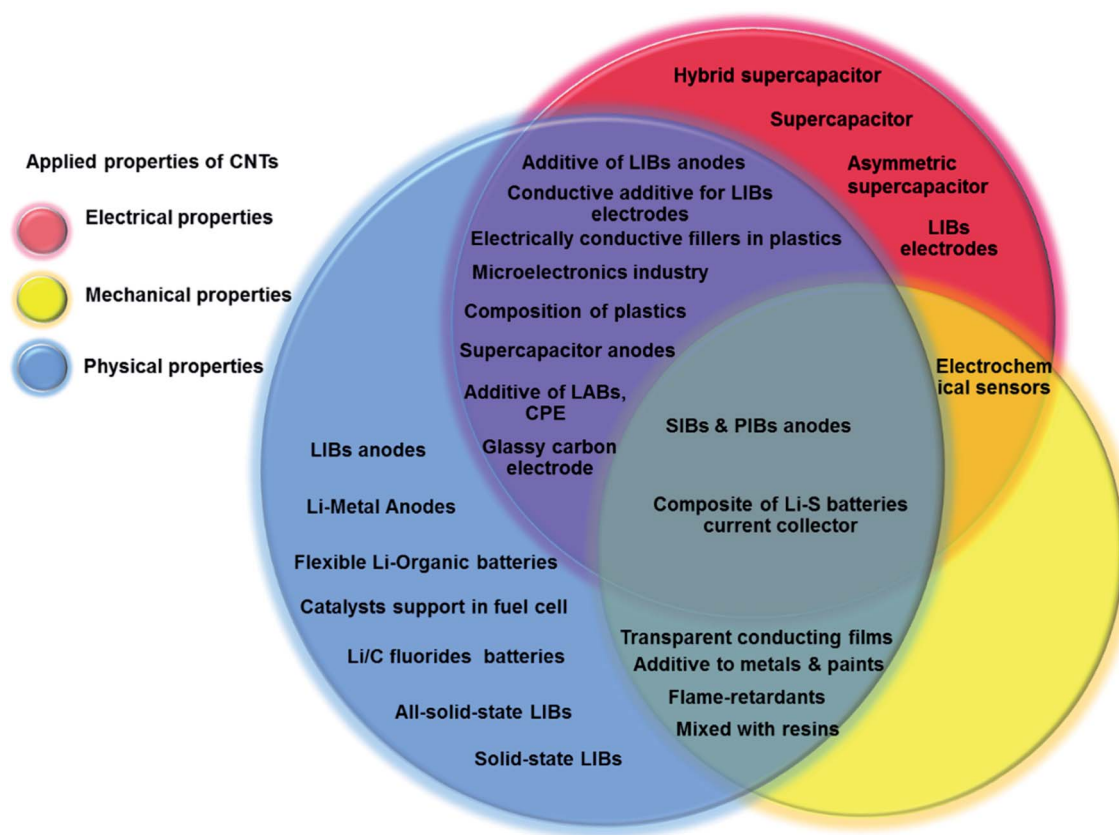| Type of CNT	Application	Applied industries	Advantages
MWCNTs	Electrical/physical	Conductive additive for LIB electrodes	Enhance the electrical connectivity and mechanical integrity;[269,270] boost the specific capacity[272]
MWCNTs	Physical	Lithium/carbon fluoride batteries, lithium-metal anodes, flexible lithium-organic batteries, solid-state lithium batteries, LIB anodes	Avoid the diffusion path of lithium ions from being plugged by the swelled LiF crystals.[273] Buffer the volume change of materials (sulphur, silicon, metal oxides, *etc.*) during cycling, to maintain a complete conductive network and improve the cycling performance.[274–278] Boost reversible capacity, accommodate volume changes and prevent structural distortion[276]
MWCNTs	Electrical/physical	Additive to LIB anodes	Suppress the dendrite growth by means of changing the local current density, controlling the lithium nucleation and accommodating the lithium deposition[279]
MWCNTs	Electrical/physical/mechanical	Assembled into current collectors for Li–S batteries	CNT-based current collectors can serve as a porous reservoir to accommodate polysulfides in Li–S batteries[280]
MWCNTs	Electrical/physical/mechanical	Incorporating CNTs into sodium-ion and potassium-ion battery (SIBs and PIBs) anodes	Alleviate poor transport kinetics and low power density of anode materials[281]
MWCNTs	Electrical	As conductive bridges of LIBs, SIBs, and PIBs	To interconnect the mixed Ni–Fe–S units and shorten the diffusion path of lithium/sodium/potassium ions, leading to enhanced charge capacity[282]
MWCNTs/SWCNTs	Electrical/physical	Additive to lead-acid batteries (LABs)	Increase the electronic conductivity and the contact among the particles. SWCNTs mitigate pronouncedly the detrimental sulfation phenomena[283]
MWCNTS	Physical	Catalyst support in fuel cells	Reduce Pt usage compared with normal carbon black.[284] The doped CNTs may not need Pt[285,286]
MWCNTS	Physical	Electrode materials for hydrogen evolution and oxygen reduction reactions (HER and ORR)	MWCNTs exhibit a high electrocatalytic performance for ORR[287]
SWCNTs	Electrical	Supercapacitors Hierarchical hybrid nanostructure CNTs Supercapacitors	Enhance the energy density, power density and lifetime[85] Electrical/physical Increase the electrical conductivity. The inter-tube structure of the open-tipped CNTs provide fast transfer channels for electrolyte ions[291]
MWCNTs	Electrical	Supercapacitors, hybrid supercapacitors, anodes of asymmetric supercapacitors	Reduce the resistance, enhance the specific capacitance and high rate cyclability.[288–290,292,294] Enhance the energy and power densities[293]
SWCNTs	Electrical/mechanical	CNT-based electrochemical sensors	Remarkable electrical and mechanical performances[295,296]
SWCNTs	Electrical/physical	Additive for carbon paste electrode (CPE) bulk for the voltammetric determination of histamine	Increased sensitivity than blank CPE[297]
MWCNTs	Electrical/physical	Gold nanoparticles-MWCNTs to modify the glassy carbon electrode (Au-MWCNTs/GCE) for the determination of anti-cancer drugs	Improve the selectivity, sensitivity and reproducibility[298]
MWCNTs	Electrical/physical	Electrically conductive fillers in plastics	To form a percolation network and enhance the conductivity of disordered polymers[299]
MWCNTs	Physical/mechanical	Composition of plastics; microelectronic industry (electromagnetic interference shielding packages and wafer carriers)	To enable electrostatic-assisted painting of mirror housings, fuel lines and filters in order to prevent electrostatic charge[85]
MWCNTs	Physical/mechanical	Resins mixed with CNTs, multifunctional coating materials (additive of paints and CNT-based transparent conducting films)	To manufacture lightweight and strong wind turbine blades and boat hulls;[300,301] reduce biofouling of ship hulls which could possibly replace the conventional environmentally hazardous biocide-containing paints.[89] A potential replacement of expensive and scarce indium tin oxide to form more flexible transparent conductors for displays[304]
MWCNTs	Physical/mechanical	As flame-retardants in plastics	Potential to replace environmentally hazardous halogenated flame retardants[302]
MWCNTs	Physical/mechanical	Additive to metals	To enhance the modulus and tensile strength[303]
SWCNTs	Physical/mechanical	Thin film coating	The surface resistivity is suitable for some applications such as CNT thin-film heaters, defrosting windows and sidewalks, but are of considerably higher price than those of the indium tin oxide coatings[309]

Fig. 7 Grouped applications of CNTs according to electrical, physical and mechanical properties.

including lightweight, mechanical durability and chemical stability, CNTs can be easily assembled into freestanding films for use as current collectors. CNT-based current collectors can serve as a porous reservoir to accommodate polysulfides in Li–S batteries.[280]

Sodium-ion and potassium-ion batteries (SIBs and PIBs) are considered as low-cost alternatives.[281] However, their poor transport kinetics and low power density of anode materials hinder the wide application of SIBs and PIBs. Incorporating CNTs into battery electrodes is a feasible strategy for alleviating the problem. Zhang et al.[282] employed CNTs with heterostructure bimetallic sulfides to form a special three-dimensional hierarchical structure, which was used as the anode for LIBs, SIBs, and PIBs and PIBs. CNTs as conductive bridges interconnected the mixed Ni–Fe–S units and shortened the diffusion path of lithium/sodium/potassium ions, leading to an enhanced charge capacity of 1535 mA h g^{-1} after 100 cycles at 0.2 A g^{-1} for LIBs, 431 mA h g^{-1} after 100 cycles at 0.1 A g^{-1} for SIBs, and 181 mA h g^{-1} at 0.1 A g^{-1} after 50 cycles for PIBs. Additionally, other types of batteries such as lead-acid batteries (LABs) are still widely employed in vehicles and popular in developing countries. Carbon nanomaterials such as MWCNTs and SWCNTs can be embedded in negative plates as sulfation-suppressing additives for high-performance LABs.[283]

CNTs can be used as catalyst supports for fuel cell electrodes since they can reduce more than half of Pt usage compared with

normal carbon black.[284] Further research has also proven that the application of doped CNTs in fuel cells may not need Pt.[285,286] Veksha et al.[287] processed plastic packaging waste (11.8 wt% polyethylene terephthalate) through catalytic-pyrolysis to produce MWCNTs and prepared them as electrode materials for the hydrogen evolution and oxygen reduction reactions (HER and ORR), respectively. Although the catalytic activity of the obtained MWCNT materials is lower than that of Pt/C electrodes in the HER, MWCNTs exhibited a higher electro-catalytic performance for ORR, where the overpotentials of MWCNT electrodes reached −0.033 V, lower than those of reported graphene-based materials.

CNTs can also be used in supercapacitors and hybrid supercapacitors.[288–290] SWCNTs have been studied for packaged cells which show a remarkable performance of using forest-grown SWCNT application. An energy density of 16 W h kg^{-1} and a power density of 10 kW kg^{-1} have been achieved for a 40 F supercapacitor, with a maximum voltage of 3.5 V. The lifetime of this supercapacitor has been forecasted to reach 16 years at 105 °C.[85] Zhou et al.[291] synthesized three-dimensional hierarchical hybrid CNT nanostructures and used them for high-performance supercapacitors. The electrical conductivity of electrode after CNT growth was elevated to 0.1 S cm^{-1}, in comparison to the initial value of 9 × 10^{-5} S cm^{-1}. The inter-tube structure of the open-tipped CNTs provided fast transfer channels for electrolyte ions, increasing the specific capacitance

to 440 F g^{-1} at 1 A g^{-1}, as well as the enhancement of cycling stability (98.4% retention of initial capacitance after 3000 cycles at 5 A g^{-1}). Natalia et al.[292] found that the addition of a small percentage of MWCNTs to a glucose-derived carbon material not only reduced the cell resistance but also promoted the formation of phenol/carbonyl surface functionalities. Correspondingly, a better capacitance of 206 F g^{-1} and a high rate cyclability (97% after 5000 cycles) were achieved. Wu et al.[293] prepared core–shell Bi–Bi$_2$O$_3$/MWCNT composites by directly annealing Bi$_2$O$_3$/MWCNTs due to the high reducibility of CNTs. A three-dimensional structure of CNTs was used as cell bodies to support Bi–Bi$_2$O$_3$ nanospheres. The Bi–Bi$_2$O$_3$/CNT electrode delivered an excellent capacitance of 714 F g^{-1} at 30 A g^{-1}. When it was used as the negative electrode for an asymmetric supercapacitor, a high energy density of 36.7 W h kg^{-1} and a maximum power density of 8000 W kg^{-1} were obtained. Wen[294] used carbon black combined with the Ni$_2$O$_3$ catalyst for catalytic carbonization of plastics and obtained CNTs with high yield and quality. Electrodes made from the synthesized CNTs displayed a higher specific capacitance than those of commercial CNTs and carbon black electrodes.

CNT-based electrochemical sensors have also been investigated extensively in recent decades, owing to their remarkable electrical and mechanical performances.[295,296] Zorica et al.[297] incorporated SWCNTs into carbon paste electrodes (CPEs) for the voltammetric determination of histamine. The SWCNT-CPE showed 50 times higher sensitivity than that observed for the blank CPE to histamine, due to enhanced conductivity and a large specific surface area. Moreover, CNTs have been used as the support of metal and metal oxides. Najari et al.[298] utilized gold nanoparticles–MWCNTs to modify a glassy carbon electrode (Au-MWCNTs/GCE) for the determination of an anticancer drug. The results showed a sharp decline in the charge-transfer resistance (R_{CT}). As a result, Au-MWCNTs/GCE has good selectivity, sensitivity and reproducibility due to the large surface area and rapid electron-transfer rate.

7.2 Applications based on physical and mechanical properties

7.2.1 Composite materials. MWCNTs can be used as electrically conductive fillers in plastics. The percolation network can be formed with only 0.01 wt% concentration of MWCNTs due to their high aspect ratio. The conductivity of disordered polymers with 10 wt% CNT composition can reach 10 000 S m^{-1}.[299] MWCNTs have also been applied in the automotive industry. By mixing CNTs into plastics, it can prevent electrostatic charge in the electrostatic-assisted painting of mirror housings, fuel lines and filters. MWCNTs can also be added to products in the microelectronic industry, such as electromagnetic interference shielding packages and wafer carriers.[85]

Due to the different features of CNTs with different diameters, aspect ratios, alignment, dispersion and interfacial interaction with the matrix, CNTs mixed with polymers or precursor resins can meaningfully improve the stiffness, strength and toughness of composite materials. It is reported in the literature that with a 1 wt% addition of CNTs into epoxy resins, the

stiffness was increased by 6% and the fracture toughness was increased by 23%.[300,301] The resins mixed with CNTs have recently been used to manufacture lightweight and strong wind turbine blades and boat hulls.

MWCNTs can also be added to plastics as flame-retardants, which can potentially replace environmentally hazardous halogenated flame retardants. The reasons for use of CNTs as flame-retardant additives are due to the changes in rheology.[302] CNTs can be added not only to polymers to form composite materials but also to metals to enhance the modulus and tensile strength. These metals with improved features can be applied in the aerospace and automotive industries.[303] For example, commercial aluminium and MWCNT mixtures have strengths close to that of stainless steel which are in the range of 0.7 to 1 GPa. However, the density is only 2.6 g cm^{-3}. The mixture of MWCNTs and aluminium provides higher strength with a lower cost than those of the Al–Li alloy.

7.2.2 Coatings and films. CNTs are emerging as multifunctional coating materials due to the development of dispersion and functionalization techniques. The addition of MWCNTs into paints could reduce biofouling of ship hulls which could possibly replace the conventional environmentally hazardous biocide-containing paints by preventing attachments of algae and barnacles on boat hulls.[89]

Indium tin oxide is commonly used in displays, touch-screen devices and photovoltaics. The price of indium tin oxide continues to rise due to a scarcity of indium.[304] As an alternative, CNT-based transparent conducting films could take the place of indium tin oxide to form more flexible transparent conductors for displays. Currently, SWCNTs films have been commercially produced. The surface resistivity is suitable for some applications such as CNT thin-film heaters, defrosting windows and sidewalks, but the price is considerably higher than those of the indium tin oxide coatings.[303]

7.3 Discussion of CNT applications

A comprehensive and most up to date list of CNT applications is summarized in Table 2 and Fig. 7. The applications of the most typical types of CNTs are summarized in Table 2 including advantages of using CNTs in the specific industry and the correlated properties with the applications. This section aims to guide the researchers to further investigate the potential applications of CNTs produced from waste materials. The initial applications of CNTs in super-capacitors, microelectronic industry and lightweight electromagnetic shields appear to have been successful. For example, using CNTs as a conductivity additive for LIB electrodes to boost the electrical connectivity[269,270] results in improved specific capacity.[269,270] CNTs can be used as multifunctional coating materials. For example, MWCNTs can be added to paints to discourage the attachment of algae and barnacles to the hulls of boats and therefore reduce bio-fouling.[89,305] MWCNTs have been used widely in LIBs by blending MWCNTs with active materials and polymer binders.[41,305,306] MWCNTs can increase the electrical connectivity and mechanical integrity with the result that the rate capacity and the life cycle of batteries have been

enhanced.[93,305,307] Considering the low electron scattering and band gap of high-quality SWCNTs, they have been used in making transistors. CNTs could also be used in biosensors and medical devices due to their chemical and dimensional compatibility with biomolecules.[305,308]

As shown in Fig. 7, most of the CNT applications are correlated with the physical properties, or electrical and mechanical properties. The applications rely on both the electrical and physical properties, such as their use as a conductive additive for LIBs, LABs and CPEs in the microelectronic industry, the composition of plastics, the anode of supercapacitors, and glassy carbon electrodes. The applications that rely on both physical and mechanical properties include their use as transparent conducting films, additives to metals and paints, flame-retardants and resins. There are a few applications that rely on the combination of electrical, physical and mechanical properties, including SIB and PIB anodes, and Li–S battery composites. There are still many applications that relate to the physical properties only, which mainly focus on battery applications, such as LIB anodes, Li-metal anodes, flexible Li-organic batteries, catalyst supports for fuel cells, Li/C fluoride batteries and all-solid-state batteries. Applications that only rely on electrical properties include supercapacitors (also include hybrid supercapacitors and asymmetric supercapacitors) and LIB anodes. There are limited applications that solely rely on their mechanical and electrical properties, which is in electrochemical sensors.

8 Conclusions, challenges and future prospects

8.1 Conclusions

Thermo-chemical conversion of waste hydrocarbons including waste tyres, plastics, biomass and crude glycerol is more desirable, compared with traditional recycling methods, as it could ease the environmental issues caused by landfilling or incineration. Also, the waste hydrocarbons can be used as an alternative feedstock for CNT production due to the much lower cost of feedstocks. Therefore, this work targets reviewing CNT production from thermo-chemical conversion of carbonaceous waste streams including waste tyres, plastics, biomass and crude glycerol and guides the researchers to use alternative resources to manufacture high-quality CNTs for furthering a broad range of applications.

The production and management of waste tyres, plastics, biomass and crude glycerol show the necessity of treatment to deal with these wastes. First, the influence of feedstocks on CNT and hydrogen production by a thermo-chemical conversion process is introduced. Then, the associated catalyst development is deliberated, including the influence of active metals, catalyst supports, synthesis methods, catalysis temperatures and reactors. The process parameters that are involved in the thermo-chemical conversion process and the effects on CNT and hydrogen production are also discussed in detail. Then, the existing applications of the CNTs were discussed according to their electrical, physical and mechanical properties, which

could be the future direction of the research, aiming to further apply the CNTs synthesised from wastes in different sectors. Finally, the review ends up with a discussion of challenge and future outlook about thermo-chemical conversion of carbonaceous waste.

8.2 Challenges and future prospects

CNTs produced from waste tyres, plastics, biomass and crude glycerol have been extensively studied for many years. However, there are still challenges to develop a techno-economic feasible process to realize the value of CNTs produced from waste materials. The CNT growth mechanism is complex and it varies with different feedstocks and reactors. Investigations are mainly carried out with lab-scale reactors and lack of research covering the applications of the CNTs produced from waste materials. Therefore, this review discusses the key challenges and future prospects on CNTs produced from waste carbonaceous materials which include the mechanism study, CNT purification and applications, and quality control and larger scale of CNT production.

8.2.1 **Mechanism study.** The first key challenge is the CNT growth mechanism from waste materials. The existing mechanism is based on the model established decades ago using pure carbon precursors by the CVD method. However, the mechanism of CNT growth from waste carbonaceous materials is far more complicated as the waste precursor is extremely complex in terms of the composition and reactors are different as well. So, there is a need to carry out an in-depth study to understand the mechanism of CNT formation from waste materials in a specific reactor.

More research studies could be conducted using pyrolysis of oil model compounds to simplify the mechanism studies. There might be differences in the behavior of different model compounds; therefore, more complicated structures of model compounds should be investigated for CNT production derived from waste carbonaceous materials. The investigation on the formation of CNTs from waste materials is worthy of further efforts, which could help to compare the particular CNT formation mechanism under different reaction regimes with the mechanism of CNT formation from the conventional CVD method. Applications of advanced metrology, such as *in situ* TEM, X-ray diffraction, X-ray photoelectron spectroscopy, Raman spectroscopy or other metrology could help to understand the growth mechanism of CNTs formed by pyrolysis-catalysis of wastes to monitor the carbon formation process on metal catalysts. There is also a need to explore a more advanced metrology to study the CNT growth mechanism.

8.2.2 **CNT purification and applications.** The CNTs produced from waste carbonaceous materials are normally formed on the surface of the catalysts and are difficult to purify, although some catalyst supports that aim to ease CNT collection have been studied, such as stainless steel meshes[265] and ceramic membranes.[310] The reported results show the advantages of using novel catalyst supports to solve the problem of the recovery of CNTs. There is a need to further develop catalyst supports for CNT recovery. The conventional purification

methods first remove the amorphous carbons by mild oxidation at low temperatures, then dissolve the metals into an acid to remove the impurities from the catalysts. However, the quality of the purified CNTs may change due to the purification performed under harsh conditions. The damage level of the conventional purification methods need to be identified. There are many applications of CNTs, but they are all synthesized from pure precursors, for example, methane. There is also a lack of research covering the application of CNTs produced from waste materials due to the impurities and uncontrollable quality of CNT production. A more simplified and less damaged purification method could assist the research on developing potential applications of CNTs produced from waste.

8.2.3 Quality control and larger scale CNT production. The quality of CNTs produced from waste varies mainly due to the complex composition of feedstocks. This could be controlled by optimizing the process conditions. However, accurate quality control of CNTs is still difficult to achieve, in relation to the chirality of the CNTs, their diameter, length, purity *etc.* This also limits the future applications of these CNTs synthesized from waste materials as the applications closely correlate with their properties and quality. A better understanding of the CNT growth mechanism directly from waste carbonaceous materials could support the realization of the CNT quality control. Therefore, a more advanced and controllable process could be developed for producing CNTs from waste materials with targeting applications. It could also support a larger scale of research and there is potential for commercialization of this technique for converting wastes to high-value products.

Author contributions

Conceptualization: Y. S. Zhang, P. T. Williams and D. J. L. Brett; visualization: Y. S. Zhang and L. Yu; writing – original draft preparation: Y. S. Zhang, H. L. Zhu and D. Xu; funding acquisition: D. J. L. Brett and P. R. Shearing; writing – review & editing: all authors.

Conflicts of interest

There are no conflicts to declare.

Acknowledgements

References

1 D. Czajczyńska, R. Krzyżyńska, H. Jouhara and N. Spencer, *Energy*, 2017, **134**, 1121–1131.

2 ETRMA, *European Tyre & Rubber Industry Statistics 2019*, European Tyre & Rubber Manufactures' Association, 2019.

3 T. A. Saleh and V. K. Gupta, *Adv. Colloid Interface Sci.*, 2014, **211**, 93–101.

4 ETRMA, *The European Tyre Industry Facts and Figures 2020*, European Tyre & Rubber Manufactures Association, 2019.

5 PlasticsEurope, *Plastics-The Facts 2019*, Plastics Europe, 2019.

6 L. Lebreton and A. Andrady, *Palgrave Commun.*, 2019, **5**, 6.

7 K. R. Vanapalli, H. B. Sharma, V. P. Ranjan, B. Samal, J. Bhattacharya, B. K. Dubey and S. Goel, *Sci. Total Environ.*, 2020, **750**, 141514.

8 M. C. Rillig and A. Lehmann, *Science*, 2020, **368**, 1430–1431.

9 S. Sharma and S. Chatterjee, *Environ. Sci. Pollut. Res.*, 2017, **24**, 21530–21547.

10 J. J. Klemeš, Y. V. Fan and P. Jiang, *Energy Sources, Part A*, 2020, 1–17.

11 B. M. Weckhuysen, *Science*, 2020, **370**, 400–401.

12 Z. Wang, D. Shen, C. Wu and S. Gu, *Green Chem.*, 2018, **20**, 5031–5057.

13 WBA, *Global Bioenergy Statistics 2019*, World Bioenergy Association, 2019.

14 J. Lehmann and S. Joseph, *Biochar for Environmental Management: Science and Technology*, 2009, vol. 1, pp. 1–12.

15 A. A. Koutinas, A. Vlysidis, D. Pleissner, N. Kopsahelis, I. L. Garcia, I. K. Kookos, S. Papanikolaou, T. H. Kwan and C. S. K. Lin, *Chem. Soc. Rev.*, 2014, **43**, 2587–2627.

16 S. Alatzas, K. Moustakas, D. Malamis and S. Vakalis, *Energies*, 2019, **12**, 1095.

17 E. J. Cho, L. T. P. Trinh, Y. Song, Y. G. Lee and H.-J. Bae, *Bioresour. Technol.*, 2020, **298**, 122386.

18 S. Kaza, L. Yao, P. Bhada-Tata and F. Van Woerden, *What a Waste 2.0: a Global Snapshot of Solid Waste Management to 2050*, The World Bank, 2018.

19 H. Daniel and B.-T. Perinaz, *What a Waste: A Global Review of Solid Waste Management, Urban development series, knowledge papers no. 15*, World Bank, Washington, DC, 2012, © World Bank, License: CC BY 3.0 IGO, https://openknowledge.worldbank.org/handle/10986/17388.

20 Eurostat, *Waste Statistics*, https://ec.europa.eu/eurostat/statistics-explained/index.php/Waste_statistics#Waste_treatment.

21 P. Agamuthu, *Solid Waste: Principles and Management: with Malaysian Case Studies*, University of Malaya Press, Kuala Lumpur, 2001.

22 N. Gupta, K. K. Yadav and V. Kumar, *J. Environ. Sci.*, 2015, **37**, 206–217.

23 M. Pagliaro, R. Ciriminna, H. Kimura, M. Rossi and C. Della Pina, *Angew. Chem., Int. Ed.*, 2007, **46**, 4434–4440.

24 National Biodiesel Board, *Biodiesel Myths*, http://www.biodiesel.org/docs/default-source/ffs-basics/biodiesel-myths-vs-facts.pdf?sfvrsn=14, accessed 25/06/2014, 2014.

25 F. Ma and M. A. Hanna, *Bioresour. Technol.*, 1999, **70**, 1–15.

26 X. Lang, A. K. Dalai, N. N. Bakhshi, M. J. Reaney and P. B. Hertz, *Bioresour. Technol.*, 2001, **80**, 53–62.

27 C. Wu, Z. Wang, P. T. Williams and J. Huang, *Sci. Rep.*, 2013, **3**, 2742.

28 European Bioenergy Board, *Biodiesel Industry calls for ambitious post 2020 transportation renewable targets*, 2014.

29 K. S. Avasthi, R. N. Reddy and S. Patel, *Procedia Eng.*, 2013, **51**, 423–429.

30 S. Adhikari, S. D. Fernando and A. Haryanto, *Energy Convers. Manage.*, 2009, **50**, 2600–2604.

31 O. Babajide, *J. Energy*, 2013, 7.

32 S. Nanda and F. Berruti, *Environ. Chem. Lett.*, 2020, 1–26.

33 P. T. Williams, *Waste Biomass Valorization*, 2021, **12**(1), 1–28.

34 M. Solis and S. Silveira, *Waste Manage.*, 2020, **105**, 128–138.

35 A. Ochoa, J. Bilbao, A. G. Gayubo and P. Castaño, *Renewable Sustainable Energy Rev.*, 2020, **119**, 109600.

36 M. Arabiourrutia, G. Lopez, M. Artetxe, J. Alvarez, J. Bilbao and M. Olazar, *Renewable Sustainable Energy Rev.*, 2020, **129**, 109932.

37 M. Checa, S. Nogales-Delgado, V. Montes and J. M. Encinar, *Catalysts*, 2020, **10**, 1279.

38 C. Wu, Z. Wang, P. T. Williams and J. Huang, *Sci. Rep.*, 2013, **3**, 2742.

39 W. M. Lewandowski, M. Ryms and W. Kosakowski, *Processes*, 2020, **8**, 516.

40 Y. Zhang, C. Wu, M. A. Nahil and P. Williams, *Proc. Inst. Civ. Eng.: Waste Resour. Manage.*, 2016, **169**, 137–145.

41 P. T. Williams, *Waste Manage.*, 2013, **33**, 1714–1728.

42 P. Williams, A. Cunliffe and A. Brindle, *J. Inst. Energy*, 2001, **74**, 100–112.

43 M. Sienkiewicz, J. Kucinska-Lipka, H. Janik and A. Balas, *Waste Manage.*, 2012, **32**, 1742–1751.

44 M. Suzuki, *Carbon*, 1994, **32**, 577–586.

45 P. T. Williams and A. J. Brindle, *J. Anal. Appl. Pyrolysis*, 2003, **67**, 143–164.

46 X. Dai, X. Yin, C. Wu, W. Zhang and Y. Chen, *Energy*, 2001, **26**, 385–399.

47 J. A. Conesa, R. Font and A. Marcilla, *Energy Fuels*, 1996, **10**, 134–140.

48 E. Aylón, A. Fernández-Colino, R. Murillo, M. Navarro, T. García and A. Mastral, *Waste Manage.*, 2010, **30**, 1220–1224.

49 C. J. Roos, *Clean Heat and Power Using Biomass Gasification for Industrial and Agricultural Projects*, Northwest CHP Application Center, 2010.

50 I. F. Elbaba, C. Wu and P. T. Williams, *Int. J. Hydrogen Energy*, 2011, **36**, 6628–6637.

51 D. Y. C. Leung and C. L. Wang, *Fuel Process. Technol.*, 2003, **84**, 175–196.

52 G. Xiao, M.-J. Ni, Y. Chi and K.-F. Cen, *Energy Convers. Manage.*, 2008, **49**, 2078–2082.

53 S. Galvagno, G. Casciaro, S. Casu, M. Martino, C. Mingazzini, A. Russo and S. Portofino, *Waste Manage.*, 2009, **29**, 678–689.

54 R. M. Dell, P. T. Moseley and D. A. J. Rand, in *Towards Sustainable Road Transport*, ed. R. M. Dell, T. Moseley and A. J. Rand, Academic Press, Boston, 2014, pp. 260–295, DOI: 10.1016/B978-0-12-404616-0.00008-6.

55 A. Zadgaonkar, *Feedstock Recycling and Pyrolysis of Waste Plastics: Converting Waste Plastics into Diesel and Other Fuels*, 2006, pp. 709–728.

56 I. de Marco Rodriguez, M. Laresgoiti, M. Cabrero, A. Torres, M. Chomon and B. Caballero, *Fuel Process. Technol.*, 2001, **72**, 9–22.

57 A. Donatelli, P. Iovane and A. Molino, *Fuel*, 2010, **89**, 2721–2728.

58 M. S. Qureshi, A. Oasmaa, H. Pihkola, I. Deviatkin, A. Tenhunen, J. Mannila, H. Minkkinen, M. Pohjakallio and J. Laine-Ylijoki, *J. Anal. Appl. Pyrolysis*, 2020, 104804.

59 C. Wu and P. T. Williams, *Appl. Catal., B*, 2009, **87**, 152–161.

60 S. Czernik and R. J. French, *Energy Fuels*, 2006, **20**, 754–758.

61 P. T. Williams, *Waste Treatment and Disposal*, 2nd edn, 2005, pp. 245–323.

62 C. Wu and P. T. Williams, *Appl. Catal., B*, 2009, **90**, 147–156.

63 Y. Chai, N. Gao, M. Wang and C. Wu, *Chem. Eng. J.*, 2020, **382**, 122947.

64 C. Wu and P. T. Williams, *Fuel*, 2010, **89**, 3022–3032.

65 S. L. Lakhapatri and M. A. Abraham, *Appl. Catal., A*, 2011, **405**, 149–159.

66 G. Sierra Gallego, J. Barrault, C. Batiot-Dupeyrat and F. Mondragón, *Catal. Today*, 2010, **149**, 365–371.

67 M. He, B. Xiao, Z. Hu, S. Liu, X. Guo and S. Luo, *Int. J. Hydrogen Energy*, 2009, **34**, 1342–1348.

68 J. Srinakruang, K. Sato, T. Vitidsant and K. Fujimoto, *Catal. Commun.*, 2005, **6**, 437–440.

69 T. Minowa, F. Zhen and T. Ogi, *J. Supercrit. Fluids*, 1998, **13**, 253–259.

70 F. H. Isikgor and C. R. Becer, *Polym. Chem.*, 2015, **6**, 4497–4559.

71 Y. Lin, H. Wang, Y. Wang, R. Huo, Z. Huang, M. Liu, G. Wei, Z. Zhao, H. Li and Y. Fang, *Energy Fuels*, 2020, **34**, 7847–7862.

72 Y. Zhang, C. Ke, W. Fu, Y. Cui, M. A. Rehan and B. Li, *Renewable Energy*, 2020, **154**, 488–496.

73 D. Yao, Q. Hu, D. Wang, H. Yang, C. Wu, X. Wang and H. Chen, *Bioresour. Technol.*, 2016, **216**, 159–164.

74 T. Valliyappan, N. N. Bakhshi and A. K. Dalai, *Bioresour. Technol.*, 2008, **99**, 4476–4483.

75 J. Gao, Y. Wang, Y. Ping, D. Hu, G. Xu, F. Gu and F. Su, *RSC Adv.*, 2012, **2**, 2358–2368.

76 I. Ahmed and A. Gupta, *Appl. Energy*, 2009, **86**, 1813–1821.

77 P. T. Williams, *Waste Treatment and Disposal*, John Wiley & Sons, 2005.

78 A. Demirbas, *J. Anal. Appl. Pyrolysis*, 2004, **72**, 243–248.

79 Y. Kodera, Y. Ishihara and T. Kuroki, *Energy Fuels*, 2006, **20**, 155–158.

80 A. Esfandiari, T. Kaghazchi and M. Soleimani, *J. Taiwan Inst. Chem. Eng.*, 2012, **43**, 631–637.

81 B. C. R. Ewan and R. W. K. Allen, *Int. J. Hydrogen Energy*, 2005, **30**, 809–819.

82 S. Authayanun, A. Arpornwichanop, W. Paengjuntuek and S. Assabumrungrat, *Int. J. Hydrogen Energy*, 2010, **35**, 6617–6623.

83 S. Iijima, *Nature*, 1991, **354**, 56–58.

84 M. Monthioux and V. L. Kuznetsov, *Carbon*, 2006, **44**, 1621–1623.

85 M. F. De Volder, S. H. Tawfick, R. H. Baughman and A. J. Hart, *Science*, 2013, **339**, 535–539.

86 B. Peng, M. Locascio, P. Zapol, S. Li, S. L. Mielke, G. C. Schatz and H. D. Espinosa, *Nat. Nanotechnol.*, 2008, **3**, 626–631.

87 B. Wei, R. Vajtai and P. Ajayan, *Appl. Phys. Lett.*, 2001, **79**, 1172–1174.

88 E. Pop, D. Mann, Q. Wang, K. Goodson and H. Dai, *Nano Lett.*, 2006, **6**, 96–100.

89 A. Beigbeder, P. Degee, S. L. Conlan, R. J. Mutton, A. S. Clare, M. E. Pettitt, M. E. Callow, J. A. Callow and P. Dubois, *Biofouling*, 2008, **24**, 291–302.

90 L. Dai, D. W. Chang, J.-B. Baek and W. Lu, *Small*, 2012, **8**, 1130–1166.

91 A. R. Köhler, C. Som, A. Helland and F. Gottschalk, *J. Cleaner Prod.*, 2008, **16**, 927–937.

92 K. Evanoff, J. Khan, A. A. Balandin, A. Magasinski, W. J. Ready, T. F. Fuller and G. Yushin, *Adv. Mater.*, 2012, **24**, 533–537.

93 C. Sotowa, G. Origi, M. Takeuchi, Y. Nishimura, K. Takeuchi, I. Y. Jang, Y. J. Kim, T. Hayashi, Y. A. Kim, M. Endo and M. S. Dresselhaus, *ChemSusChem*, 2008, **1**, 911–915.

94 D. A. Heller, S. Baik, T. E. Eurell and M. S. Strano, *Adv. Mater.*, 2005, **17**(23), 2793–2799.

95 M. Endo, T. Hayashi and Y.-A. Kim, *Pure Appl. Chem.*, 2006, **78**, 1703–1713.

96 Q. Zhang, J. Q. Huang, M. Q. Zhao, W. Z. Qian and F. Wei, *ChemSusChem*, 2011, **4**, 864–889.

97 M. Kumar and Y. Ando, *J. Nanosci. Nanotechnol.*, 2010, **10**, 3739–3758.

98 A. Bazargan and G. McKay, *Chem. Eng. J.*, 2012, **195**, 377–391.

99 W.-W. Liu, S.-P. Chai, A. R. Mohamed and U. Hashim, *J. Ind. Eng. Chem.*, 2014, **20**, 1171–1185.

100 P. N. H. D. P. Petit, *Science*, 1996, **273**, 483–487.

101 K. Dasgupta, J. B. Joshi and S. Banerjee, *Chem. Eng. J.*, 2011, **171**, 841–869.

102 E. Boellaard, P. K. de Bokx, A. J. H. M. Kock and J. W. Geus, *J. Catal.*, 1985, **96**, 481–490.

103 N. M. Rodriguez, M. S. Kim and R. T. K. Baker, *J. Catal.*, 1993, **144**, 93–108.

104 H. Boehm, *Carbon*, 1973, **11**, 583IN1587–1586IN5590.

105 N. Behabtu, C. C. Young, D. E. Tsentalovich, O. Kleinerman, X. Wang, A. W. Ma, E. A. Bengio, R. F. ter Waarbeek, J. J. de Jong and R. E. Hoogerwerf, *Science*, 2013, **339**, 182–186.

106 E. L. K. Mui, V. K. C. Lee, W. H. Cheung and G. McKay, *Energy Fuels*, 2008, **22**, 1650–1657.

107 V. B. Mortola, S. Damyanova, D. Zanchet and J. M. C. Bueno, *Appl. Catal., B*, 2011, **107**, 221–236.

108 J. Nishikawa, K. Nakamura, M. Asadullah, T. Miyazawa, K. Kunimori and K. Tomishige, *Catal. Today*, 2008, **131**, 146–155.

109 K. Hernadi, A. Fonseca, J. Nagy, D. Bernaerts and A. Lucas, *Carbon*, 1996, **34**, 1249–1257.

110 J. Kong, A. M. Cassell and H. Dai, *Chem. Phys. Lett.*, 1998, **292**, 567–574.

111 S. Fan, M. G. Chapline, N. R. Franklin, T. W. Tombler, A. M. Cassell and H. Dai, *Science*, 1999, **283**, 512–514.

112 B. C. Satishkumar, A. Govindaraj and C. N. R. Rao, *Chem. Phys. Lett.*, 1999, **307**, 158–162.

113 W. Z. Li, S. S. Xie, L. X. Qian, B. H. Chang, B. S. Zou, W. Y. Zhou, R. A. Zhao and G. Wang, *Science*, 1996, **274**, 1701–1703.

114 R. Sen, A. Govindaraj and C. N. R. Rao, *Chem. Phys. Lett.*, 1997, **267**, 276–280.

115 B. Q. Wei, R. Vajtai, Y. Jung, J. Ward, R. Zhang, G. Ramanath and P. M. Ajayan, *Nature*, 2002, **416**, 495–496.

116 P. Nikolaev, M. J. Bronikowski, R. K. Bradley, F. Rohmund, D. T. Colbert, K. A. Smith and R. E. Smalley, *Chem. Phys. Lett.*, 1999, **313**, 91–97.

117 A. Weidenkaff, S. G. Ebbinghaus, P. Mauron, A. Reller, Y. Zhang and A. Züttel, *Mater. Sci. Eng., C*, 2002, **19**, 119–123.

118 D. Venegoni, P. Serp, R. Feurer, Y. Kihn, C. Vahlas and P. Kalck, *Carbon*, 2002, **40**, 1799–1807.

119 A. Morançais, B. Caussat, Y. Kihn, P. Kalck, D. Plee, P. Gaillard, D. Bernard and P. Serp, *Carbon*, 2007, **45**, 624–635.

120 R. Philippe, B. Caussat, A. Falqui, Y. Kihn, P. Kalck, S. Bordère, D. Plee, P. Gaillard, D. Bernard and P. Serp, *J. Catal.*, 2009, **263**, 345–358.

121 Q. Li, X. Zhang, R. F. DePaula, L. Zheng, Y. Zhao, L. Stan, T. G. Holesinger, P. N. Arendt, D. E. Peterson and Y. T. Zhu, *Adv. Mater.*, 2006, **18**, 3160–3163.

122 C. H. See and A. T. Harris, *Aust. J. Chem.*, 2007, **60**, 541–546.

123 C. H. See, O. M. Dunens, K. J. MacKenzie and A. T. Harris, *Ind. Eng. Chem. Res.*, 2008, **47**, 7686–7692.

124 W. Qian, T. Liu, F. Wei, Z. Wang and Y. Li, *Appl. Catal., A*, 2004, **258**, 121–124.

125 Y. Wei, G. Eres, V. Merkulov and D. Lowndes, *Appl. Phys. Lett.*, 2001, **78**, 1394–1396.

126 W. Fang, C. Pirez, M. Capron, S. Paul, T. Raja, P. L. Dhepe, F. Dumeignil and L. Jalowiecki-Duhamel, *RSC Adv.*, 2012, **2**, 9626–9634.

127 W. Li, J. Wen and Z. Ren, *Appl. Phys. A: Mater. Sci. Process.*, 2002, **74**, 397–402.

128 A. Moisala, A. G. Nasibulin and E. I. Kauppinen, *J. Phys.: Condens. Matter*, 2003, **15**, S3011.

129 J. Kong, A. M. Cassell and H. Dai, *Chem. Phys. Lett.*, 1998, **292**, 567–574.

130 Z.-J. Liu, R. Che, Z. Xu and L.-M. Peng, *Synth. Met.*, 2002, **128**, 191–195.

131 N. Li, X. Chen, L. Stoica, W. Xia, J. Qian, J. Aßmann, W. Schuhmann and M. Muhler, *Adv. Mater.*, 2007, **19**, 2957–2960.

132 O. A. Nerushev, S. Dittmar, R.-E. Morjan, F. Rohmund and E. E. B. Campbell, *J. Appl. Phys.*, 2003, **93**, 4185–4190.

133 R. E. Morjan, O. A. Nerushev, M. Sveningsson, F. Rohmund, L. K. L. Falk and E. E. B. Campbell, *Appl. Phys. A: Mater. Sci. Process.*, 2004, **78**, 253–261.

134 R. T. K. Baker, M. A. Barber, P. S. Harris, F. S. Feates and R. J. Waite, *J. Catal.*, 1972, **26**, 51–62.

135 R. Andrews, D. Jacques, A. M. Rao, F. Derbyshire, D. Qian, X. Fan, E. C. Dickey and J. Chen, *Chem. Phys. Lett.*, 1999, **303**, 467–474.

136 M. Kumar and Y. Ando, *Chem. Phys. Lett.*, 2003, **374**, 521–526.

137 K. Hata, D. N. Futaba, K. Mizuno, T. Namai, M. Yumura and S. Iijima, *Science*, 2004, **306**, 1362–1364.

138 M. Kumar, K. Kakamu, T. Okazaki and Y. Ando, *Chem. Phys. Lett.*, 2004, **385**, 161–165.

139 D. Ding, J. Wang, Z. Cao and J. Dai, *Carbon*, 2003, **41**, 579–582.

140 T. Murakami, T. Sako, H. Harima, K. Kisoda, K. Mitikami and T. Isshiki, *Thin Solid Films*, 2004, **464–465**, 319–322.

141 B. Kitiyanan, W. E. Alvarez, J. H. Harwell and D. E. Resasco, *Chem. Phys. Lett.*, 2000, **317**, 497–503.

142 C. Mattevi, C. T. Wirth, S. Hofmann, R. Blume, M. Cantoro, C. Ducati, C. Cepek, A. Knop-Gericke, S. Milne, C. Castellarin-Cudia, S. Dolafi, A. Goldoni, R. Schloegl and J. Robertson, *J. Phys. Chem. C*, 2008, **112**, 12207–12213.

143 C. L. Cheung, A. Kurtz, H. Park and C. M. Lieber, *J. Phys. Chem. B*, 2002, **106**, 2429–2433.

144 H. Hongo, M. Yudasaka, T. Ichihashi, F. Nihey and S. Iijima, *Chem. Phys. Lett.*, 2002, **361**, 349–354.

145 C. Mirodatos, H. Praliaud and M. Primet, *J. Catal.*, 1987, **107**, 275–287.

146 Z. Zhang and X. E. Verykios, *Appl. Catal., A*, 1996, **138**, 109–133.

147 I. Willems, Z. Kónya, J. F. Colomer, G. Van Tendeloo, N. Nagaraju, A. Fonseca and J. B. Nagy, *Chem. Phys. Lett.*, 2000, **317**, 71–76.

148 M. Kumar and Y. Ando, *Carbon*, 2005, **43**, 533–540.

149 E. Couteau, K. Hernadi, J. W. Seo, L. Thiên-Nga, C. Mikó, R. Gaál and L. Forró, *Chem. Phys. Lett.*, 2003, **378**, 9–17.

150 J. F. Colomer, C. Stephan, S. Lefrant, G. Van Tendeloo, I. Willems, Z. Kónya, A. Fonseca, C. Laurent and J. B. Nagy, *Chem. Phys. Lett.*, 2000, **317**, 83–89.

151 J. W. Ward, B. Q. Wei and P. M. Ajayan, *Chem. Phys. Lett.*, 2003, **376**, 717–725.

152 H. Ago, K. Nakamura, S. Imamura and M. Tsuji, *Chem. Phys. Lett.*, 2004, **391**, 308–313.

153 N. Nagaraju, A. Fonseca, Z. Konya and J. B. Nagy, *J. Mol. Catal. A: Chem.*, 2002, **181**, 57–62.

154 G. Busca, U. Costantino, T. Montanari, G. Ramis, C. Resini and M. Sisani, *Int. J. Hydrogen Energy*, 2010, **35**, 5356–5366.

155 J. O. Alves, Y. A. Levendis and J. A. S. Tenório, *Carbon*, 2012, **85**, 82.

156 N. Sano, Y. Hori, S. Yamamoto and H. Tamon, *Carbon*, 2012, **50**, 115–122.

157 J. Amadou, D. Begin, P. Nguyen, J. P. Tessonnier, T. Dintzer, E. Vanhaecke, M. J. Ledoux and C. Pham-Huu, *Carbon*, 2006, **44**, 2587–2589.

158 R. L. Vander Wal and L. J. Hall, *Carbon*, 2003, **41**, 659–672.

159 T. Ebbesen, P. Ajayan and K. Tanigaki, *Nature*, 1994, **367**, 519.

160 Y.-Q. Xu, H. Peng, R. H. Hauge and R. E. Smalley, *Nano Lett.*, 2005, **5**, 163–168.

161 J.-M. Moon, K. H. An, Y. H. Lee, Y. S. Park, D. J. Bae and G.-S. Park, *J. Phys. Chem. B*, 2001, **105**, 5677–5681.

162 M. Kumar and Y. Ando, in *Nanotechnology and Nanomaterials; Carbon Nanotubes-Synthesis, Characterisation, Application*, ed. S. Yellampalli, INTECH Open Access Publisher, 2011, pp. 148–170.

163 L. Ma, X. Dong, M. Chen, L. Zhu, C. Wang, F. Yang and Y. Dong, *Membranes*, 2017, **7**, 16.

164 J. P. Tessonnier and D. S. Su, *ChemSusChem*, 2011, **4**, 824–847.

165 A. Rinaldi, J. P. Tessonnier, M. E. Schuster, R. Blume, F. Girgsdies, Q. Zhang, T. Jacob, S. B. Abd Hamid, D. S. Su and R. Schlögl, *Angew. Chem., Int. Ed.*, 2011, **50**, 3313–3317.

166 R. Baker, P. Harris, R. Thomas and R. Waite, *J. Catal.*, 1973, **30**, 86–95.

167 S. Shukrullah, N. M. Mohamed, M. S. Shaharun and M. Y. Naz, *Mater. Chem. Phys.*, 2016, **176**, 32–43.

168 N. Yang, S. K. Youn, C. E. Frouzakis and H. G. Park, *Carbon*, 2018, **130**, 607–613.

169 R. Li, E. F. Antunes, E. Kalfon-Cohen, A. Kudo, L. Acauan, W.-C. D. Yang, C. Wang, K. Cui, A. H. Liotta, A. G. Rajan, J. Gardener, D. C. Bell, M. S. Strano, J. A. Liddle, R. Sharma and B. L. Wardle, *Angew. Chem., Int. Ed.*, 2019, **58**, 9204–9209.

170 A. Ashok, A. Kumar, J. Ponraj and S. A. Mansour, *Carbon*, 2020, **170**, 452–463.

171 C. Wu and P. T. Williams, *Appl. Catal., B*, 2010, **96**, 198–207.

172 A. Ebshish, Z. Yaakob, Y. H. Taufiq-Yap, A. Bshish and S. M. Tasirin, *Proc. Inst. Mech. Eng., Part A*, 2012, **226**, 1060–1075.

173 N. Das, A. Dalai, J. S. Soltan Mohammadzadeh and J. Adjaye, *Carbon*, 2006, **44**, 2236–2245.

174 H. Ago, N. Uehara, N. Yoshihara, M. Tsuji, M. Yumura, N. Tomonaga and T. Setoguchi, *Carbon*, 2006, **44**, 2912–2918.

175 I. F. Elbaba and P. T. Williams, *Appl. Catal., B*, 2012, **125**, 136–143.

176 I. F. Elbaba and P. T. Williams, *Fuel*, 2013, **106**, 528–536.

177 I. F. Elbaba and P. T. Williams, *Energy Fuels*, 2014, **28**, 2104–2113.

178 I. F. Elbaba, C. Wu and P. T. Williams, *Energy Fuels*, 2010, **24**, 3928–3935.

179 W. Yang, W. J. Sun, W. Chu, C. F. Jiang and J. Wen, *Chin. Chem. Lett.*, 2012, **23**, 363–366.

180 L. E. Murr, D. K. Brown, E. V. Esquivel, T. D. Ponda, F. Martinez and A. Virgen, *Mater. Charact.*, 2005, **55**, 371–377.

181 S. Poyraz, Z. Liu, Y. Liu and X. Zhang, *Curr. Org. Chem.*, 2013, **17**, 2243–2248.

182 C. Wu, Z. Wang, L. Wang, P. T. Williams and J. Huang, *RSC Adv.*, 2012, **2**, 4045–4047.

183 E. F. Kukovitskii, L. A. Chernozatonskii, S. G. L'vov and N. N. Mel'nik, *Chem. Phys. Lett.*, 1997, **266**, 323–328.

184 J. Liu, Z. Jiang, H. Yu and T. Tang, *Polym. Degrad. Stab.*, 2011, **96**, 1711–1719.

185 X. Jie, W. Li, D. Slocombe, Y. Gao, I. Banerjee, S. Gonzalez-Cortes, B. Yao, H. AlMegren, S. Alshihri and J. Dilworth, *Nat. Catal.*, 2020, 1–11.

186 L. He, S. Hu, L. Jiang, G. Liao, L. Zhang, H. Han, X. Chen, Y. Wang, K. Xu, S. Su and J. Xiang, *Fuel*, 2017, **210**, 307–314.

187 S. Zhang, S.-F. Jiang, B.-C. Huang, X.-C. Shen, W.-J. Chen, T.-P. Zhou, H.-Y. Cheng, B.-H. Cheng, C.-Z. Wu, W.-W. Li and H. Jiang, *Nat. Sustain.*, 2020, **3**(9), 753–760.

188 A. Romero, M. Jobbágy, M. Laborde, G. Baronetti and N. Amadeo, *Appl. Catal., A*, 2014, **470**, 398–404.

189 Y. Zhang, C. Wu, M. A. Nahil and P. Williams, *Energy Fuels*, 2015, **29**, 3328–3334.

190 S. Ucar, S. Karagoz, A. R. Ozkan and J. Yanik, *Fuel*, 2005, **84**, 1884–1892.

191 E. Kwon and M. J. Castaldi, *Environ. Sci. Technol.*, 2008, **42**, 2175–2180.

192 R. R. Soares, D. A. Simonetti and J. A. Dumesic, *Angew. Chem., Int. Ed.*, 2006, **45**, 3982–3985.

193 H. Brown and Y. Shah, in *Clean Production*, ed. K. B. Misra, Springer Berlin Heidelberg, 1996, ch. 28, pp. 647–683, DOI: 10.1007/978-3-642-79940-2_28.

194 S. Claude, *Lipid/Fett*, 1999, **101**(3), 101–104.

195 T. Valliyappan, N. N. Bakhshi and A. K. Dalai, *Bioresour. Technol.*, 2008, **99**, 4476–4483.

196 D. Simonetti, E. Kunkes and J. Dumesic, *J. Catal.*, 2007, **247**, 298–306.

197 A. P. G. Peres, N. D. L. Da Silva and M. R. W. Maciel, *Int. J. Energy Convers.*, 2013, **1**(1), 2013.

198 B. Dou, V. Dupont, G. Rickett, N. Blakeman, P. T. Williams, H. Chen, Y. Ding and M. Ghadiri, *Bioresour. Technol.*, 2009, **100**, 3540–3547.

199 V. Chiodo, S. Freni, A. Galvagno, N. Mondello and F. Frusteri, *Appl. Catal., A*, 2010, **381**, 1–7.

200 N. D. Charisiou, K. N. Papageridis, G. Siakavelas, V. Sebastian, S. J. Hinder, M. A. Baker, K. Polychronopoulou and M. A. Goula, *Catal. Today*, 2019, **319**, 206–219.

201 Z. Abu El-Rub, E. A. Bramer and G. Brem, *Ind. Eng. Chem. Res.*, 2004, **43**, 6911–6919.

202 J. C. Acomb, C. Wu and P. T. Williams, *Appl. Catal., B*, 2016, **180**, 497–510.

203 Y. Zhang, J. Huang and P. T. Williams, *Energy Fuels*, 2017, **31**(8), 8497–8504.

204 Y. Zhang and P. T. Williams, *J. Anal. Appl. Pyrolysis*, 2016, **122**, 490–501.

205 Y. Zhang, C. Wu, M. A. Nahil and P. Williams, *Proc. Inst. Civ. Eng.: Waste Resour. Manage.*, 2016, **169**, 137–145.

206 Y. Zhang, Y. Tao, J. Huang and P. Williams, *Waste Manage. Res.*, 2017, **35**(10), 1045–1054.

207 A. C. Freitas and R. Guirardello, *Int. J. Hydrogen Energy*, 2014, **39**(31), 17969–17984.

208 S. Adhikari, S. Fernando and A. Haryanto, *Catal. Today*, 2007, **129**, 355–364.

209 S. Czernik, R. French, C. Feik and E. Chornet, *Ind. Eng. Chem. Res.*, 2002, **41**, 4209–4215.

210 S. Adhikari, S. D. Fernando and A. Haryanto, *Chem. Eng. Technol.*, 2009, **32**, 541–547.

211 S. Adhikari, S. D. Fernando, S. F. To, R. M. Bricka, P. H. Steele and A. Haryanto, *Energy Fuels*, 2008, **22**(2), 1220–1226.

212 D. Sutton, B. Kelleher and J. R. H. Ross, *Fuel Process. Technol.*, 2001, **73**, 155–173.

213 W. B. Hauserman, *Int. J. Hydrogen Energy*, 1994, **19**, 413–419.

214 I. N. Buffoni, F. Pompeo, G. F. Santori and N. N. Nichio, *Catal. Commun.*, 2009, **10**, 1656–1660.

215 B. Zhang, X. Tang, Y. Li, Y. Xu and W. Shen, *Int. J. Hydrogen Energy*, 2007, **32**, 2367–2373.

216 A. Iriondo, V. L. Barrio, J. F. Cambra, P. L. Arias, M. B. Güemez, R. M. Navarro, M. C. Sánchez-Sánchez and J. L. G. Fierro, *Top. Catal.*, 2008, **49**, 46–58.

217 A. Iriondo, V. L. Barrio, J. F. Cambra, P. L. Arias, M. B. Güemez, R. M. Navarro, M. C. Sanchez-Sanchez and J. L. G. Fierro, *Catal. Commun.*, 2009, **10**, 1275–1278.

218 Y. Hao, Z. Qunfeng, W. Fei, Q. Weizhong and L. Guohua, *Carbon*, 2003, **41**, 2855–2863.

219 A. A. Aboul-Enein and A. E. Awadallah, *Chem. Eng. J.*, 2018, **354**, 802–816.

220 D. Yao, C. Wu, H. Yang, Y. Zhang, M. A. Nahil, Y. Chen, P. T. Williams and H. Chen, *Energy Convers. Manage.*, 2017, **148**, 692–700.

221 L. He, S. Hu, X. Yin, J. Xu, H. Han, H. Li, Q. Ren, S. Su, Y. Wang and J. Xiang, *Fuel*, 2020, **276**, 118116.

222 D. Yao, H. Li, Y. Dai and C.-H. Wang, *Chem. Eng. J.*, 2020, 127268, DOI: 10.1016/j.cej.2020.127268.

223 N. Cai, H. Yang, X. Zhang, S. Xia, D. Yao, P. Bartocci, F. Fantozzi, Y. Chen, H. Chen and P. T. Williams, *Waste Manage.*, 2020, **109**, 119–126.

224 D. Yao, Y. Zhang, P. T. Williams, H. Yang and H. Chen, *Appl. Catal., B*, 2018, **221**, 584–597.

225 A. Iriondo, V. L. Barrio, J. F. Cambra, P. L. Arias, M. B. Guemez, M. C. Sanchez-Sanchez, R. M. Navarro and J. L. G. Fierro, *Int. J. Hydrogen Energy*, 2010, **35**, 11622–11633.

226 M. Slinn, K. Kendall, C. Mallon and J. Andrews, *Bioresour. Technol.*, 2008, **99**, 5851–5858.

227 T. Hirai, N.-o. Ikenaga, T. Miyake and T. Suzuki, *Energy Fuels*, 2005, **19**, 1761–1762.

228 R. Kikuchi, H. Sato, Y. Matsukura and T. Yamamoto, *Fuel Process. Technol.*, 2005, **86**, 1279–1296.

229 L. P. R. Profeti, E. A. Ticianelli and E. M. Assaf, *Int. J. Hydrogen Energy*, 2009, **34**, 5049–5060.

230 Y. Cui, V. Galvita, L. Rihko-Struckmann, H. Lorenz and K. Sundmacher, *Appl. Catal., B*, 2009, **90**, 29–37.

231 A. Slagtern, Y. Schuurman, C. Leclercq, X. Verykios and C. Mirodatos, *J. Catal.*, 1997, **172**, 118–126.

232 A. Le Valant, N. Bion, F. Can, D. Duprez and F. Epron, *Appl. Catal., B*, 2010, **97**(1–2), 72–81.

233 S. Adhikari, S. D. Fernando and A. Haryanto, *Renewable Energy*, 2008, **33**(5), 1097–1100.

234 I. Rossetti, A. Gallo, V. Dal Santo, C. L. Bianchi, V. Nichele, M. Signoretto, E. Finocchio, G. Ramis and A. Di Michele, *ChemCatChem*, 2013, **5**, 294.

235 T. Miyazawa, T. Kimura, J. Nishikawa, S. Kado, K. Kunimori and K. Tomishige, *Catal. Today*, 2006, **115**, 254–262.

236 M. Inaba, K. Murata, M. Saito and I. Takahara, *Energy Fuels*, 2006, **20**, 432–438.

237 L. He, S. Hu, L. Jiang, G. Liao, X. Chen, H. Han, L. Xiao, Q. Ren, Y. Wang, S. Su and J. Xiang, *Fuel Process. Technol.*, 2018, **176**, 7–14.

238 C. Wu, L. Dong, J. Onwudili, P. T. Williams and J. Huang, *ACS Sustainable Chem. Eng.*, 2013, **1**, 1083–1091.

239 M. Zhao, N. H. Florin and A. T. Harris, *Appl. Catal., B*, 2009, **92**, 185–193.

240 D. Yao, H. Yang, H. Chen and P. T. Williams, *Appl. Catal., B*, 2018, **227**, 477–487.

241 S. Bepari and D. Kuila, *Int. J. Hydrogen Energy*, 2020, **45**, 18090–18113.

242 D. Yao, H. Yang, H. Chen and P. T. Williams, *Appl. Catal., B*, 2018, **239**, 565–577.

243 M. U. Zahid, E. Pervaiz, A. Hussain, M. I. Shahzad and M. B. K. Niazi, *Mater. Res. Express*, 2018, **5**, 052002.

244 P. A. Simell, J. O. Hepola and A. O. I. Krause, *Fuel*, 1997, **76**, 1117–1127.

245 A. M. Venezia, *Catal. Today*, 2003, **77**, 359–370.

246 H. E. Lim, Y. Miyata, R. Kitaura, Y. Nishimura, Y. Nishimoto, S. Irle, J. H. Warner, H. Kataura and H. Shinohara, *Nat. Commun.*, 2013, **4**(1), 1–7.

247 L. Bokobza and J. Zhang, *eXPRESS Polym. Lett.*, 2012, **6**, 601–608.

248 N. Giannakeas, A. Lea-Langton, V. Dupont and M. V. Twigg, *Appl. Catal., B*, 2012, **126**, 249–257.

249 C. Courson, E. Makaga, C. Petit and A. Kiennemann, *Catal. Today*, 2000, **63**, 427–437.

250 Y. Zhang, Y. Tao, J. Huang and P. Williams, *Waste Manage. Res.*, 2017, **35**, 1045–1054.

251 X. Wang, M. Li, S. Li, H. Wang, S. Wang and X. Ma, *Fuel Process. Technol.*, 2010, **91**, 1812–1818.

252 Y. Zhang, J. Huang and P. T. Williams, *Energy Fuels*, 2017, **31**, 8497–8504.

253 M. Kyari, A. Cunliffe and P. T. Williams, *Energy Fuels*, 2005, **19**, 1165–1173.

254 I. de Marco Rodriguez, M. F. Laresgoiti, M. A. Cabrero, A. Torres, M. J. Chomón and B. Caballero, *Fuel Process. Technol.*, 2001, **72**, 9–22.

255 A. M. Cunliffe and P. T. Williams, *J. Anal. Appl. Pyrolysis*, 1998, **44**, 131–152.

256 D. Leung, X. Yin, Z. Zhao, B. Xu and Y. Chen, *Fuel Process. Technol.*, 2002, **79**, 141–155.

257 C. Roy, B. Labrecque and B. de Caumia, *Resour., Conserv. Recycl.*, 1990, **4**, 203–213.

258 A. Napoli, Y. Soudais, D. Lecomte and S. Castillo, *J. Anal. Appl. Pyrolysis*, 1997, **40**, 373–382.

259 J.-H. Zhou, Z.-J. Sui, P. Li, D. Chen, Y.-C. Dai and W.-K. Yuan, *Carbon*, 2006, **44**, 3255–3262.

260 T. Zhao, W. Sun, X. Gu, M. Rönning and D. Chen, *Appl. Catal., A*, 2007, **323**, 135–146.

261 A. Magrez, J. W. Seo, R. Smajda, B. Korbely, J. C. Andresen, M. Mionic, S. Casimirius and L. s. Forró, *ACS Nano*, 2010, **4**, 3702–3708.

262 Y. Zhang, J. M. Gregoire, R. Van Dover and A. J. Hart, *J. Phys. Chem. C*, 2010, **114**, 6389–6395.

263 M. Motta, A. Moisala, I. Kinloch and A. Windle, *J. Nanosci. Nanotechnol.*, 2008, **8**, 2442–2449.

264 Y. Zhang, *Hydrogen and carbon nano-materials from the pyrolysis-catalysis of wastes*, University of Leeds, 2017.

265 Y. Zhang, M. A. Nahil, C. Wu and P. T. Williams, *Environ. Technol.*, 2017, **38**, 1–9.

266 R. Schmuch, R. Wagner, G. Hörpel, T. Placke and M. Winter, *Nat. Energy*, 2018, **3**, 267–278.

267 R. Fang, K. Chen, L. Yin, Z. Sun, F. Li and H. M. Cheng, *Adv. Mater.*, 2019, **31**, e1800863.

268 P. G. Bruce, S. A. Freunberger, L. J. Hardwick and J.-M. Tarascon, *Nat. Mater.*, 2012, **11**, 19–29.

269 L. Dai, D. W. Chang, J. B. Baek and W. Lu, *Small*, 2012, **8**, 1122.

270 K. Evanoff, J. Khan, A. A. Balandin, A. Magasinski, W. J. Ready, T. F. Fuller and G. Yushin, *Adv. Mater.*, 2012, **24**, 533–537.

271 J. Wang, X. Yan, Z. Zhang, H. Ying, R. Guo, W. Yang and W. Q. Han, *Adv. Funct. Mater.*, 2019, **29**, 1904819.

272 Y. Cao, A.-Q. Zhang, H. Zhang, G.-Q. Ding and L.-S. Zhang, *Inorg. Chem. Commun.*, 2020, **111**, 107633.

273 Y. Li, Y. Feng and W. Feng, *Electrochim. Acta*, 2013, **107**, 343–349.

274 Y. Wu, J. Wang, K. Jiang and S. Fan, *Front. Phys.*, 2014, **9**, 351–369.

275 M. Zhang, R. Lu, H. Yuan, K. Amin, L. Mao, W. Yan and Z. Wei, *ACS Appl. Mater. Interfaces*, 2019, **11**, 20873–20880.

276 Q. Zhang, G. Peng, J. P. Mwizerwa, H. Wan, L. Cai, X. Xu and X. Yao, *J. Mater. Chem. A*, 2018, **6**, 12098–12105.

277 D. Gueon and J. H. Moon, *Chem. Commun.*, 2019, **55**, 361–364.

278 W. Mao, G. Ai, Y. Dai, Y. Fu, Y. Ma, S. Shi, R. Soe, X. Zhang, D. Qu, Z. Tang and V. S. Battaglia, *J. Power Sources*, 2016, **310**, 54–60.

279 Y. Li, X. Wu, C. Liu, S. Wang, P. Zhou, T. Zhou, Z. Miao, W. Xing, S. Zhuo and J. Zhou, *J. Mater. Chem. A*, 2019, **7**, 7128–7137.

280 L. Zhang, R. A. Senthil, J. Pan, A. Khan, X. Jin and Y. Sun, *Ionics*, 2019, **25**, 4761–4773.

281 P. K. Nayak, L. Yang, W. Brehm and P. Adelhelm, *Angew. Chem.*, 2018, **57**, 102–120.

282 S. Zhang, G. Wang, B. Wang, J. Wang, J. Bai and H. Wang, *Adv. Funct. Mater.*, 2020, **30**, 2001592.

283 A. Banerjee, B. Ziv, E. Levi, Y. Shilina, S. Luski and D. Aurbach, *J. Electrochem. Soc.*, 2016, **163**, A1518–A1526.

284 T. Matsumoto, T. Komatsu, K. Arai, T. Yamazaki, M. Kijima, H. Shimizu, Y. Takasawa and J. Nakamura, *Chem. Commun.*, 2004, 840–841.

285 A. Le Goff, V. Artero, B. Jousselme, P. D. Tran, N. Guillet, R. Métayé, A. Fihri, S. Palacin and M. Fontecave, *Science*, 2009, **326**, 1384–1387.

286 K. Gong, F. Du, Z. Xia, M. Durstock and L. Dai, *Science*, 2009, **323**, 760–764.

287 A. Veksha, K. Yin, J. G. S. Moo, W. D. Oh, A. Ahamed, W. Q. Chen, P. Weerachanchai, A. Giannis and G. Lisak, *J. Hazard. Mater.*, 2020, **387**, 121256.

288 T. Kshetri, D. T. Tran, D. C. Nguyen, N. H. Kim, K.-t. Lau and J. H. Lee, *Chem. Eng. J.*, 2020, **380**, 122543.

289 A. Afzal, F. A. Abuilaiwi, A. Habib, M. Awais, S. B. Waje and M. A. Atieh, *J. Power Sources*, 2017, **352**, 174–186.

290 Y. Liu, K. Shi and I. Zhitomirsky, *Electrochim. Acta*, 2017, **233**, 142–150.

291 F. Zhou, Q. Liu, D. Kang, J. Gu, W. Zhang and D. Zhang, *J. Mater. Chem. A*, 2014, **2**, 3505–3512.

292 N. Rey-Raap, M. Enterria, J. I. Martins, M. F. R. Pereira and J. L. Figueiredo, *ACS Appl. Mater. Interfaces*, 2019, **11**, 6066–6077.

293 H. Wu, J. Guo and D. a. Yang, *J. Mater. Sci. Technol.*, 2020, **47**, 169–176.

294 X. Wen, X. Chen, N. Tian, J. Gong, J. Liu, M. H. Rummeli, P. K. Chu, E. Mijiwska and T. Tang, *Environ. Sci. Technol.*, 2014, **48**, 4048–4055.

295 N. X. Viet, S. Kishimoto and Y. Ohno, *ACS Appl. Mater. Interfaces*, 2019, **11**, 6389–6395.

296 T. Rasheed, F. Nabeel, M. Adeel, K. Rizwan, M. Bilal and H. M. N. Iqbal, *J. Mol. Liq.*, 2019, **292**, 111425.

297 Z. S. Stojanović, E. Mehmeti, K. Kalcher, V. Guzsvány and D. M. Stanković, *Food Anal. Methods*, 2016, **9**, 2701–2710.

298 S. Najari, H. Bagheri, Z. Monsef-Khoshhesab, A. Hajian and A. Afkhami, *Ionics*, 2018, **24**, 3209–3219.

299 W. Bauhofer and J. Z. Kovacs, *Compos. Sci. Technol.*, 2009, **69**, 1486–1498.

300 T.-W. Chou, L. Gao, E. T. Thostenson, Z. Zhang and J.-H. Byun, *Compos. Sci. Technol.*, 2010, **70**, 1–19.

301 F. Gojny, M. Wichmann, U. Köpke, B. Fiedler and K. Schulte, *Compos. Sci. Technol.*, 2004, **64**, 2363–2371.

302 T. Kashiwagi, F. Du, J. F. Douglas, K. I. Winey, R. H. Harris and J. R. Shields, *Nat. Mater.*, 2005, **4**, 928–933.

303 S. R. Bakshi and A. Agarwal, *Carbon*, 2011, **49**, 533–544.

304 Z. Wu, Z. Chen, X. Du, J. M. Logan, J. Sippel, M. Nikolou, K. Kamaras, J. R. Reynolds, D. B. Tanner and A. F. Hebard, *Science*, 2004, **305**, 1273–1276.

305 M. F. De Volder, S. H. Tawfick, R. H. Baughman and A. J. Hart, *Science*, 2013, **339**(6119), 535–539.

306 P. T. Williams, S. Besler and D. T. Taylor, *Proc. Inst. Mech. Eng., Part A*, 1993, **207**, 55–63.

307 J. D. Martínez, N. Puy, R. Murillo, T. García, M. V. Navarro and A. M. Mastral, *Renewable Sustainable Energy Rev.*, 2013, **23**, 179–213.

308 A. Evans and R. Evans, *The Composition of a Tyre: Typical Components, the Waste & Resource Action Programme*, Banbury, 2006.

309 S. De and J. N. Coleman, *MRS Bull.*, 2011, **36**, 774–781.

310 X. Liu, B. Shen, Z. Wu, C. M. Parlett, Z. Han, A. George, P. Yuan, D. Patel and C. Wu, *Chem. Eng. Sci.*, 2018, **192**, 882–891.